Physiological Chemistry and Physics and Medical NMR Volume 38, Number 2, 2006

Addresses of Chief Editor and Editorial College

Toshihiko Ubuka
Department of Clinical Nutrition
Kawasaki University of Medical Welfare
Kurashiki, Okayama, 701-0193, Japan

Denys Wheatley
Department of Cell Pathology
University of Aberdeen
Aberdeen AB24 4FA, Scotland
United Kingdom

EDITORIAL AND BUSINESS OFFICE

Physiological Chemistry and Physics
and Medical NMR
P.O. Box 1452
Melville, New York 11747

Editor In Chief, Dr. Gilbert N. Ling
Managing Editor, Margaret M. Ochsenfeld

SCOPE: PCP provides a forum for the review and publication of reports of original research in a broad range of subjects in biophysics, biochemistry and cellular physiology. Reports of direct applications of basic knowledge to human studies are invited; examples would include the measurements of relaxation times as part of NMR imaging. Single experiments, conclusions based on inadequate statistics, purely speculative papers, and clinical case reports are not accepted.

POLICY: The pages of PCP are accessible to competing viewpoints, interpretations, theories and opinions. Debate is invited via Editorial Comments and Letters to the Editor. Criteria for evaluating submissions include soundness of the study and clarity of presentation, and papers are not rejected on the basis of interpretation or theory, however controversial. PCP believes that scientific issues should be settled by investigation and open debate, not by an appeal to anonymous authority.

PCP attempts to achieve a balance between freedom of expression and constructive peer review. All papers are refereed by reviewers who may remain anonymous, but the Chief Editors make all final decisions, and will handle appeals from authors who feel their papers are unfairly reviewed.

The Editors endeavor to make decisions regarding acceptance or rejection of manuscripts quickly, and have set self-imposed deadlines for doing so. Referees also are given deadlines.

TYPES OF PAPERS: *Regular papers* may be experimental or theoretical. *Short notes, Priority notes* and *Letters* in response to published papers are invited. *Reviews* are desired, but authors are urged to contact an Editor before sending a finished review manuscript. *Symposia* may be published as regular or supplemental issues.

SUBSCRIPTIONS: Price is US$80.00 per volume in the United States and US$87.00 outside the United States. *Physiological Chemistry and Physics and Medical NMR* is published biannually, 2 issues per year, the volume numbered yearly. New subscriptions will start with the first issue of the volume in progress, unless the subscriber directs otherwise. Most back issues are available

Instructions to Authors

SUBMISSIONS: An original and two copies of all material are requested. The original must be typewritten on one side only. Papers should be sent to Dr. Gilbert N. Ling, Editor, P.O. Box 1452, Melville, New York 11747 U.S.A. Manuscripts should be submitted only to this journal and not have been published in part or whole in another publication, except as short preliminary notes, abstracts, or as unpublished work in reviews or symposia. Be sure to keep a copy of your manuscript.

NOTE: Referees will be instructed to destroy their copies of the manuscript after reviewing them. We will return only the original manuscript to you for revision or if rejected.

MANUSCRIPTS: All material should be typed double-spaced with margins at least one inch wide and pages numbered consecutively beginning with the title page. In addition to a paper copy, send an IBM- or Macintosh-compatible file on a floppy disk or CD, in Word or Wordperfect. *Title Page* should include title (of at most 100 characters and spaces), full names of authors as you wish them to be published, names and cities of institutional affiliation(s) of authors and of institution(s) where the studies were performed, and name, full address, telephone number, fax number and e-mail address of the person to whom correspondence, proofs, and reprint requests are to be sent. Four to six *key words* should be listed on the title page. These words will assist indexers. Also, at bottom of title page include a short running title of 40 characters or less.

Abstract should be concise and no longer than 225 words. *Body* may or may not be divided into Introduction, Materials and Methods, Results and Discussion, depending on the length and nature of the paper. Introductory remarks should indicate clearly the significance of the work presented. *References* may be indicated in the text and listed in the reference list in whatever style the author prefers, but we prefer that titles of articles be omitted.

TABLES: Tables should be typewritten on separate sheets and identified by roman numerals (eg. Table III) and titles. Table notes should be keyed by superscript italic lower-case letters (eg. [a]Control). The approximate locations of *tables* and *figures* should be indicated in the margins of the manuscript.

ILLUSTRATIONS: Original artwork or glossy photostatic prints, together with two photocopies (like Xerox copies) should be provided. Each illustration should be numbered on the back in pencil, along with the authors' names. It is preferred that line drawings be made on paper that is not larger than 8 1/2 by 13 inches, and that the drawing be its intended size in the printed paper. Most figures will occupy 1/2 to full column, that is 5 inches wide. Lines and lettering should be thick enough to allow reduction. A drawing of overall dimension of 8 by 10 inches that will be reduced to 1/4 of its original size should be lettered with 18-point (capitals 6 mm high, lower-case 4 mm high) or larger lettering. Glossy photostatic prints are acceptable, and should be attached firmly to a sheet of paper the same size as the manuscript. Postacceptance: If possible send figures as an image file using TIFF or JPEG formatting scanned at a resolution of 600 dpi.

PHOTOGRAPHS: High-quality black and white glossy prints should be provided in triplicate, and may be provided as one print plus two photocopies if the photocopies are sufficiently clear to portray the original to referees. Photographs should be attached firmly to a sheet of paper the same size as the manuscript. Photographs that have been scanned and stored as a TIFF file with a resolution of 300 dpi may also be submitted.

REFEREES: Two anonymous referees will be sought for each paper. Authors are encouraged to suggest names and addresses of suitable referees. Referees will be given deadlines for mailing manuscripts back or phoning reviews in, and will be invited to provide editorial statements or Letters that deal with issues raised by submitted papers.

REPRINTS: An order form is enclosed with proofs sent to authors.

PAGE CHARGES: Page charge is $20.00 per published page. It may be waived in the case of severe international exchange difficulties. An additional charge of $15.00 will be levied for photographs that require screening (eg., E.M's, chromatograms, scans).

Physiol. Chem. Phys. & Med. NMR (2006) *38*: 77–83

Effects of Acetaminophen on Hepatic Gene Expression in Mice

Sun-Young Jeong[1], Jung-Sun Lim[1], Han-Jin Park[1], Jae-Woo Cho[2], Suresh VS Rana[3] & Seokjoo Yoon[1*]

[1]*Toxicogenomics Team,* [2]*Histopathology Team, Korea Institute of Toxicology, 100 Jangdong, Yuseong, Daejeon, 305-343, Republic of Korea,* [3]*Toxicology Laboratory, Department of Zoology, Ch. Charan Singh University, Meerut, 250004, India.*

**Correspondence to: Seokjoo Yoon, Toxicogenomics Team, Korea Institute of Toxicology, 100 Jang-dong, Yuseong, Daejeon, 305-343, Republic of Korea. E-mail: sjyoon@kitox.re.kr*

Abstract: Acetaminophen (APAP) is one of the most commonly used drugs for the safe and effective treatment of fever and pain. However, it is a well-established hepatotoxin. The objective of this study was to identify alternation in various genes in liver of mice after administration of low and high doses of APAP. Male C57BL/6J mice received APAP (30 or 300 mg/kg, i.p.). They were sacrificed after 6 hr and 24 hr for assessment of alanine aminotransferase (ALT) and aspartate aminotransferase (AST), total RNA isolation, cDNA microarray analysis and histopathological analysis of liver injury. Low dose of APAP did not cause hepatotoxicity in mice. However, it was toxic at a high dose. Using microarray technology, we selected changed genes more than 1.5 fold. Gene expression changes were recorded even at a low dose treatment with APAP. Six (6) hr after APAP treatment at low dose, 6 genes were up-regulated and 25 genes were down-regulated. However, 24 hr after treatment at low dose 8 genes were up-regulated and 34 genes were down-regulated. 6 hr after of high dose treatment 29 genes were down-regulated and none was up-regulated. A 24 hr treatment with high dose up-regulated 6 genes and down-regulated 18 genes. These expression patterns provide information on high versus low dose mechanisms of APAP toxicity. Gene expression signatures recorded after a nontoxic dose of APAP strongly support the validity of gene expression changes as meaningful markers of hepatotoxicity.

KEY WORDS: acetaminophen; hepatotoxicity; gene expression

ACETAMINOPHEN (APAP) is an extensively used analgesic. Typical therapeutic doses of APAP are not hepatotoxic. Metabolites produced by APAP are reactive electrophiles

Abbreviations: APAP, acetaminophen; ALT, alanine aminotransferase; AST, aspartate aminotransferase; NAPQI, N-acetyl-*p*-benzoquinone imine; H&E, hematoxylin and eosin; PAS, periodic acid-Schiff.

which are oxidized to electrophilic quinones. APAP is converted to a quinoneimine, namely N-acetyl-*p*-benzoquinone imine (NAPQI), a cytotoxic electrophile that binds to cellular proteins. The formation of this toxic metabolite by cytochrome P450 causes centrilobular necrosis of the liver. NAPQI is conjugated with glutathione to form nontoxic cysteine and mercapturic acid conjugates and is eliminated unless glutathione stores become depleted. The portion of NAPQI not detoxified to APAP mercapturate, binds covalently to critical intracellular molecules which eventually lead to toxicity and cell death (1–3). Many of these covalently bound proteins are within the mitochondria (4), resulting in reduced respiration (5) and increased superoxide production (6). Superoxide either reacts with nitric oxide to produce peroxynitrite (7) or dismutase to hydrogen peroxide, whereby it can oxidize cellular macromolecules. The induction of nitric oxide by APAP (8) is thought to block propagation of lipid peroxidation (9). It is now generally accepted that loss of mitochondrial function and concomitant generation of oxidative stress are central to APAP-induced hepatotoxiciy (10,11). Recently, Lucas *et al*. (12) discussed the role of cycloxygenase in APAP toxicity. However, the mechanisms of APAP toxicity have not been correlated with gene expression changes. Since observations on gene expression profiling can serve as a guide for specific genes and/or proteins that could be used as biomarkers of incipient toxicity or can predict pathological changes, we have tried to detect subtle cellular disturbances caused by APAP at an acute and overtly toxic dose, in the liver of mice.

Materials and Methods

Chemicals

APAP was purchased from Sigma-Aldrich (USA). APAP was dissolved in a saline. Trizol was purchased from InVitrogen (USA).

Animal treatments

Ten week old male C57BL/6 mice were obtained from Orient Co. Ltd (Korea). They were acclimatized to laboratory conditions for two weeks, and maintained on a 12 h light/dark cycle in the animal room at 23±1 °C and humidity 50±5 %. After acclimatization, mice were randomly divided into 5 groups each containing 3 mice. Mice of group A received 30 mg/kg APAP through intraperitoneal injection and sacrificed by diethyl ether after 6 hrs. Whereas mice of group B received the same dose of APAP through same route but sacrificed 24 hrs after APAP injection. Mice of group C received 300 mg/kg APAP through intraperitoneal injection and sacrificed after 6 hrs. Mice of group D received APAP in the same dose and manner as the mice of group C but sacrificed after 24 hrs. Control group received intraperitoneal injections of saline only and sacrificed after 24 hrs. After respective treatments, liver samples were carefully removed from each mouse and processed further for histopathological, biochemical and cDNA microarray expression studies.

Histopathological observations

Small liver samples collected from treated and control groups were fixed in 10 % neutral buffered formalin and embedded in paraffin. The 4 μm thick paraffin sections were cut on a RM2165 microtome (Leica, Germany), stained with hematoxylin and eosin (H&E) and periodic acid-Schiff (PAS) and examined under a light microscope (Nikon, Japan).

Biochemical observations

Blood from each mouse was collected from the inferior vena cava. Serum was separated by centrifugation. Alanine aminotransferase (ALT) and aspartate aminotransferase (AST) were determined using an automated clinical chemistry analyzer (Fuji Drichem 3500, Japan). Data was calculated as mean ± S.D.. The statistical inference was drawn applying one-way ANOVA followed by the Dunnett test.

Isolation of RNA

The left lateral lobe of the liver was removed and processed for RNA extraction. Total RNA was extracted using the TRIzol reagent (InVitrogen, USA) according to the instructions of the manufacturer and purified using RNeasy total RNA isolation kit (Qiagen, Germany). Total RNA was quantified by NanoDrop ND-1000 (Nanodrop, USA) and its integrity was assessed by Bioanalyzer 2100 (Agilent, USA).

cDNA microarray

For microarray analysis, fluorescent-labeled cDNA was prepared from the coupled Cy3-dUTP or Cy5-dUTP using Superscript II (InVitrogen, USA). Single stranded cDNA probes were purified using a PCR purification kit (Qiagen, Germany). Probes were resuspended in hybridization solution. The mouse TwinChip 7.4K cDNA chip (DigitalGenomics, Korea) was used for microarray study.

Analysis of fluorescence spots

After washing the probes, the slides were scanned using Scannarray (Packard, USA) and analyzed with GenePlex software (Istech, Korea). The log gene expression ratios were normalized by LOWLESS regression. The genes that were expressed above 1.5 fold induction or below 2-fold repression after APAP treatment as compared with control samples were considered for statistical analysis. Significant differences between control and treated groups were determined using Student's t test.

Results

Low dose (30 mg/kg) treatments with APAP for 6 hr and 24 hr did not cause hepatotoxic effects in mice. High dose (300 mg/kg) treatments, however, were found to be hepatotoxic. Highly significant elevation in the activities of AST and ALT were recorded in mice treated with high dose of APAP for 24 hr (Table I).

TABLE I. AST and ALT activities in the sera of APAP treated mice

Time after APAP treatment	Dose	AST	ALT
Control (Saline)		51.70±2.55	30.40±2.83
6 hr	Low	52.50±4.53	33.95±0.21
6 hr	High	65.90±0.14	46.85±2.05
24 hr	Low	54.45±13.22	30.65±7.14
24 hr	High	478.40±105.08**	445.70±45.85**

**$p<0.01$ vs. control, t-test (Dunnett).

Histopathological observations supported the results on serum transaminases. 24 hr high dose treatment of mice with APAP induced centrilobular necrosis (Figure 1).

After 6 hr of APAP treatment at low dose, 6 genes were up-regulated and 25 genes were down-regulated. However, after 24 hr of APAP treatment at low dose, 8 genes were up-regulated and 34 genes were down-regulated. Results were different between low dose and high dose treatments. At high dose treatment for 6 hr, 29 genes were down-regulated and none was up-regulated. 24 hr treatment at high dose up-regulated 6 genes and down-regulated 18 genes. Significant up-regulated genes included *Pklr*, *Cyp2a4*, *Igh-VJ558*, and *Nsdhl*. Down-regulated genes included *Slc10a3*, *Ifi205*, *Hspa5*, *Tnfrs7*, *Selenbp1*, *Cyp4a14*, and *Cyp4a10* (Table II, III).

Discussion

The present study on APAP shows that alteration in gene expression does occur even when no apparent toxicity is detected using routine histopathological and clinical chemistry measurements. Heinloth *et al*. (13) demonstrated that a subtoxic dose of APAP (150 mg/kg) induced oxidative stress after 6 hr of APAP treatment. Other studies have reported elevated levels of nitrotyrosine protein adducts that precede and/or accompany APAP induced hepatotoxicity in mice (7, 11). We explain this possibility by the inhibition of GSH peroxidase. Down-regulation selenium binding protein actually impairs GSH peroxidase. Inhibition of GSH peroxidase by APAP has already been reported by Gaut *et al*. (14). Furthermore, the down-regulation of tumor necrosis factor and proteins of cytochrome P450 family 4 all support the ROS dependent mechanism of APAP toxicity. It is interesting to note that genes Cyp450, family 2A4 are up-regulated as are those GOT and NAD(P) dependent dehydrogenase. Moreover, down-regulated heat shock proteins (*Hsp70*) again suggest the role of ROS in APAP hepatotoxicity. Jia *et al*. (15) have shown that transcription co-activator peroxisome proliferators-activated receptor binding protein (*PBP*) that functions as a transcription co-activator for nuclear receptors is abrogated in APAP hepatotoxicity. Our results show down-regulation of nuclear receptor subfamily 1 and thus find a support from their report.

In general, the acceptance of microarray expression data as a reliable endpoint in any toxicological study requires careful interpretation and validation. Minami *et al*. (16) while analyzing DNA microarray containing 1097 drug response genes also considered cytochrome P450s, other phase I and phase II enzymes, nuclear receptors, signal transducers and transporters as indicators of hepatotoxicity. They identified 10 up-regulated and 10 down-regulated genes as potential markers of APAP, bromobenzene, and carbon tetrachloride in Sprague-Dawley rats (6 weeks old). In addition to these molecular markers, we have studied those encoding for tumor necrosis factor and heat shock proteins. Expression of gene encoding for *Hsp70* has been studied by Welch *et al*. (17) in APAP induced liver disease in susceptible and resistant strains of mice. They also suggested protective role of this protein against APAP hepatotoxicity.

Time course expression profiles for selected genes created after APAP administration showed that most active gene expression occurs around 4 hr after a toxic dose of APAP (18). They also observed the down-regulation of these genes after 24 hr, coinciding with the development of hepatotoxicity. However, differential expression of hepatic transporter genes was observed in mice after APAP and carbon tetrachloride treatments (19). There seems to be a coordinated regulation of both transport and detoxification genes during liver injury.

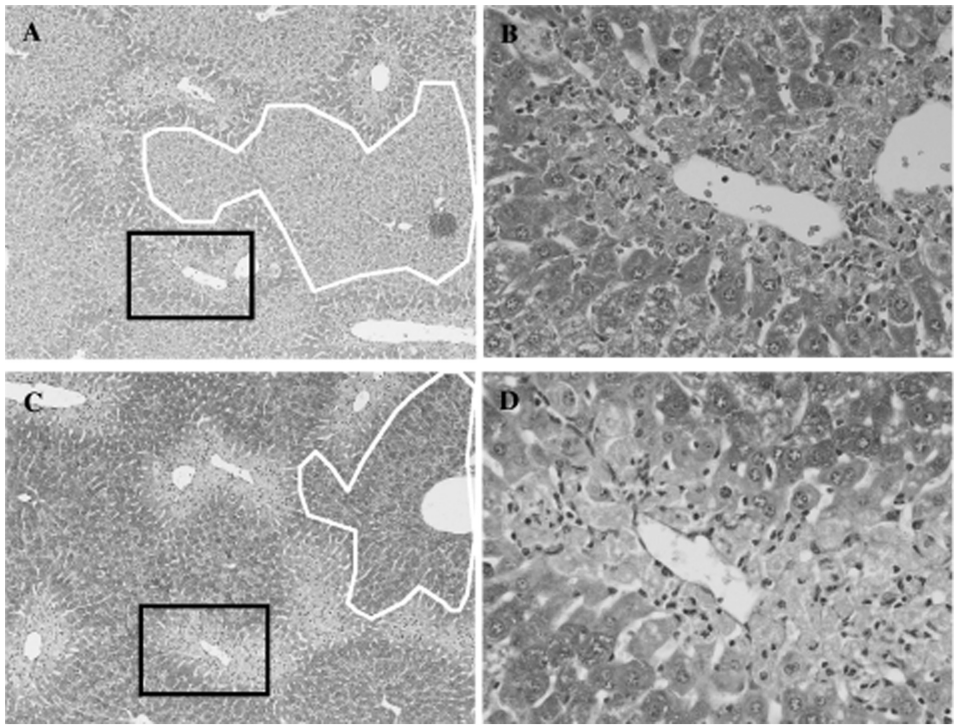

FIGURE 1. H&E and PAS stained sections from mice liver 24 hr after high dose of APAP. (A) H&E staining. Black lined box: centrilobular necrosis; white lined area: normal tissue, X100. (B) Enlarged picture from black lined box A, X400. (C) PAS staining. Black lined box: centrilobular necrosis; white lined area: normal tissue, X100. (D) Enlarged picture from black lined box of C, X400.

Table II. 1.5 folds up-regulated genes in at least one group.

Genbank No.	6h		24h		Gene Name
	Low	High	Low	High	
NM_011267	1.04	0.94	0.23	0.16	*Rgs16*, Regulator of G-protein signaling 1
NM_009127	0.93	0.08	–0.03	0.34	*Scd1*, Stearoyl-Coenzyme A desaturase 1
NM_009980	0.80	0.45	0.06	0.33	*Ctbp2*, C-terminal binding protein 2
NM_011983	0.74	0.83	–0.08	0.23	*Homer2*, Homer homolog 2 (Drosophila)
NM_008227	0.74	0.59	0.24	0.26	*Pklr*, Pyruvate kinase liver and red blood
NM_009997	0.97	1.85	0.27	1.08	*Cyp2a4*, Cytochrome P450, family 2, subfamily a, polypeptide 4
NM_010324	0.18	1.10	0.24	–0.11	*Got1*, Glutamate oxaloacetate transaminase 1
NM_032002	0.33	0.89	0.09	0.06	*Nrg4*, Neuregulin 4
	0.48	0.76	0.16	0.07	*Igh-VJ558*, Immunoglobulin heavy chain (J558 family)
NM_134469	–0.14	–0.17	0.16	1.02	*Fdps*, Farnesyl diphosphate synthetase
	0.17	–0.03	0.38	0.78	*Nsdhl*, NAD(P) dependent steroid dehydroge
NM_007654	0.86	0.70	0.89	0.78	*Cd72*, CD72 antigen
	0.25	0.33	0.40	0.64	Similar to acidic ribosomal phosphoprotein P1

The numbers mean relative fold change of treated group versus control and are presented as log base 2.

Table III. 2 folds down-regulated genes in at least one group

Genbank No.	6h		24h		Gene Name
	Low	High	Low	High	
NM_011315	–4.39	–2.95	–2.49	–3.17	*Saa3*, Serum amyloid A 3
NM_174848	–3.98	–2.16	–2.07	–2.31	CDNA sequence BC043118
NM_011318	–2.97	–2.91	–2.12	–1.64	*Apcs*, Serum amyloid P-component
NM_172775	–1.95	–1.53	–2.43	–2.90	*Plxnb1*, Plexin B1
NM_008407	–1.64	–1.44	–1.07	–1.08	*Itih3*, Inter-alpha trypsin inhibitor, heavy chain 3
NM_145406	–1.43	–1.36	–0.84	–0.96	*Slc10a3*, Sodium/bile acid cotransporter family, member 3
NM_028030	–1.33	–1.24	–1.15	–1.07	*Rbpms2*, RNA binding protein with multiple splicing 2
NM_133661	–1.31	–1.33	–0.18	–0.19	*Slc6a12*, Solute carrier family 6, member 12
	–1.28	–0.93	–0.14	–0.26	*Tubb2*, Tubulin, beta 2
	–1.24	–0.96	–1.33	–1.04	*Ifi205*, Interferon activated gene 205
NM_022310	–1.17	–1.17	–0.80	–0.43	*Hspa5*, Heat shock 70kD protein 5 (glucose-regulated protein)
	–1.16	–1.23	–0.19	–0.35	Transcribed locus
NM_020577	–1.16	–0.93	–0.81	–0.66	*As3mt*, Arsenic (+3 oxidation state) methyltransferase
NM_017371	–1.13	–1.13	–0.80	–1.00	*Hpxn*, Hemopexin
NM_010196	–1.13	–0.95	–0.94	–0.78	*Fga*, Fibrinogen, alpha polypeptide
	–1.08	–0.89	–0.48	–0.60	*Tnfrsf7*, Tumor necrosis factor receptors
NM_133191	–1.04	–1.31	–0.27	–0.51	*Eps8l2*, EPS8-like 2
NM_018793	–1.00	–0.85	–0.94	–0.78	*Tyk2*, Tyrosine kinase 2
NM_009150	–0.90	–0.17	–1.33	–1.50	*Selenbp1*, Selenium binding protein 1
	–0.80	–1.15	–0.97	–1.02	*Itih4*, Inter alpha-trypsin inhibitor, hea
NM_007822	–0.76	–1.58	–1.54	–0.65	*Cyp4a14*, Cytochrome P450, family 4, subfamily a, polypeptide 14
NM_008341	–0.66	–0.17	–0.93	–1.00	*Igfbp1*, Insulin-like growth factor binding protein 1
NM_146101	–0.64	–1.01	–0.56	–0.77	*Habp2*, Hyaluronic acid binding protein 2
NM_145942	–0.42	–1.32	0.11	0.81	*Hmgcs1*, 3-hydroxy-3-methylglutaryl-Coenzyme A synthase 1
NM_010011	–0.36	–1.00	–0.39	–0.04	*Cyp4a10*, Cytochrome P450, family 4, subfamily a, polypeptide 10
NM_145434	0.31	–1.03	0.17	0.58	*Nr1d1*, Nuclear receptor subfamily 1, group D, member 1

The numbers mean relative fold change of treated group versus control and are presented as log base 2.

The present study, however, provides predictive information to understand high- versus low dose mechanisms of APAP toxicity. Furthermore protective role of *HSP70* is also envisaged. In summary, present study suggests that mechanistic differences may exist in APAP metabolism between subtoxic and overtly toxic doses in mice. Thus gene expression profiling helps in detecting subtle cellular disturbances at doses and times that could not be detected by classical toxicological methods. Generating gene signatures as biomarkers of hepatotoxicity seems to be the most warranted research in predictive toxicology.

This work was supported by the Ministry of Science and Technology for the 2005 Advanced Project for an International Accreditation of the Preclinical Safety Evaluation System for Korea Institute of Toxicology. Prof. SVS Rana thanks Korea Science and Engineering Foundation for a visiting fellowship.

References

1. Mitchel, J.R., Jollow, D.J., Potter, W.Z., Davis, D.C., Gillette, J.R. and Brodie, B.B. (1973) *J. Pharmacol. Exp. Ther. 187*: 185.
2. Dahlin, D.C., Miwa, G.T., Lu, A.Y. and Nelson, S.D. (1984) *Proc. Natl. Acad. Sci. USA. 81*: 1327.
3. Cohen, S.D., Pumford, N.R., Khairallah, E.A., Boekelheide, K., Pohl, L.R., Amouzadeh, H.R. and Hinson, J.A. (1997) *Toxicol. Appl. Pharmacol. 143*: 1.
4. Qiu, Y., Benet, L.Z. and Burlingame, A.L. (2001) *Adv. Exp. Med. Biol. 500*: 663.
5. Donnelly, P.J., Walker, R.M. and Racz, W.J. (1994) *Arch. Toxicol. 68*: 110.
6. Jaeschke, H. (1990*) J. Pharmacol. Exp. Ther. 255*: 935.
7. Hinson, J.A., Pike, S.L., Pumford, N.R. and Mayeux, P.R. (1998) *Chem. Res. Toxicol. 11*: 604.
8. Gardner, C.R., Heck, D.E., Yang, C.S., Thomas, P.E., Zhang, X.J., DeGeorge, G.L., Laskin, J.D. and Laskin, D.L. (1998) *Hepatology 27*: 748.
9. O'Donnell, V.B., Chumley, P.H., Hogg, N., Bloodsworth, A., Darley-Usmar, V.M. and Freeman, B.A. (1997) *Biochemistry 36*: 15216.
10. James, L.P., Mayeux, P.R. and Hinson, J.A. (2003) *Drug Metab. Dispos. 31*: 1499.
11. James, L.P., McCullough, S.S., Lamps, L.W. and Hinson, J.A. (2003) *Toxicol. Sci. 75*: 458.
12. Lucas, R., Warner, T.D., Vojnovic, I. and Mitchell, J.A. (2005) *FASEB J.19*: 635.
13. Heinloth, A.N., Irwin, R.D., Boorman, G.A., Nettesheim, P., Fannin, R.D., Sieber, S.O., Snell, M.L., Tucker, C.J., Li, L., Travlos, G.S., Vansant, G., Blackshear, P.E., Tennant, R.W., Cunningham, M.L. and Paules, R.S. (2004) *Toxicol. Sci. 80*: 193.
14. Gaut, J.P., Byun, J., Tran, H.D., Lauber, W.M., Carroll, J.A., Hotchkiss, R.S., Belaaouaj, A. and Heinecke, J.W. (2002) *J. Clin. Invest.109*: 1311.
15. Jia, Y., Guo, G.L., Surapureddi, S., Sarkar, J., Qi, C., Guo, D., Xia, J., Kashireddi, P., Yu, S., Cho, Y.W., Rao, M.S., Kemper, B., Ge, K., Gonzalez, F.J. and Reddy, J.K. (2005) *Proc. Natl. Acad. Sci. USA. 102*: 12531.
16. Minami, K., Saito, T., Narahara, M., Tomita, H., Kato, H., Sugiyama, H., Katoh, M., Nakajima, M. and Yokoi, T. (2005) *Toxicol. Sci. 87*: 296.
17. Welch, K.D., Reilly, T.P., Bourdi, M., Hays, T., Pise-Masison, C.A., Radonovich, M.F., Brady, J.N., Dix, D.J. and Pohl, L.R. (2006) *Chem. Res. Toxicol. 19*: 223.
18. Williams, D.P., Garcia-Allan, C., Hanton, G., LeNet, J.L., Provost, J.P., Brain, P., Walsh, R., Johnston, G.I., Smith, D.A. and Park, B.K. (2004) *Chem. Res. Toxicol. 17*: 1551.
19. Aleksunes, L.M., Goedken, M. and Manautou, J.E. (2006) *World J. Gastroenterol. 12*: 1937.

Received November 13, 2006;
accepted January 31, 2007.

Physiol. Chem. Phys. & Med. NMR (2006) *38*: 85–92

Basic Study on Biochemical Mechanism of Thoron and Thermal Therapy

Takahiro Kataoka, Yutaka Aoyama, Akihiro Sakoda, Shinya Nakagawa, and Kiyonori Yamaoka*

Graduate School of Health Sciences, Okayama University, 5-1 Shikata-cho, 2-chome, Okayama 700-8558, Japan
**Author for correspondence. E-mail: yamaoka @ md.okayama-u.ac.jp*

Abstract: Exposure to water in hot springs containing thoron is thought to exercise beneficial effects on hypertension and diabetes mellitus. To put to a test this hypothesis we examined the time dependent changes in the levels of lipid peroxide, vasoactive- and diabetes associated substances in human blood in order to throw further light on the possible beneficial influence of thoron and thermal therapy on the mechanism of hypertension and diabetes mellitus. Every 2 days, nasal inhalation of vapor containing thoron was performed for 40 min. Blood samples were collected after each treatment at 1, 2, and 3 weeks after the first treatment. Results show that the treatment decreased the lipid peroxide levels. The finding suggests that the treatment contributes to the prevention of peroxidation reaction related to hypertension and diabetes mellitus. Moreover, the changes in vasoactive-associated substances indicate an increase in tissue perfusion, suggesting that the treatment plays a role in alleviating hypertension. The treatment decreased the total ketone body levels and the finding suggests that the treatment contributes to the prevention of diabetes mellitus related to the insulin deficiency.

KEY WORDS: thoron and thermal therapy / hypertension / diabetes mellitus / antioxidant function / tissue perfusion

RADON (^{222}Rn) is a radioactive gaseous element that mainly emits α-rays. If radon is inhaled, the lungs will be subjected to the actions of free radicals created by the radiation and may suffer inflammation. Although radon inhalation has been thought to be hazardous in general, radon springs have been reported to have therapeutic effects on senile brain disorder and hypertension (1). Another known effect of a radon spring is to promote the

Abbreviations: ANP -atrial natriuretic polypeptide; IRMA- immunoradiometric assay; 3-OHBA - 3-hydroxy butyric acid; SOD- superoxide dismutase

effects of such tissue perfusion agents as adrenaline in plasma; that is, the level of plasma adrenaline is increased by radon inhalation (2,3). So far, no epidemiologic data exists on the hazardous effects of radon (4).

We have reported that low-dose, unlike high-dose, irradiation enhanced the antioxidation function and reduced oxidative damage (5). Moreover low-dose irradiation enhanced the immune and anti-oxidation functions (6).

The therapy using radon gas, which is volatilized from radon-enriched water, is performed for various diseases, such as osteoarthritis and asthma (7). Several attempts have been made to clarify its mechanism, but there have been only a few studies on radon therapy in humans (8,9).

As the pilot study, the effect of the radioactivity of radon and the thermal effect were compared at room temperature or a hot spring condition with the same chemical component by using as the parameters the activity of superoxide dismutase (SOD), which is an oxidation inhibitor, and the levels of lipid peroxide, which is closely involved with arteriosclerosis. The results were about 2-fold larger in the radon effects than in the thermal effects. This suggests that the antioxidation function was more enhanced by radon therapy than by thermal therapy, and that radon therapy might help to prevent the causes of life style-related diseases such as arteriosclerosis (10).

Considering this background, in this study, we evaluated dynamic changes in human blood components in order to throw light on the alleged beneficial influence of thoron and thermal therapy on the mechanism of hypertension and diabetes mellitus.

Subjects and Methods

Fifteen persons, 40 to 60 years of age were studied; five were patients with hypertension, five were patients with diabetes mellitus and five were healthy persons (no hypertension and no diabetes). In this study, hypertension or diabetes mellitus is defined as systolic blood pressure above 140 mmHg or diastolic blood pressure above 90 mmHg, or that blood glucose level is above 126 mg/dL, respectively. The subjects were in a hot bath room with a high concentration of thoron. The room temperature was 42 °C, and the air concentration in the thoron hot spring bath room was about 4900 Bq/m^3. Subjects did not bathe but only stayed in the above bath room. Nasal inhalation was used because the uptake of thoron is most efficient by this method. Every 2 days, nasal inhalation of vapor from the hot spring in the room was performed for 40 min once a day under a condition of high humidity (90 %). Blood pressures were measured and blood samples were collected after each treatment (before meal) at 1, 2, and 3 weeks after the first treatment. Blood pressure was measured and a blood sample was collected before the first treatment to be used as the control. The written informed consent was obtained from all subjects.

We entrusted the biochemical assays of the blood samples to the special clinical analysis service. Briefly, each biochemical indicator was measured; lipid peroxide level in serum by the hemoglobin methylene blue method, atrial natriuretic polypeptide (ANP) level in EDTA plasma by the immunoradiometric assay (IRMA), blood glucose level by enzymatic method, and total ketone body, free fatty acid, acetoacetic acid, and 3-hydroxy butyric acid (3-OHBA) by enzymatic method.

Data values are presented as the mean ± SEM. The statistical significance of differences was determined by using Student's *t*-test for comparison between two groups or two-way ANOVA and Dunnett tests for multiple comparison.

Results

Time Dependent Changes in Blood Pressures

Before the first treatment, both the maximum blood pressures and the minimum blood pressures in the hypertensive group were significantly higher than those in the non-hypertensive group. The maximum blood pressures in the non-hypertensive group (on weeks 2 and 3 after the first treatment) and those in the hypertensive group (on week 3) were significantly decreased compared with the control (before the first treatment). On weeks 1 and 3, the minimum blood pressures in the non-hypertensive group were significantly decreased compared with the control. No significant changes were observed in the other experimental conditions (Figure 1).

Time Dependent Changes in Blood Glucose Level

Before the first treatment, the blood glucose level in the diabetes group was significantly higher than that in the non-diabetic group. The blood glucose level in the non-diabetic group (on week 3) was significantly decreased compared with the control. No significant changes were observed in the other experimental conditions (Figure 2).

Time Dependent Change in Lipid Peroxide Level

Before the first treatment, the lipid peroxide level in the hypertensive group or the non-diabetic group were not significantly different from that in the non-hypertensive and non-diabetic group. The lipid peroxide levels in the non-hypertensive and non-diabetic group or the diabetic group (on weeks 2 and 3) and that in the hypertensive group (on week 2) were significantly decreased compared with the control respectively. No significant changes were observed in the other experimental condition (Figure 3).

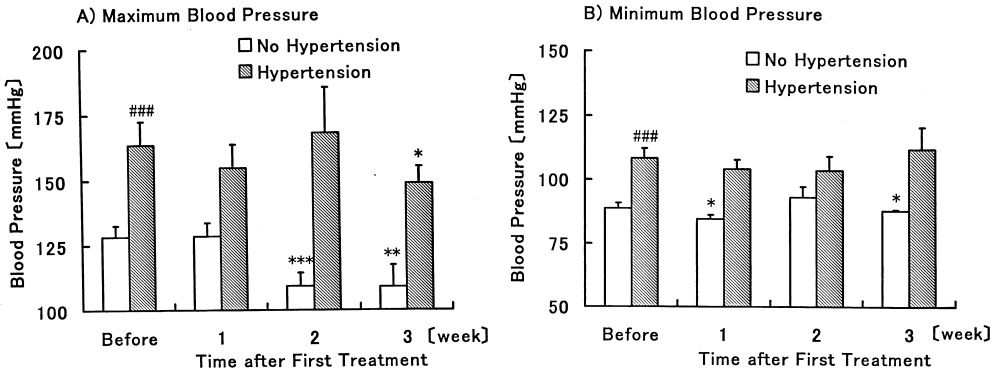

FIGURE 1. Time dependent changes in maximum blood pressures (A) and minimum blood pressures (B) of patients with hypertension and without hypertension after first thoron and thermal treatment. Each value represents the Mean ± SEM. The number of subjects in each experiment is five. *P<0.05, **P<0.01, ***P<0.001, hypertensive group or non-hypertensive group value *vs*. each control (before treatment) value. $^{\#}$P<0.05, $^{\#\#\#}$P<0.001, hypertensive group value *vs*. non-hypertensive group value.

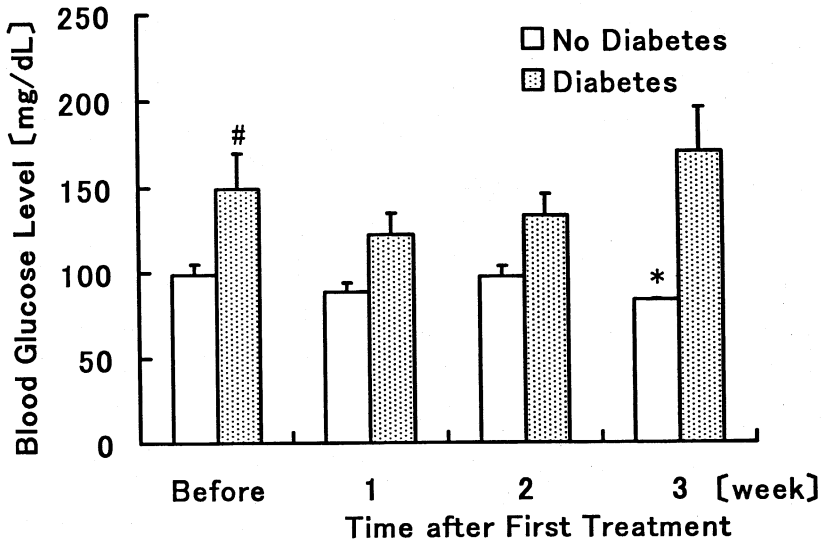

FIGURE 2. Time dependent changes in blood glucose level in blood of patients with diabetes and without diabetes after first thoron and thermal treatment. The number of subjects in each experiment is five. $^{\#}P<0.05$, diabetic group value *vs*. non-diabetic group, *P<0.05, **P<0.01, diabetic group value *vs*. control value.

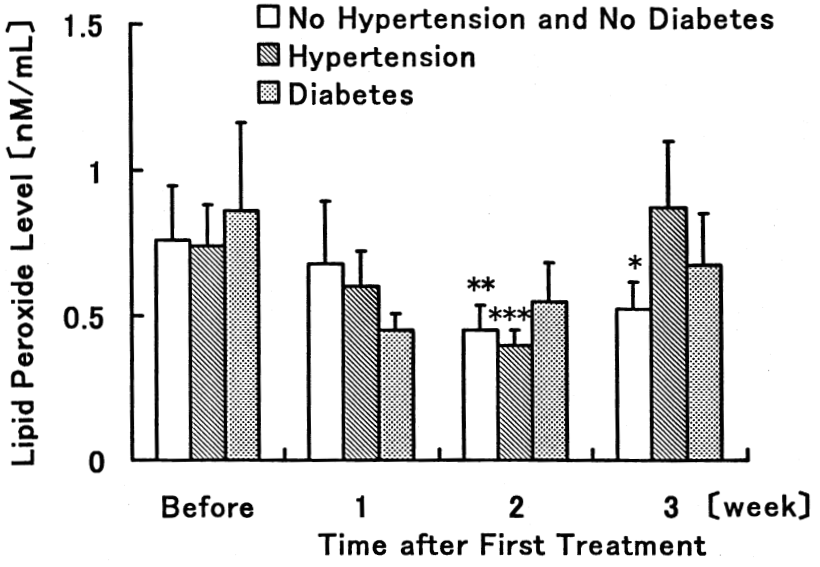

FIGURE 3. Time dependent changes in lipid peroxide levels in blood of patients with hypertension or diabetes, and without hypertension or diabetes after first thoron and thermal treatment. The number of subjects in each experiment is five. *P<0.05, **P<0.01, ***P<0.001, non-hypertensive and non-diabetic group value *vs*. each control value.

Time Dependent Change in Vasoactive-associated Substance Level

Before the first treatment, the a-ANP level in the hypertensive group was significantly higher than that in the non-hypertensive group. The α-ANP levels in the non-hypertensive group (on weeks 1 and 2) and that in the hypertensive group (on week 3) were significantly increased compared with each control, respectively. No significant changes were observed in the other experimental conditions (Figure 4).

Time Dependent Changes in Diabetes-associated Substances Levels

The acetoacetic acid in the non-diabetic group (on week 2) and those in the diabetic group (on week 2) were significantly decreased compared with the control. The 3-OHBA and total ketone body in the diabetic group (on weeks 2 and 3) were significantly decreased compared with the control. Moreover, the free fatty acid in the group with diabetes mellitus (on week 2) was significantly decreased compared with the control. No significant changes were observed in the other experimental conditions (Figure 5).

Discussion

Radon is an inert gas and as such does not react with any chemical component of the body. On entry through lungs or through the skin, it reaches the blood stream and is then distributed throughout the body. Because it is rather lipid soluble, radon tends to accumulate in organs rich in fat, such as the endosecretory glands, and also nerve fibers, which

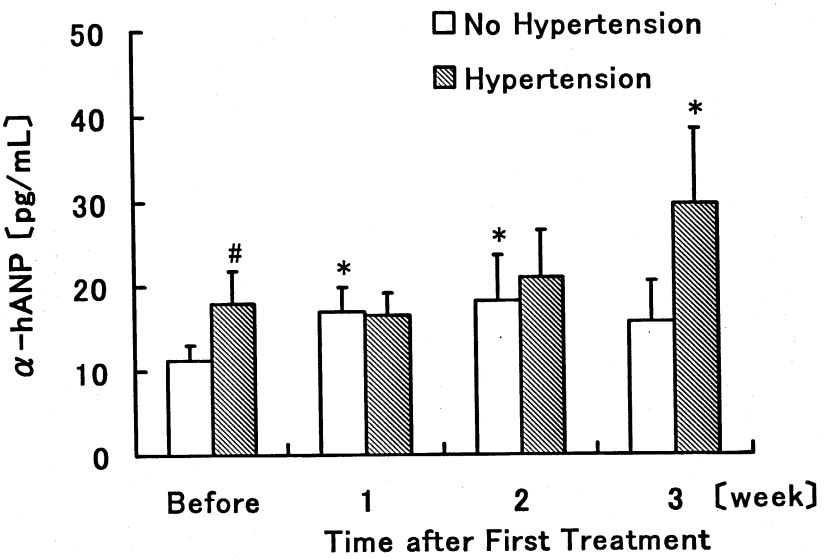

FIGURE 4. Time dependent changes in vasoactive-associated substances level in blood of patients with hypertension and without hypertension after first thoron and thermal treatment. The number of subjects in each experiment, and significance are as described in Figure 1.

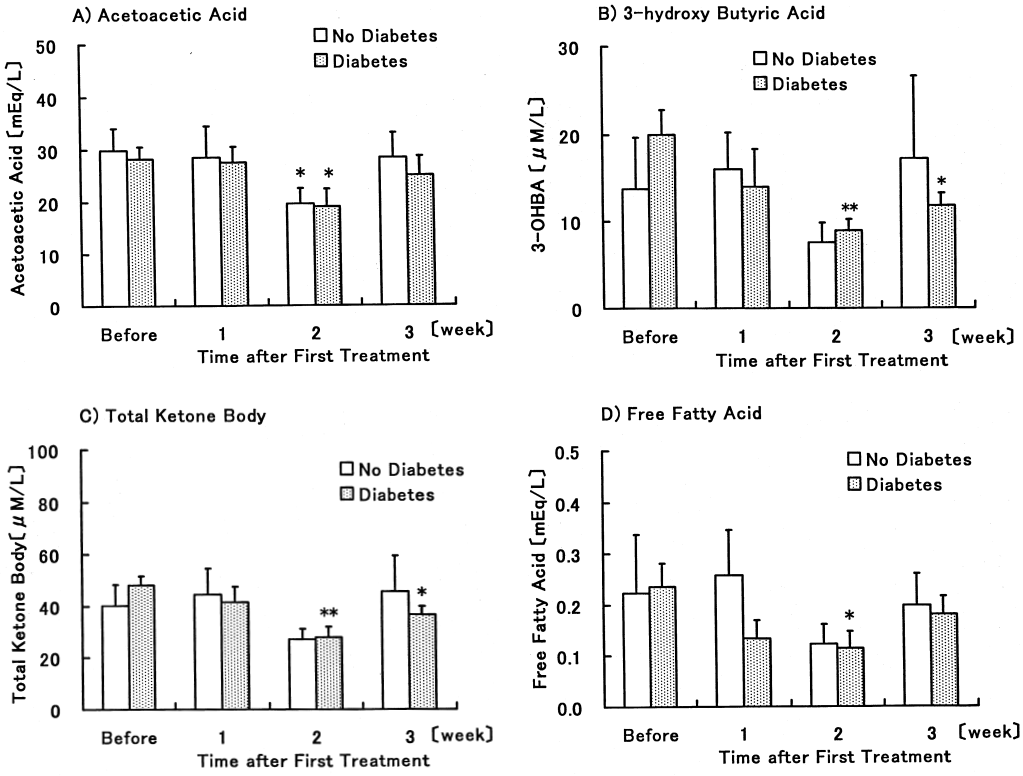

FIGURE 5. Time dependent changes in diabetes-associated substances levels in blood of patients with diabetes and without diabetes after first thoron and thermal treatment. The number of subjects in each experiment, and significance are as described in Figure 2.

are surrounded and protected by a lipid-containing layer. Retention time in the body is short; 50 % disappears after only 15 to 30 min. It is during this short period, however, while radon is in contact with the tissue, that it launches the stimulus effects. Radon is a source of α-rays, and it can only travel a distance of about 20 μm through body tissues. The relatively large transfer of energy that is associated with the absorption of α-particles causes a series of complicated reactions within the tissues. As yet the molecular processes involved are still poorly understood. It is safe, however, to assume that radiolytic radicals are released, and these in turn stimulate detoxification processes and also might stimulate such processes as cell metabolism and energy conversion within mitochondria as well as biosynthesis of enzymes and other proteins or bioactive peptides (7).

It has been known that the activity of SOD, which is a scavenger of superoxide radicals, is increased in cultured cells (11) and in various organs of rats (12) and rabbits (13) by exposure to radon. We also showed that the lipid peroxide level was reduced in rabbits by radon inhalation (13). While the induction by a low dose of α-ray irradiation with inhalation of enzymes such as SOD and catalase, which inhibit lipid peroxidation in the body, i.e., an activation of the protective mechanisms of the body, may also be related to this decrease in total cholesterol level (10). Moreover we have reported that the results on

week 1 were about 2-fold larger in the radon group than in the thermo group (10). This suggests that the anti-oxidation function was more enhanced by the radon effect than by the thermo effect, and suggests that radon inhalation may prevent the causes of life style-related diseases such as hypertension and diabetes mellitus.

In this study, the lipid peroxide levels in the blood of the patients with hypertension or diabetes mellitus were found to be decreased by low dose α-rays irradiation with thoron inhalation. The decrease in the lipid peroxide level may be linked to the thoron and thermal effects on membrane structure. This possibility, however, was not evaluated in this study.

Moreover the thoron and thermal treatment increases the level of α-ANP, which decreases blood pressure by relaxation of the vascular smooth muscle, in the blood of hypertension patients. This finding indicates what may be a part of the mechanism for the increase in tissue perfusion, namely, the decrease in blood pressure brought about by the treatment.

Total ketone body consists of acetoacetic acid, 3-OHBA, and acetone. When insulin decreases, the ketone body is induced to maintain blood glucose level. Diabetic ketoacidosis is developed by insulin deficiency or impaired insulin action. The insulin deficiency induces high blood glucose level with inhibition of the glucose absorption into cells. Fatty acid is degraded to gain another energy. Therefore diabetic ketoacidosis develops by insulin deficiency and the ketone body, especially 3-OHBA, is accumulated in the blood. In this study, the acetoacetic acid, the 3-OHBA, and total ketone body decreased at about 2 or 3 weeks after first treatment. These findings suggest that thoron inhalation prevents diabetic ketoacidosis.

On the other hand, the half-life of thoron (^{220}Rn, 55.6 sec), which is the isotope of radon, is shorter than that of radon (3.82 days), and the α particle energy of thoron (6.29 MeV) is larger than that of radon (5.49 MeV). Moreover, α particles emitted by ^{222}Rn progeny and ^{220}Rn progeny are mainly responsible for the biological effects on the respiratory organs, because most radon, an inert gas, is exhaled after it is inhaled. Therefore, the potential α energy concentrations of them were evaluated. For example, the potential α energy concentrations of the progeny were summed up for the case where the atmospheric ^{222}Rn concentration in a hot bathroom with a high concentration of radon (at Misasa Medical Center of Okayama University Medical School) was equal to that of ^{220}Rn concentrations in a bathroom of an artificial thoron hot spring. We assumed that the atmospheric concentration of ^{222}Rn progeny were equal to that of ^{220}Rn progeny, this because of the great difficulty in measuring them. Consequently, the total potential α energy concentrations of ^{220}Rn progeny were about 17 times as high as those of ^{222}Rn progeny. It is likely that ^{220}Rn therapy has more biological effects on a bronchus and lung than ^{222}Rn therapy when atmospheric ^{220}Rn and their progeny concentrations in the bathroom are equal to that of ^{222}Rn and their progeny.

These findings suggest that an appropriate amount of active oxygen is produced in the body after the treatment, and this contributes to the alleviation of the symptoms of active oxygen diseases, such as hypertension and diabetes mellitus *via* certain processes such as activation of the biological defense mechanism, or promoting these physiological changes such as tissue perfusion (2,3), in contrast to the toxic effects of thoron inhalation at higher concentrations.

In the future, clarification in detail of the mechanisms of these phenomena will be helpful toward understanding the effects of thoron and thermal treatment on the functions of

the living body. Moreover, in order to enhance the beneficial effects of thoron inhalation, the optimal doses of thoron should be determined together with the development of precise microdosimetry. Further, we will conduct studies on the biochemical comparison between the radon effects and the thoron effects when the radioactive concentration of thoron is equal to that of radon.

The authors are indebted to Dr. Chunosuke Sugie (Sugie Clinic, Japan) and Dr. Shoji Futatsugawa (Japan Radioisotope Association) for their excellent technical advice.

Reference

1. Ooshima, Y. (1996) *System of Current Internal Medicine II*. Nakayama Shoten, Tokyo, pp 124–144.
2. Komoto, Y., Kohmoto, T., Nakao, T., Sunakawa, M., Yorozu, H. (1988) Tissue perfusion with perfusion with CO_2. *Z. Phys. Med. Baln. Med. Klim. 17:* 72–78.
3. Suzuka, I., Yamaoka, K., Komoto, Y. (1991) Adrenal secretion of catecholamines by inhalation of radon water in relation to an increase of the tissue perfusion rate in rabbit. *J. Jpn. Coll. Angiol. 31:* 1182
4. Mifuna, M., Sobue, T., Arimoto, H., Komoto, Y., Kondo, S., Tanaoka, H. (1992) Cancer mortality survey in a spa area (Misasa, Japan) with a high radon background. *Jpn. J. Cancer. Res. 83:* 1–5.
5. Kataoka, T., Nomura, T., Da-Hong Wang, Taguchi, T., Yamaoka, K. (2005) Effects of post low-dose X-ray irradiation on carbon tetrachloride-induced acatalasemic mice liver damage. *Physiol. Chem. Phys. Med. NMR 37:* 109–126.
6. Kataoka, T., Mizuguchi, Y., Notohara, K., Taguchi, T., Yamaoka, K. (2006) Histological changes in spleens of radio-sensitive and radio-resistant mice exposed to low-dose X-ray irradiation. *Physiol. Chem. Phys. Med. NMR 38:* 21–29.
7. Deetjen, P. (1997) Epidemiology and biological effects of radon. In *Radon in der Kur Medizin,* Pratzel H.G., Deetjen P. eds., Verlag Geretsried. pp 32–38.
8. Yamaoka, K., Mitsunobu, F., Hanamoto, K., Mori, S., Tanizaki, Y., Sugita, K. (2004) Study on biologic effects of radon and thermal therapy on osteoarthritis. *J. Pain. 5:* 20–25.
9. Mitsunobu, F., Yamaoka, K., Hanamoto, K., Kojima, S., Hosaki, Y., Ashida, K., Sugita, K., Tanizaki, Y. (2003) Elevation of antioxidant enzymes in the clinical effects of radon and thermal therapy for bronchial asthma. *J. Radiat. Res. 44:* 95–99.
10. Yamaoka, K., Mitsunobu, F., Hanamoto, K., Shibuya, K., Mori, S., Tanizaki, Y., Sugita, K. (2004) Biochemical comparision between radon effects and thermal effects on humans in radon hot spring therapy. *J. Radiat. Res. 45:* 83–88.
11. Frick, H., Pfaller, W. (1988) Die auswirkung niedriger astrahlendosis auf epitheliale zellkulturen. *Z. Phys. Med. Baln. Med. Klim. 17:* 23–30.
12 Ma, J., Yonehara, H., Ikebuchi, M., Aoyama, T. (1996) Effect of radon exposure on superoxide dismutase (SOD) activity in rat. *J. Radiat. Res. 37:* 12–19.
13. Yamaoka, K., Komoto, Y., Suzuka, I., Edamatsu, R., Mori, A. (1993) Effects of radon inhalation on biological function-Lipid peroxide level, superoxide dismutase activity and membrane fluidity. *Arch. Biochem. Biophys. 302:* 37–41.

Received March 16, 2007;
accepted May 24, 2007.

Physiol. Chem. Phys. & Med. NMR (2006) *38*: 93–104

Tissue Magnesium Loss during Prolonged Hypokinesia in Magnesium Supplemented and Unsupplemented Rats

Yan G. Zorbas[1], Kostas K. Kakuris[2]*, Viktor A. Denogradov[1] and Kosmas B. Yerullis[2]

[1]*Higher Institute of Biochemistry, Gomel, Belarus;*
[2]*European Foundation of Environmental Sciences, Athens, Greece*
*Corresponding Author: Dr. Kostas K. Kakuris, European Foundation of Environmental Sciences
Odos Kerasundos 2, GR-162 32 Athens, Greece
Email:kkakuris@in.gr

Abstract: This study aims at showing that during hypokinesia (HK) tissue magnesium (Mg^{2+}) content decreases more with higher Mg^{2+} intake than with lower Mg^{2+} intake and that Mg^{2+} loss increases more with higher than lower tissue Mg^{2+} depletion due to inability of the body to use Mg^{2+} during HK.

Studies were conducted on male Wistar rats during a pre-HK period and a HK period. Rats were equally divided into four groups: unsupplemented vivarium control rats (UVCR), unsupplemented hypokinetic rats (UHKR), supplemented vivarium control rats (SVCR) and supplemented hypokinetic rats (SHKR). SVCR and SHKR consumed 42 mEq Mg^{2+} per day.

The gastrocnemius muscle and right femur bone Mg^{2+} content decreased significantly, while plasma Mg^{2+} level and urine and fecal Mg^{2+} loss increased significantly in SHKR and UHKR compared with their pre-HK values and their respective vivarium controls (SVCR and UVCR). However, muscle and bone Mg^{2+} content decreased more significantly and plasma Mg^{2+} level, and urine and fecal Mg^{2+} loss increased more significantly in SHKR than in UHKR.

The greater tissue Mg^{2+} loss with higher Mg^{2+} intake and the lower tissue Mg^{2+} loss with lower Mg^{2+} intake shows that the risk of higher tissue Mg^{2+} depletion is directly related to the magnitude of Mg^{2+}intake. The higher Mg^{2+} loss with higher tissue Mg^{2+} depletion and the lower Mg^{2+}loss with lower Mg^{2+} tissue depletion shows that the risk of greater Mg^{2+} loss is directly related to the magnitude of tissue Mg^{2+} depletion. It was concluded that tissue Mg^{2+} depletion increases more when

Abbreviations: HK, hypokinesia; UHKR, unsupplemented hypokinetic rats; UVCR, unsupplemented vivavium control rats; SHKR, supplemented hypokinetic rats; SVCR, supplemented vivarium control rats.

the Mg^{2+} intake is higher and that Mg^{2+} loss increases more with higher than lower tissue Mg^{2+} depletion indicating that during prolonged HK the tissue Mg^{2+} depletion is not due to the Mg^{2+} shortage in food but to the inability of the body to use Mg^{2+}.

KEY WORDS: magnesium deposition, tissue magnesium depletion, cell injury, energy depletion, enzyme deficiencies, ion transport alterations, physical inactivity.

HYPOKINESIA (diminished movement) is associated with a reduction in flow of afferent and thus, efferent impulsation, and the body is deprived of its constant regulatory influence (1–4). A change from increased to decreased muscular activity contributes to the formation of hypokinetic stress (1, 2), and the greater the magnitude of the differences between these two conditions, the stronger the effect of stress is on the body during prolonged hypokinesia (HK) (1, 2).

The coefficient of distribution of electrolytes in muscle and blood, and between muscle and blood is the integral characteristic of the functional condition of the skeletal muscles. Being involved in finely regulated processes of active membrane transport and intracellular phases, electrolytes are distributed in muscles according to the functional condition of the system of membranomyo-fibril conjugation (5), metabolic activity of cell (6), and chemical composition of cytoplasmic template that carries fixed charges (7). Any condition which affects the muscular activity, would inevitably lead to the redistribution of electrolytes in the body resulting in tissue electrolyte changes (8–15). Although muscle electrolyte redistribution has not been established, it has been shown that during HK the skeletal muscle electrolyte content is easily affected (8–15). There is little information available on the effect of HK on muscle electrolyte content and no additional information was retrieved from the different medical data bases other than the unrelated information from non-hypokinetic studies, i.e., bed rest, weightlessness, immersion, detraining, etc. Thus, determination of the skeletal muscle electrolyte content during prolonged HK deserves further studies.

During HK, tissue electrolyte content decreases either with higher or lower electrolyte intake (8–15). The decreased tissue electrolyte content is accompanied by a higher plasma electrolyte level and a greater bodily electrolyte loss from the animal. Other studies suggest that the underlying mechanism for this triple response—tissue electrolyte depletion, increased plasma electrolyte level and electrolyte loss from animal—might not be the same as a similar triple response produced by normal muscular activity, since other factors have been shown to contribute to the higher plasma electrolyte level and bodily loss of electrolyte with tissue electrolyte depletion (8–15). On the other hand, higher plasma electrolyte level and bodily electrolyte loss with tissue electrolyte depletion might be linked to muscle cell membrane changes (16).

Until now there has been little information on magnesium (Mg^{2+}) deposition in tissues. Thus, we do not know how total bodily loss of Mg^{2+} is related to tissue Mg^{2+} depletion or whether tissue Mg^{2+} depletion comes from Mg^{2+} shortage in the food consumed or from an inability of the body to accumulate this electrolyte (10–13). Now, each electrolyte has a well-defined and separate homeostatic mechanism to regulate that electrolyte's content in a tissue at both the cell membrane level and higher organ level (e.g., bone, renal, gastrointestinal and hormonal). For this reason, it is important to study the effect of prolonged HK on tissue Mg^{2+} content in order to determine the potential of lower Mg^{2+} deposition and higher Mg^{2+} loss with tissue Mg^{2+} depletion.

To this end the objective of this study was to show that tissue Mg^{2+} content decreases more with higher than with lower Mg^{2+} intake and that Mg^{2+} loss increases more with higher than lower tissue Mg^{2+} depletion due to the inability of the body to use Mg^{2+} and not due to the Mg^{2+} shortage in food. Measurements of bone and muscle Mg^{2+} content, plasma Mg^{2+} levels and Mg^{2+} loss in urine and feces of rats with higher and lower Mg^{2+} intake during HK were made.

Methods and Materials

Two hundred forty 13-week-old male Wistar rats were obtained from a local breeding animal laboratory. On arrival they were given an adjusting dietary period of 9-days during which they were fed a commercial laboratory diet. During this pre-HK period of 9-days rats were kept under vivarium control conditions. At the start of the investigation, all rats were about 90-days old and weighed 370 to 390 g. Rats were housed in individual metabolic cages where light (07:00 to 19:00 h), temperature (25 ± 1 °C) and relative humidity (65%) were automatically controlled. Cages were cleaned daily in the morning before feeding. The studies were approved by the Committee for the Protection of Animals.

Assignment of animals into four groups was conducted randomly and their conditions were:

Group one: sixty unrestrained rats were housed in individual cages for 98-days under vivarium control conditions. They served as unsupplemented vivarium control rats (UVCR).

Group two: sixty restrained rats were kept in small individual cages for 98-days. They served as unsupplemented hypokinetic rats (UHKR).

Group three: sixty unrestrained rats were housed in individual cages for 98-days under vivarium control conditions. They were supplemented with 42 mEq of magnesium acetate per day and they served as supplemented vivarium control rats (SVCR).

Group four: sixty restrained rats were kept in small individual cages for 98-days. They were supplemented with 42 mEq of magnesium acetate per day and they served as supplemented hypokinetic rats (SHKR).

Protocol

Studies during HK were preceded by a pre-HK period of 9-days which involved a series of biochemical testing and conditioning of animals to their new laboratory conditions. This preparation period was carried out for collecting pre-HK values with regard to bone and muscle Mg^{2+} content, plasma, urine and fecal Mg^{2+} values. This period of adaptation was aimed at minimizing hypokinetic stress induced by diminished muscular activity (1, 2).

Simulation of Hypokinesia

Hypokinetic rats were kept for 98-days in small individual wooden cages. The dimensions of the cages were 195 x 80 x 65 mm and allowed movements to be restricted in all directions without hindering food and water intakes. The hypokinetic rats could still assume a natural position that allowed them to groom different parts of their body. When

necessary, the conditions of individual cages could be changed using special wood inserts. The cages were constructed so that their size could be changed in accordance with the size of each animal, thus the degree of restriction of muscular activity throughout the study could be maintained at a relatively constant degree.

Food and fluid consumption

Food intake was measured and 90% of a daily intake (12 g) was mixed with deionized distilled water (1:2 wt/vol) to form a slurry which was divided into two meals. Rats were pair-fed and daily food intakes were measured during pre-HK and HK. Control rats were allowed to eat approximately the same amounts of food as hypokinetic rats. The daily dietary intake of food was placed in individual feeders formed by the little trough and wood partitions. Food for the entire study was from the same production lots that contained all essential nutrients, i.e., 19% protein, 4% fat, 38% carbohydrates, 16% cellulose, vitamins, A, D, E, 0.6% phosphorus, 0.6% sodium chloride, 0.7% calcium, 0.65% magnesium and 0.9% potassium per one g diet and kept in a cold chamber (4 °C). Food intake was measured daily by weighing (Mettler PL 200 top load balance) the slurry food containers. Rats received deionized-distilled water *ad libitum*. Water dispensers (120 to 150 mL) were secured onto a wooden plate installed on front cage panels and filled daily.

Plasma, feces and urine sample collection

Plasma samples were collected every 6-days, while urine and feces were collected from each rat every day and pooled to form 6-day composites. Six-day (consecutive day) pooled samples were collected during pre-HK and HK periods. Blood samples were 2.0 mL and were obtained *via* a cardiac puncture from ether-anesthetized animals with syringes containing heparin. To obtain plasma, blood samples were transferred to polypropylene tubes, and centrifuged immediately in a refrigerated centrifuge. Aliquots for plasma Mg^{2+} analysis were stored at −20 °C. A stainless steel urine-feces separating funnel (Hoeltge, model HB/SS Hoeltge Inc., Cincinnati, OH, USA) was placed beneath each animal to collect 24 h urine samples uncontaminated by stools. To ensure 24 hr urine collections creatinine excretion was measured by colorimetric method. Urine was collected in a beaker with layers of mineral oil to prevent evaporation. Beakers were replaced daily. Urine for each 24 h period was collected in acidified acid-wash containers and was stored at −4 °C until Mg^{2+} analysis. Fecal samples were collected in plastic bags, dried-ashed in a muffle furnace at 600°C overnight. Ashed samples were dissolved in 5% nitric acid. To ensure complete recovery of feces polyethylene glycol was used as a marker.

Tissue preparations, electrolyte extraction and analysis

Samples were collected during pre-HK and HK and mean ± SD of muscle water-electrolyte levels are presented. Six rats from each group were exsanguinated under ether anesthesia by cardiac puncture. Six hypokinetic and six control rats from each group were decapitated on the 1st, 7th and 9th day of pre-HK period, and on the 3rd, 7th, 15th, 30th, 50th, 70th and 98th of the HK period. Muscle (gastrocnemius) and bone (right femur) data are represented as the average of six rats. We have studied the right femur because during HK it is affected more than left femur (17–19).The femur bones were cleaned of

soft tissues, dried to a constant weight, weighed, reduced to ash in a muffle furnace at 600 degrees for 144 minute, then the ash was weighed and dissolved in 0.05 N HCl and, as a chloride solution, analyzed for Mg^{2+}. Gastrocnemius muscles were excised immediately after decapitating the rats. Muscles were thoroughly cleaned of connective tissues, fatty inclusions and large vessels, weighed on Teflon liners and placed in a drying chamber at 110 °C. After drying to a constant weight muscle was transferred to quartz tubes for mineralization by means of concentrated HNO_3, distilled off in a quartz apparatus. After ashing, the residue was dissolved in 0.05 M HCl and, as chloride solution, analyzed for Mg^{2+}.

Tissue magnesium measurements

Samples were analyzed in duplicate and appropriate standards were used for measurements. Mg^{2+} in gastrocnemius muscle and femur bone, and Mg^{2+} levels in plasma, feces and urine were measured. Urine and fecal samples were diluted as necessary and aspirated directly into an atomic absorption spectrophotometer (Perkin-Elmer 3030 model, Perkin-Elmer Corp., Norwalk, CT).

Data analyses

The results were analyzed with a 2 (hypokinetic *vs*. active controls) X 2 (supplemented *vs* unsupplemented) X 2 (pre-intervention *vs*. post-intervention) ANOVA with repeated measures on the last factor. The ANOVA test followed by Tukey's test was used to establish which means were significantly different from each other. The predetermined level of significance was set at alpha <0.05. The results obtained were reported as mean ± SD (Standard Deviation).

Results

Pre-hypokinetic tissue magnesium changes with and without magnesium supplementation

Muscle and bone Mg^{2+} content, plasma Mg^{2+} level, and urine and fecal Mg^{2+} loss (Table I) showed no difference between hypokinetic and control groups of rats. The Mg^{2+}supplementation did not affect muscle and bone Mg^{2+} content, plasma Mg^{2+} level, and urine and fecal Mg^{2+} loss in supplemented hypokinetic and control groups of rats (Table I).

Hypokinetic tissue magnesium changes with and without magnesium supplementation

Muscle and bone Mg^{2+} content, plasma Mg^{2+} level, and urine and fecal Mg^{2+} loss did not change in UVCR and SVCR compared with their pre-HK values (Table I). Muscle and bone Mg^{2+} content decreased significantly ($p<0.05$), while plasma Mg^{2+} level, and urine and fecal Mg^{2+} loss increased significantly ($p<0.05$) in SHKR and UHKR compared with their pre-HK values and values in their respective vivarium controls (SVCR and UVCR) (Table I). However, muscle and bone Mg^{2+} content decreased more significantly ($p<0.05$), while plasma Mg^{2+} level, and urine and fecal Mg^{2+} loss increased more significantly ($p<0.05$) in SHKR than in UHKR (Table I).

TABLE I. Plasma Magnesium, Urine and Fecal Magnesium, and Gastrocnemius Muscle and Right Femur Bone Magnesium Levels Measured in Rats at Pre-hypokinesia and During Vivarium Control and Hypokinesia both With and Without Magnesium Supplementation.

Days	Plasma (mEq/L)	Urine (mEq/days)	Feces (mEq/days)	Gastrocnemius muscle (mEq/kg wet tissue)	Right Femur Bone (mg/100 g ash)
			Unsupplemented Vivarium Control Rats (UVCR), n=60		
Pre-HK	2.4 ± 0.3	0.40 ± 0.03	14.11 ± 2.4	21.2 ± 1.4	751.0 ± 40.3
3rd	2.3 ± 0.4	0.38 ± 0.04	13.83 ± 2.3	21.3 ± 1.3	752.3 ± 45.2
7th	2.2 ± 0.2	0.40 ± 0.03	14.07 ± 2.0	21.2 ± 1.4	751.2 ± 27.0
15th	2.4 ± 0.5	0.39 ± 0.02	13.71 ± 2.2	21.5 ± 1.3	753.5 ± 42.2
30th	2.3 ± 0.4	0.40 ± 0.03	14.01 ± 2.3	21.4 ± 1.5	752.3 ± 36.0
50th	2.2 ± 0.2	0.38 ± 0.04	13.80 ± 2.0	21.6 ± 1.4	754.7 ± 33.3
70th	2.3 ± 0.3	0.39 ± 0.03	14.02 ± 2.3	21.5 ± 1.4	753.5 ± 40.4
98th	2.2 ± 0.5	0.40 ± 0.04	13.54 ± 2.4	21.7 ± 1.3	755.7 ± 31.4
			Unsupplemented Hypokinetic Rats (UHKR), n=60		
Pre-HK	2.4 ± 0.2	0.40 ± 0.03	14.07 ± 2.5	21.7 ± 1.5	751.3 ± 40.2
3rd	2.7 ± 0.3*	0.53 ± 0.06*	19.06 ± 2.7*	19.4 ± 1.2*	660.7 ± 36.3*
7th	2.6 ± 0.4*	0.51 ± 0.05*	18.45 ± 3.0*	19.6 ± 1.4*	675.6 ± 42.0*
15th	2.7 ± 0.3*	0.55 ± 0.07*	21.03 ± 2.8*	18.7 ± 1.2*	641.8 ± 35.6*
30th	2.6 ± 0.4*	0.53 ± 0.05*	19.87 ± 3.4*	18.9 ± 1.3*	651.1 ± 42.2*
50th	2.8 ± 0.2*	0.57 ± 0.07*	22.00 ± 2.7*	18.0 ± 1.2*	638.0 ± 30.7*
70th	2.7 ± 0.3*	0.55 ± 0.04*	21.67 ± 3.3*	18.3 ± 1.3*	647.4 ± 44.0*
98th	2.8 ± 0.3*	0.60 ± 0.05*	23.85 ± 2.8*	17.8 ± 1.4*	628.3 ± 38.5*
			Supplemented Vivarium Control Rats (SVCR), n=60		
Pre-HK	2.5 ± 0.4	0.44 ± 0.03	16.13 ± 2.3	22.0 ± 1.5	772.1 ± 43.2
3rd	2.6 ± 0.5	0.49 ± 0.01	18.35 ± 3.0	22.2 ± 1.4	774.0 ± 50.6
7th	2.5 ± 0.4	0.47 ± 0.03	17.80 ± 2.0	22.1 ± 1.6	773.7 ± 38.7
15th	2.6 ± 0.5	0.50 ± 0.03	18.32 ± 2.5	22.3 ± 1.4	775.5 ± 45.4
30th	2.5 ± 0.5	0.48 ± 0.02	17.76 ± 2.4	22.2 ± 1.6	774.4 ± 51.3
50th	2.5 ± 0.4	0.50 ± 0.01	18.45 ± 2.2	22.5 ± 1.5	776.8 ± 36.5
70th	2.6 ± 0.6	0.47 ± 0.03	17.80 ± 3.0	22.3 ± 1.4	775.6 ± 41.4
98th	2.5 ± 0.5	0.49 ± 0.02	18.41 ± 2.3	22.6 ± 1.5	777.8 ± 32.3
			Supplemented Hypokinetic Rats (SHKR), n=60		
Pre-HK	2.5 ± 0.5	0.44 ± 0.01	16.33 ± 2.5	22.5 ± 2.0*+	773.0 ± 40.5*+
3rd	2.9 ± 0.6*+	0.73 ± 0.04*+	28.22 ± 2.7*+	18.0 ± 1.5*+	607.2 ± 55.6*+
7th	2.8 ± 0.4*+	0.67 ± 0.02*+	24.70 ± 2.9*+	18.2 ± 1.4*+	615.8 ± 43.7*+
15th	3.0 ± 0.5*+	0.83 ± 0.03*+	33.02 ± 3.0*+	17.4 ± 1.3*+	591.2 ± 54.5*+
30th	2.9 ± 0.7*+	0.75 ± 0.04*+	27.84 ± 2.8*+	17.6 ± 1.2*+	603.5 ± 40.7*+
50th	3.1 ± 0.5*+	0.87 ± 0.05*+	36.53 ± 3.1*+	16.6 ± 1.4*+	587.1 ± 51.4*+
70th	3.0 ± 0.6*+	0.79 ± 0.04*+	32.97 ± 2.7*+	16.9 ± 1.2*+	594.6 ± 46.6*+
98th	3.2 ± 0.5*+	0.98 ± 0.03*+	40.21 ± 3.3*+	16.4 ± 1.5*+	578.3 ± 47.5*+

*$p<0.05$ significant differences between vivarium control and hypokinetic groups of rats. Each of the hypokinetic groups was compared with their respective vivarium controls (UVCR *vs* UHKR and SVCR *vs* SHKR).
+$p< 0.05$ significant difference between supplemented and unsupplemented hypokinetic groups.

Discussion

Pre-hypokinetic tissue magnesium changes with and without magnesium supplementation

During pre-HK, control and hypokinetic rats did not show any changes in muscle and bone Mg^{2+} content, plasma Mg^{2+} level and Mg^{2+} loss in urine and feces. This is because most Mg^{2+} was taken up for deposition and was used to great extent by tissues (10–13). The stability of bone and muscle Mg^{2+} content, plasma Mg^{2+} level and Mg^{2+} loss in urine and feces show that Mg^{2+} is readily bound to bone and muscle (10–13). This was more clearly expressed in supplemented than in unsupplemented rats because with the higher Mg^{2+} intake, tissue Mg^{2+} content, plasma Mg^{2+} level and Mg^{2+} loss did not show any changes. During pre-HK, Mg^{2+} content in bone and muscle with differences in their weight-bearing supporting function and morphology did not show any changes with or without Mg^{2+} supplementation because the consumed Mg^{2+} was taken up for deposition and was used to great extent by the body which protected tissue from any changes.

Hypokinetic tissue magnesium changes with and without magnesium supplementation

Tissue Mg^{2+} depletion during normal muscular activity is usually accompanied by a lower Mg^{2+} loss, while tissue Mg^{2+} depletion during HK was always accompanied by a higher Mg^{2+} loss. The greater Mg^{2+} loss with tissue Mg^{2+} depletion shows reduced Mg^{2+} deposition because electrolyte loss cannot occur with tissue electrolyte depletion unless electrolyte deposition decreases (8–15). Decreased Mg^{2+} deposition is related to several factors: the reduced fluid volume, impaired energy production, enzyme deficiencies, sodium pump and membrane cell changes, etc. Higher bodily Mg^{2+} loss with tissue Mg^{2+} depletion during HK indicates a different kind of mechanism than those involved in the lowered Mg^{2+} loss with tissue Mg^{2+} depletion during normal muscular activity. During the initial days of HK, bodily Mg^{2+} loss (with tissue Mg^{2+} depletion) could have been due to hypokinetic stress (1, 2). In subsequent days, bodily Mg^{2+} loss with tissue Mg^{2+} depletion could have been due to decreased Mg^{2+} deposition and/or HK (10–13). As duration of HK increased, both the bodily loss of this ion and its depletion in the tissue become greater. This indicates that Mg^{2+} deposition mechanism continues to deteriorate under HK. Since the Mg^{2+} deposition mechanism is not functioning properly, tissue Mg^{2+} content cannot be normalized by alteration of Mg^{2+} intake alone (10–13). Other data available indicate that tissue electrolyte depletion cannot be normalized unless muscular activity resumes (8–15).

With higher tissue Mg^{2+} depletion, the higher Mg^{2+} loss in SHKR than in UHKR is attributable to a more degraded Mg^{2+} deposition capability in SHKR than in UHKR, because with the higher tissue electrolyte depletion, the lower electrolyte deposition and the higher electrolyte loss followed (11–15). Since SHKR with higher tissue Mg^{2+} depletion lost more Mg^{2+} than UHKR, SHKR were experiencing lower Mg^{2+} deposition than UHKR. The fact that with tissue Mg^{2+} depletion Mg^{2+} loss increases more in SHKR than in UHKR supports the view that SHKR were experiencing a more degraded Mg^{2+} deposition capability than UHKR.With tissue Mg^{2+} depletion the differences in Mg^{2+} loss among SHKR and UHKR, shows that Mg^{2+} deposition decreases more in SHKR than in UHKR. However, it is unknown for what reason SHKR with higher tissue Mg^{2+} depletion

and higher Mg^{2+} intake would have shown higher Mg^{2+} loss than UHKR. It is possible that the higher Mg^{2+} intake accounts for higher Mg^{2+} loss with lower tissue Mg^{2+} content in SHKR than in UHKR (11–15) because SHKR (with lower tissue Mg^{2+} content) had lost more Mg^{2+} than UHKR. It has also been shown (13, 14) that excessive electrolyte intake contributes to the decrease in amino acid pool in the blood and this decrease aggravates the impact of HK in causing Mg^{2+} loss. The fact that SHKR showed lower tissue Mg^{2+} content and higher bodily Mg^{2+} loss than UHKR indicates that the more Mg^{2+} is ingested, the lesser is Mg^{2+} deposition and the lesser Mg^{2+} deposition, the higher the bodily Mg^{2+} loss. This resembles a vicious circle: i.e., the higher Mg^{2+} intake, the lower its deposition; the lower is Mg^{2+} deposition, the greater the Mg^{2+} loss. As more Mg^{2+} is removed from the blood, it cannot help to correct tissue Mg^{2+} depletion.

Rats with and without Mg^{2+} supplementation show a significantly lower Mg^{2+} content in bone and muscle with differences in their weight-bearing supporting function and morphology as compared with control rats. The severity of muscle and bone Mg^{2+}depletion was different in right femur and gastrocnemius muscle which have a different weight-bearing supporting function and morphology. The Mg^{2+} content decreased more in gastrocnemius muscle with less weight-bearing supporting morphology and function than in right femur with more weight bearing supporting function and morphology. Normally, electrolyte content decreases more in bone and muscle that have a weight supportive heavier function and morphology. The mechanism by which Mg^{2+} decreases differently in bone and muscle with different weight-bearing supporting function and morphology is unclear. There are grounds to indicate that tissue electrolyte level decreases more with than without electrolyte supplementation (8–15) and that electrolyte content decreases more in muscle and bone with less weight-bearing supporting function and morphology (17–19). This is ensured by the differences in electrolyte intake and electrolyte deposition which could have decreased more in tissue with less weight-bearing supporting function and morphology.

Skeletal muscle cell injury mechanisms of magnesium loss with tissue magnesium depletion

The potential mechanisms of HK-induced Mg^{2+} loss with tissue Mg^{2+} depletion may be related to many factors primarily to the energy depletion, cell injury, enzyme deficiencies and are as follows. The change from increased to decreased muscular activity results in redistribution of fluid in the body (8, 14, 15). This could be attributable to the absence of muscular activity (8, 14, 15). Fluid redistribution leads to decreased blood volume and thus to hyperelectrolemia (8, 14, 15). This leads to the reverse reflex increase of electrolyte loss with hypovolemia and tissue electrolyte depletion (8, 14, 15). Because electrolyte loss develops with hypovolemia and tissue electrolyte depletion, it occurs in the nature of a reverse fluid and electrolyte volume regulating reflex (20). However, the mechanism of electrolyte loss with tissue electrolyte depletion and hypovolemia has not been established. It has been assumed that fluid redistribution which results in the decreased blood volume could potentially lead to the hyperelectrolemia and electrolyte loss with tissue electrolyte depletion (8, 14, 15). The decreased blood volume can also result in skeletal muscle cell injury which alters the integrity of the sarcolemma and leads to the eventual release of intracellular contents into the plasma (8, 14, 15). The process also in-

cludes inadequate blood perfusion and decreased electrolyte deposition. This could have been one of the potential mechanisms for the Mg^{2+} loss with tissue Mg^{2+} depletion and hypovolemia during prolonged HK.

During HK there is no need to split adenosine triphosphate (ATP) as a source of energy for muscle contraction (3, 4). Because there is no need to split ATP there is no formation of ADP (adenosine diphosphate). The ADP is a stimulator of oxygen uptake and formation of new ATP molecules in the course of oxidative phosphorylation a process which is drastically decreased (3, 4). The reduction of mitochondrial number and/or function suggested as the most likely culprit to explain the decreased oxidative phosphorylation. Because there is very little creatine phosphate there is very little release of energy to cause bonding of a new phosphate ion to ADP to reconstitute the ATP. There is limitation of reserves of ATP due to inhibition of formation of ADP and decreased synthesis of ATP. The ATP becomes energetically less efficient, and for the production of ATP more substrates are used, which causes even greater shortage of the already sparse reserves of ATP (3, 4). Any condition which directly or indirectly impairs the production or use of ATP by skeletal muscle, or leads to ATP depletion can result to cell injury. The process includes inadequate blood perfusion due to HK-induced hypovolemia. The HK can also indirectly affects the skeletal muscle cell (16), thereby interfering with production or use of ATP (3, 4).

The intracellular substances and their associated positive ions tend to cause osmosis of water to the interior of cell all the time. If some factors should not overcome the continual tendency of water to enter the cell, then the cell would eventually swell. During normal muscular activity, this sodium transport mechanism opposes this tendency of the cell to shrink by continually transporting sodium to the exterior that initiates an opposite osmotic tendency to move water out of the cell. However, during HK this function of the sodium pump aimed at preventing the swelling of cells is decreased (21, 22) and sodium transport mechanisms cannot overcome the continual tendency of water to enter the cell and the cell eventually shrink (21, 22). When energy from ATP is not enough (3, 4) to keep the sodium pump operating properly the cell mass decreases (21, 22). The ATP depletion may inhibit the Na^{+}-K^{+} pump since there is a significant correlation between the Na^{+}-K^{+} pump and ATP depletion. The decreased cell mass results in the diminished holding capacity for Mg^{2+} which leads during this condition to the Mg^{2+} loss with tissue Mg^{2+} depletion (11–15). Thus, Mg^{2+} supplementation would fail to prevent tissue Mg^{2+} depletion when muscular activity restricted allowing cell mass to shrink further (21, 22).

During HK a change in the sarcolemma develops (16). A change in viscosity of sarcolemma is caused by the activation of phospholipase A. This results in the higher permeability of the sarcolemma, permitting leakage of intracellular contents, and increase in the entry of sodium (Na^{+}) ions into the cell. The increase of intracellular sodium ion concentration activates Na^{+}, K^{+}-ATPase, a process which requires energy when there energy production is decreased (3, 4). This and the impaired synthesis of ATP eventually exhausts the supplies of ATP and thus decreases cellular transport (23). The increase of the cellular Na^{+} level leads to accumulation of intracellular calcium (Ca^{2+}) level, which activates neutral proteases within the cell, causing further cellular injury (24). However, it has been suggested that irrespective of mechanisms involved, there is a final common pathway (8, 14, 15) namely during HK the intracellular Ca^{2+} increases significantly. This increases the activity of intracellular proteolytic enzymes, leading to the further destruction of intracel-

lular structures. Increase of intracellular free Ca^{++} plays an important role in deterioration of cell structure that occurs during ATP depletion. On the other hand a form of independent cell injury due to glycine deficiency has been shown.

Severe K^+ depletion, especially that associated with significant reduction in the intracellular muscle K^+, has been implicated in the development of hypokinetic-induced hyperelectrolemia. The glycogen synthesis is impaired in tissue K^+ depletion as well as during HK while *de novo* synthesis of glycogen is inhibited (25), leading to the decreased energy production (3, 4). The tissue K^+ depletion has been shown experimentally to decrease muscle cell transmembrane voltage and to cause muscle damage (26), thereby interfering with the electrolyte deposition.

The Mg^{2+} loss with tissue Mg^{2+} depletion may also be associated with Ca^{2+} and K^+ changes because Mg^{2+}changes are closely linked to Ca^{2+} and K^+ changes. The Ca^{2+} flux across the cell membrane is regulated by Ca^{2+}, Mg^{2+}-ATPase pump and tissue Mg^{2+} depletion leads to the higher intracellular Ca^{2+} level and Ca^{2+} influx across external cellular membrane which plays a crucial role in regulation of cellular excitation, contraction and impulse propagation. Studies on the Ca^{2+} fluxes across cell membrane have shown this because Mg^{2+} changes are closely linked to the Ca^{2+} and K^+ changes (8, 14, 15). Since Mg^{2+} is transported by all cell membranes in much the same manner as Na^+ and K^+ and because HK affects Na^+ and K^+ transport by all cell membranes this would also affect Mg^{2+} transport in the same manner as that of Na^+ and K^+. This eventually leads to higher Mg^{2+} loss with tissue Mg^{2+} depletion. Irrespective of the mechanisms involved, there is a common factor, namely with tissue Mg^{2+}depletion the Mg^{2+} deposition decreases which leads to Mg^{2+} shifting into plasma and Mg^{2+} loss with tissue Mg^{2+} depletion (8, 14,15). The Mg^{2+} loss increases with tissue Mg^{2+} depletion and supplementation of Mg^{2+}does not alter the tissue Mg^{2+} because Mg^{2+} deposition cannot be restored during HK unless muscular activity is restored (8, 14, 15). Failure to prevent tissue Mg^{2+} depletion with Mg^{2+} supplementation shows that tissue Mg^{2+} depletion is not a matter of Mg^{2+} shortage in the food as the inability of the body to deposit Mg^{2+}. Evidence of decreased Mg^{2+}deposition arises from the persistent increase of plasma Mg^{2+} level and Mg^{2+} loss with Mg^{2+} depletion.

Conclusion

The higher tissue Mg^{2+} depletion in SHKR with higher Mg^{2+} intake than in UHKR with lower Mg^{2+} intake shows that tissue Mg^{2+} loss is greater with higher Mg^{2+} intake. The higher total bodily Mg^{2+}loss in SHKR than in UHKR in turn shows that the bodily loss of Mg is directly related to the magnitude of tissue Mg^{2+} depletion. The dissociation of tissue Mg^{2+} depletion and bodily Mg^{2+} loss shows that reduced Mg^{2+}deposition is the main cause of tissue Mg^{2+} depletion. With enhanced tissue Mg^{2+} depletion, bodily Mg^{2+} loss would increase unless factors contributing to the decreased Mg^{2+} deposition are reversed. It is concluded that that tissue Mg^{2+} depletion increases more with higher than lower Mg^{2+} intake and that bodily Mg^{2+} loss increases more with higher than lower tissue Mg^{2+} depletion. In all, tissue Mg^{2+}depletion is not due to Mg^{2+} shortage in the foods consumed. Rather, it is due to the inability of the tissue to take up Mg^{2+} during HK.

References

1. Kovalenko, E.A. and Gurovskiy, H.H. (1980) *Hypokinesia*. Meditsina Pres, Moscow, Russia, p. 320.
2. Krupina, T.N. Mikhaylovskiy, G.P., and Tizul, A. Ya. (1970) Hormonal changes as an indicator of hypokinetic stress, in: *Adaptation to Muscular Activity and Hypokinesia*. Meditsina Press, Moscow, Russia, pp. 94–96.
3. Fedorov, I.V. (1982) *Metabolism under Hypokinetic Conditions*. Izdatelstvo Nauka, Moscow Russia, p. 254.
4. Fedorov, I.V., Chernyy, A.V. and Fedorov, A.I. (1977) Synthesis and catabolism of tissue proteins in animals during hypodynamia and resumption of muscular activity. *Fiziol. Zh. SSSR 63:* 1128–1133.
5. Katz, B. (1966) *Nerves, Muscles and Synapses*. McGraw-Hill, New York, p. 380.
6. Dee, E. and Kerman, R.P. (1963) Energetics of sodium transport in ram puppies. *J. Physiol. (London) 165:* 550–558.
7. Ling, G.N. (1965) The membrane theory and other views for solute permeability, distribution and transport in living cells. *Perspective Biol. Med. 9,* 87–106.
8. Biryukov, Ye. N. (1978) Changes in mineral deposition in bone tissue and calcium balance during experimental hypokinesia and kosmic flights. PhD thesis, Interkosmos Council, Academy of Sciences USSR and Directorate of Kosmic Biology and Medicine, Ministry of Health USSR, Moscow, Russia.
9. Zorbas, Y.G., Ivanov, A.L. and Federenko, Y.F. (1995) Electrolyte and water content in organs and tissues of rats during and after exposure to prolonged restriction of motor activity. *Rev. Esp. Fisiol. 51:* 155–162.
10. Zorbas, Y.G., Verentsov, G.E., Bobylev, V.R., Yaroshenko, Y.N. and Federenko, Y.F. (1996) Electrolyte metabolic changes in rats during and after exposure to hypokinesia. *Physiol. Chem. Phys. Med. NMR 28:* 267–277.
11. Zorbas, Y.G., Kakurin, V.J., Yaroshenko, Y.Y., Charapakhin, K.P., Kuznetsov, N.K. and Yarullinm V.L. (1998) Daily magnesium supplements effect on magnesium deficiency in rats during prolonged restriction of motor activity. *Metabolism 47:* 903–907.
12. Zorbas, Y.G., Federenko, Y.F. and Naexu, K.A. (1994) Renal excretion of magnesium in rats subjected to prolonged restriction of motor activity and magnesium supplementation. *Magnesium-Bulletin 16:* 64–70.
13. Zorbas, Y.G., Andreyev, V.G., Verentsov, G.E. and Yaroshenko, Y.N. (1997) Daily magnesium supplementation on serum and urinary magnesium changes in rats during prolonged restriction of motor activity. *Biological Trace Element Research 58:* 103–116.
14. Krotov, V.P. (1981) Kinetics and regulation of fluid-electrolyte metabolism in animals and humans during hypokinesia. PhD thesis, Interkosmos Council, Academy of Sciences USSR and Directorate of Kosmic Biology and Medicine, Ministry of Health USSR, Moscow, Russia.
15. Zorbas, Y.G., Kakuris, K.K., Deogenov, V.A. and Yerullis, K.B. (In press) Skeletal muscular calcium in supplemented and unsupplemented healthy subjects during prolonged hypokinesia. *Clinical Biochemistry*.
16. Portugalov, V.V and Rhoklenko, K.D. (1969) Changes in striated muscle fibers of mice under hypokinetic conditions. *Kosmicheskaya Biol. 3:* 45–52.
17. Zorbas, Y.G., Charapakhin, K.P., Kakurin, V.J. and Deogenov, V.A. (2000) Electrolyte content in femur of rats during prolonged restriction of motor activity. *Acta Astronautica 47:* 781–788.
18. Mikhaleva, N.P., Yefimenko, G.D., and Bobrovnitskiy, I.P. (1978) Electrolyte content of the myocardium, skeletal muscles and blood of rats during prolonged hypokinesia and readaptation. *Kosmicheskaya Biol. 12:* 80–81.

19. Zorbas, Y.G., Kakuris, K.K., Neofitos, E.A. and Afoninos, N.I. (2005) Water-electrolyte utilization in skeletal and cardiac muscles during prolonged hypokinesia in rats. *Physiol. Chem. Phys. Med. NMR 37:* 127–140.
20. Tsiamis, C.B. (1998) Fluid-volume-regulation during prolonged hypokinesia. *Acta Physiological Bulgarica 97:* 330–355.
21. Svets, V.N. (1978) *Mechanisms of Regulation of the Blood System*. Meditsina Pres, Krasnoyarsk, Russia, pp. 185–196.
22. Makarov, G.A. (1974) *Molecular Aspects of Control of Erythropoiesis*. Meditsina Pres, Ryazan, Russia, pp. 132–151.
23. Rubin, B., Liauw, S., Tittley, J., Romaschin, A. and Walker, P. (1992) Prolonged adenine nucleotide resynthesis and reperfusion in jury in post-ischemic skeletal muscle. *Am. J. Physiol. 262:* H1538–1547.
24. Armstrong, R., Warren, G. and Warren, J. (1991) Mechanisms of exercise-induced muscle fiber injury. *Sports Med. 12:* 184–207.
25. Chernyy, A.V. (1981) Effect of hypodynamia on animals' reactions to the administration of glucose, epinephrine and insulin referable to some parameters of carbohydrate metabolism, PhD thesis, Interkosmos Council, Academy of Sciences USSR and Directorate of Kosmic Biology and Medicine, Ministry of Health USSR, Moscow, Russia.
26. Larner, A.J. (1994) Potassium depletion and rhabdomyolysis. *Br. Med. J. 308:* 136–145.

Received October 23, 2006;
accepted March 6, 2007.

Physiol. Chem. Phys. & Med. NMR (2006) *38*: 105–145

An Ultra Simple Model of Protoplasm to Test the Theory of Its Long-range Coherence and Control So Far Tested (and Affirmed) Mostly on Intact Cell(s)

Gilbert Ling

Damadian Foundation of Basic and Cancer Research
Tim and Kim Ling Foundation of Basic and Cancer Research
c/o Fonar Corporation, 110 Marcus Drive
Melville, NY 11747
Email: gilbertling@dobar.org

Abstract: According to the association-induction hypothesis, the core of living phenomena lies in the long-range, one-on-many connectedness among all three major components of living protoplasm: protein, water and K^+ (and the controlling agents, called the cardinal adsorbents.) This article describes simple experimental models that could cogently test the theory of this connectedness and its control by drugs and other cardinal adsorbents.

IN VOLUME, the largest component of all living cells is water; the next is proteins. In number, the largest component is again water; but the next largest is K^+. From these, one concludes that the living cell is largely an assembly of water, proteins and K^+.

As part of what became known later as Ling's fixed charge hypothesis (LFCH) (Ling 1962, p. 218), I first suggested in 1952 that on *statistical mechanical* and *energy* grounds, K^+ in living cells is not free as widely taught (Ling 1952.) Rather, all or virtually all K^+ in living cells are in close-contact, one-on-one adsorption on the β-, and γ-carboxyl groups carried respectively on aspartic and glutamic residues of intracellular proteins. In a recent review (Ling 2005), I have shown that by the year 2005, this suggestion has been

Abbreviations: AI Hypothesis (association-induction hypothesis); EDC (electron-donating cardinal adsorbent); EWC (electron-withdrawing cardinal adsorbent); LFCH (Ling's Fixed Charge Hypothesis); PCS (pseudo-cardinal site); PM theory (polarized-oriented multilayer theory of cell water); POM theory (polarized-oriented multilayer theory of cell water).

fully verified by theoretical and experimental advances made in my own laboratory and by others including the earlier work of Kern (1948) and later definitive work of Edelmann (1977, 1980, 1983, 1998.)

In 1965 I introduced another theory, called the polarized multilayer theory — later modified to polarized-oriented multilayer theory (POM or PM) theory of cell water (Ling 1965.) In this theory, all or virtually all water molecules in most living cells are adsorbed as polarized-oriented multilayers on the exposed NHCO groups on arrays of fully-extended cell proteins. In two recent reviews, I have shown that here too progress in both theory and experimental studies made in the preceding 39 years have fully verified the validity of the POM theory (Ling 2004, 2006.)

Considering at once these two conclusions, one reaches a third conclusion. That is, the three major components of the living cell — water, proteins and K^+ — are in direct or indirect contact with one another.

This is a landmark perception in the study of living phenomenon on its own merit. More important, this conclusion affirms the association arm of the much broader unifying theory of the living cell called the ***association-induction (AI) hypothesis***, which I introduced in 1962. And, it is the one and only (surviving) unifying theory of cell physiology known then or now. The near-completion of the association aspect of the AI Hypothesis already achieved shifts attention to the less extensively studied induction-arm of the AI hypothesis, which actually also began in 1952 as part of the LFCH, when it addressed the question, why is the K^+ accumulated in living cells lost on cell death? What follows was the answer offered.

As an expression of an equilibrium phenomenon, this postulated (selective adsorption and hence) accumulation of one ion (K^+) over another (e.g., Na^+) does not demand a continual energy expenditure as in the now completely disproved membrane-pump hypothesis (Ling 1997.) Nonetheless, over the long run and in particular after work-performance, metabolic energy is required to recharge the system back to its high (negative) energy-low entropy *resting living state* (Ling 1962, p. xxii, 1992, p. 32, 2001, p. 154.) That energy is provided by the adsorption of the ultimate end-product of aerobic and anaerobic metabolism, ATP.

Figure 1, reproduced from my paper of 1952, shows diagrammatically how ATP adsorption on controlling sites — later named "cardinal sites" (Ling 1962 p. 118, p. 420) — *electronically* regulates and maintains the selective adsorption on β-, and γ-carboxyl groups near and far — as part of the maintained resting living state.

The electronic mechanism suggested in that 1952 paper can be called the direct electrostatic effect or D-effect. In years following, this was modified to what is known as the F-effect, incorporating both the D-effect mediated through space and inductive, or I-effect, mediated through intervening atoms (Ling 1962, pp. 57–58.) As more time went by, however, it became clear that the inductive or I-effect plays the predominant role.

How such a short-range inductive effect could be marshaled and organized to bring about action at a distance and in a one-on-many manner became a central theme of the association-induction hypothesis.

With the introduction of the POM theory of cell water in 1965 (Ling 1965), it was suggested that ATP does not just control and maintain the selective adsorption of (cationic) partners of the β-, and γ-carboxyl groups like K^+, ATP adsorption on cardinal site also controls and maintains the polarization and orientation of all the bulk-phase water molecules.

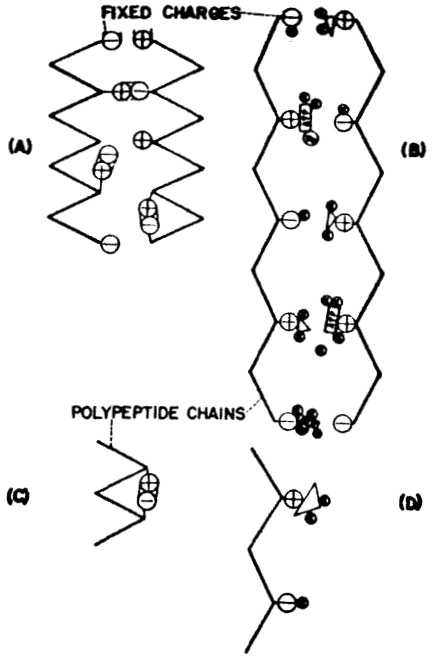

FIGURE 1. Diagrammatic illustration of the hypothetical unfolding of protein chains as a result of the adsorption of ATP. (from Ling 1952, by permission of the Johns Hopkins University Press)

And, it does so, according to the AI Hypothesis, by its action as an *electron-withdrawing cardinal adsorbent* or EWC (for definition, see Ling 1992, pp. 144–145, Ling 2001, pp. 167–168.) A mechanism was introduced and steadily improved to show how such an EWC can produce a uniform, across-the-board electron reduction at a large number of β-, and γ-carboxyl groups, near and far (Ling 2001, pp. 171–175. For earlier versions see Ling 1964 p. 254, Ling 1969, p. 45, Ling 1992 pp. 147–149.) In addition, it can at the same time, produce an electron density reduction of the oxygen atom of a vast number of backbone *carbonyl* groups (CO) of the CONH links near and far. The important consequence of this change will be made clear below.

Somewhere along the way, the need to build a broader quantitative theory became apparent. To that end, I began by introducing a parameter called the c-value (Ling 1958, 1961 p. 156, 1962 p. 58.) Measured in Ångstrom units, the c-value is roughly speaking a measure of the effective density of electrons of the singly charged oxygen atom of an oxyacid group such as a β-, or γ-carboxyl group.

(By analogy, a c'-value was introduced for the cationic charge of fixed cations including the ϵ-amino groups of lysine residue and guanidyl groups of arginine residues. A further extension was in the introduction of the c-value analogue for the oxygen atom of the CONH peptide group and the c' value analogue of the positively charge H atom of the CONH peptide link (Ling 1962 p. 60.) Unlike the carboxyl and amino groups, these CO and NH groups do not carry net electric charges and are bipolar. This means that the negative charges of the oxygen atom of CONH groups are due to the lone pairs of electrons and thus seen only at short range. The same holds for the positive charge due to the H atom of the NH component of the NHCO group.)

With the c-value defined, we went on to construct the so-called Linear Model and proceeded from there to compute the adsorption energies of the five alkali-metal ions (Li^+, Na^+, K^+, Rb^+ and Cs^+) in addition to H^+ and NH_4^+on β-, or γ-carboxyl groups at different c-values. (NH_4^+ is also seen as a prototype of the fixed cationic ϵ-amino groups carried on lysine side chains and guanidyl groups carried on arginine side chains.) The details of this theoretical model was presented in the fourth chapter of my first book, *A Physical Theory of the Living State: the Association-Induction Hypothesis* (Ling 1962.) This book has long since been out of print. Since I own its copyright, I have reproduced this entire chapter as an Appendix (Appendix 1) at the end of this article.

Figure 2 — which is a copy of Figure 4-11 in Appendix 1 — indicates that for any pair of any two monovalent cations, the relative preference indicated by a higher (negative) adsorption (association) energy shown on the ordinate of the figure reverses itself sooner or later as the c-value increases. However, for the simple objectives on hand, all we need to remember here is that at low c-value, K^+ is preferred over Na^+; at higher c-value, Na^+ may be preferred over K^+.

A similar relation exists also between K^+ and a fixed cation (i.e., ϵ-amino group and guanidyl group) but here the fixation of these fixed cations adds a favorable entropy element in the bargain, making a fixed cation more preferred even when their respective $-\Delta E$'s are equal. However, this entropy contribution due to salt-linkage formation between a fixed anion and a fixed cation is constant and does not change with c-value change.

In 1981, another basic concept of the AI Hypothesis was made more quantitative (Ling 1981.) It shows that the electron density of the carbonyl oxygen of the polypeptide chain — characterized by the *c-value analogue* mentioned above with the c-value — plays a similar role as the c-value (of the β-, and γ-carboxyl groups) in deciding which one of the alternative partners of adsorption is energetically favored.

More specifically, the c-value analogue decides the preference of the backbone peptide linkage for one or the other of the two alternative partners. These partners are respectively, (i) the NHCO groups on the third amino acid residue up or down the same protein chain (thus forming an α-helical fold) or (ii) multiple layers of water molecules. At high c-value analogue the polypeptide chain prefers to form α-helical folds; at low c-value analogue, the polypeptide chain prefers to adsorb multilayers of water molecules.

In consequence of the c-value decrease and c-value analogue decrease brought on by an electron-withdrawing cardinal adsorbent (EWC) like ATP, the β-, and γ-carboxyl groups would enhance its propensity toward adsorbing K^+ (over Na^+ or fixed cation) and the backbone NHCO groups would prefer to stay fully-extended and adsorb multilayers of water molecules. Figure 3 is the latest version of a series of more or less similar illustrations published between 1952 and 2001 (Ling 2001, p. 153.)

Thus far, experimental testing of this model during the past forty years has been performed mostly on intact living cells — where the physiological attribute involved determines what part of the cell and hence what kind of protoplasm is involved. The overall results are highly encouraging and reviewed in a sister article soon to be published. The title of that article is: *Reinstating the (redefined) protoplasm as the physical basis of life* (Ling 2007.)

However, to help gain a more and deeper understanding of the complex phenomenon, it would be ideal if we could deal with a model system that is much simpler than a living

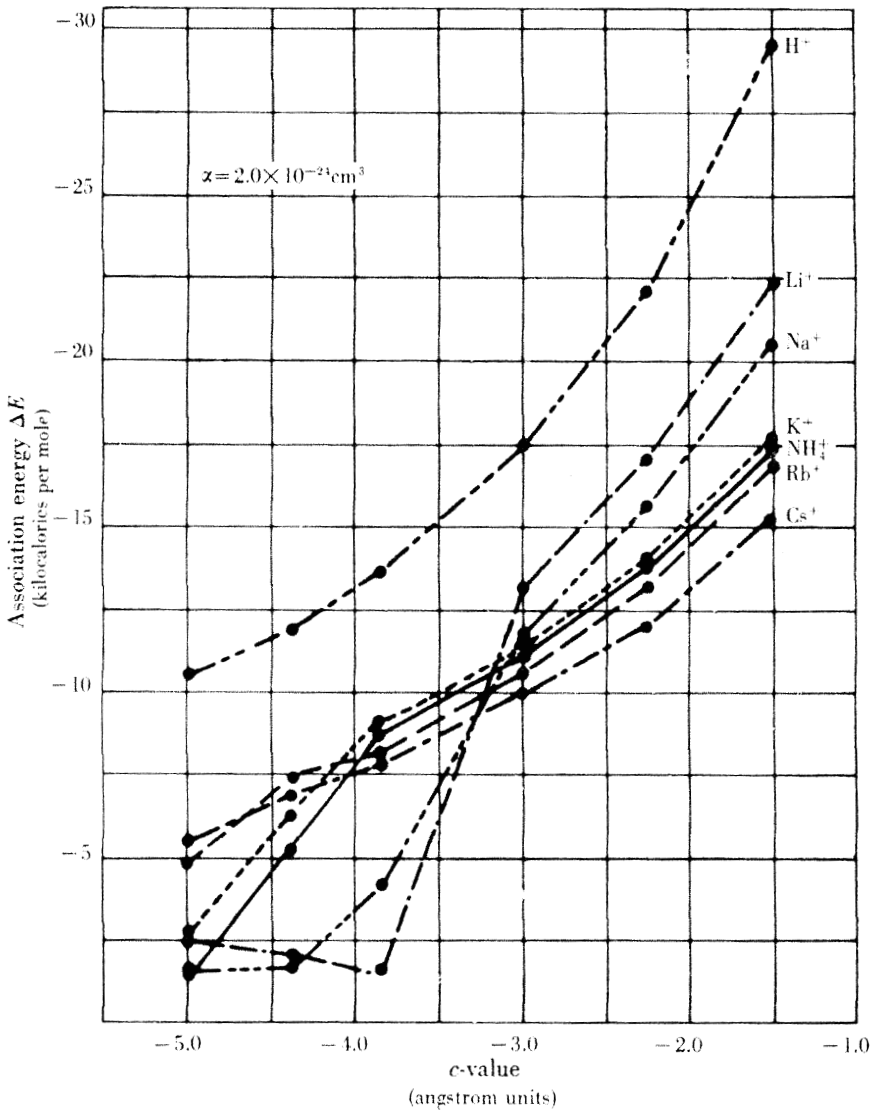

FIGURE 2. The theoretically computed adsorption (association) energies in kilogram calories per mole of H^+, Li^+, Na^+, K^+, Rb^+, Cs^+ and NH_4^+ respectively on a singly charged oxyacid group with a polarizability of 2.0 x $10^{-24}cm^3$ and c-value as shown on the abscissa. An ion, say K^+, which shows a higher negative energy of adsorption of 8.3 kcal/mole on the fixed oxyacid anion at a c-value of –4.0 Å is preferentially adsorbed over Na^+ , which at the same c-value, shows a lower negative adsorption (association) energy of 3.3 kcal/mole. However, at a higher c-value of –2.5 Å, the preference is reversed since at this c-value, the negative adsorption energy of Na^+ at 14.3 kcal/mole is higher than that of K^+ at 13 kcal/mole. (from Ling 1962, the relevant chapter 4 is attached to the end of the article as Appendix 1)

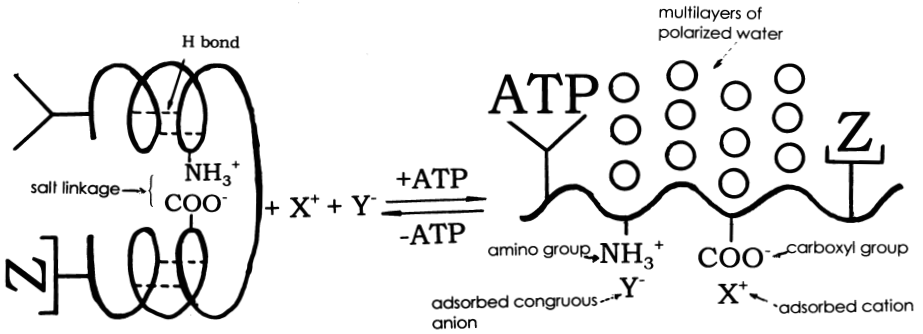

FIGURE 3. Diagrammatic illustration of how adsorption of the cardinal adsorbent ATP on the ATP-binding cardinal site and "helpers" including the *congruous anions* (shown here as "adsorbed congruous anions") and *Protein-X* (shown here as Z) unravels the introverted (folded) secondary structure shown on the left-hand side of the figure. As a result, selective K^+ adsorption can now take place on the liberated β-, and γ-carboxyl groups (shown on the right hand side figure as "carboxyl groups") and multilayer water polarization and orientation can now occur on the exposed backbone NHCO groups and the resting living state is thus achieved and maintained. (from Ling 2001)

cell. In theory, the ideal model would contain all the key elements of the protoplasm according to the AI Hypothesis. They include the polypeptide chain and functional groups on short side chains, in particular, the β-, and γ-carboxyl groups, their alternative partners (K^+ , Na^+ , fixed cations) and the alternative partners for the backbone NHCO groups, i.e., other CONH groups, three amino acid residues up or down the chain and bulk-phase water molecules.

It may produce a moment of disbelief to realize that all these requirements are present in an aqueous solution of a protein plus KCl or NaCl. All with the exception of one missing player, the cardinal site. So we will have to invent one. It is our next task to describe how.

1.0 Inventing a cardinal site

Inventing the cardinal site — which includes what are widely known as receptor sites (for drugs and hormones) — begins with a postulation. It says that all real-life cardinal sites are made of the same ingredients that make up proteins. In other words, each cardinal site is a gathering of different or similar amino acid side chains and stretches of the polypeptide chain posed in a geometric configuration.

On the basis of this postulation, we would suggest that many pure proteins may contain within their normal primary structure segments of the protein chain that have the potential of acting fully or in part like real-life cardinal sites of one kind or another seen in living protoplasm. As a result of this fortuitous event and the fundamental attributes and activities of living protoplasm seen in the light of the association-induction hypothesis, reaction of these proteins with real-life cardinal adsorbents might produce long-range, one-on-many impact on distant sites of the protein. For convenience of discussion, I shall call these sites, ***pseudo-cardinal sites*** (PCS)**.** Having said that, I must add that only future study can determine if a pseudo-cardinal site demonstrated is truly pseudo.

With the only missing component of the *ad minimum* protoplasm model made up in theory by the invented *pseudo-cardinal sites,* our next task is to lay out outlines of how

to test the theory of protoplasmic coherence and connectedness and all its basic postulations in experiments simple enough to be done by the real vanguard of future cell physiologists worldwide rich or poor as they may be.

2.0 Testing for the existence of "pseudo-cardinal sites" (PCS) and (if they do) how they can interact with one or more specific real-life cardinal adsorbents and bring about the predicted one-to-many, from-here-to-there response in the simplest model of protoplasm suggested

In theory, the successful binding of a cardinal adsorbent onto a "psudo-cardinal site" on a protein molecule could create an across-the-board change of the electron density and hence the preferred partners of the backbone peptide groups and of all functional groups on short side chains. This then provides the basis for the new kind of experimental testing outlined below.

2.1 Functional groups on short side chains

The most prominent among these functional groups on short side chains are the β-, and γ-carboxyl groups because they are most numerous in many isolated proteins, usually making up about 10% of all the amino acid residues of the protein (see Table 0-2 on page xxvii in Ling 1962 and also Ling 2007.) One advantage offered by its high concentration lies in greater ease in detecting small changes. For this reason, we will begin with the study of the β-, and γ-carboxyl groups. Once we have gained some experience in following this new approach, we can then look into other functional groups on short side chains. They may include SH groups on cysteine side chains, phenol on tyrosine side chains, tryptophane on phenylalanine side chains and even prosthetic groups like heme anchored onto imidazole groups on histidine side chains. But all that is on a future menu.

Let us begin with the mono-valent cation that is most strongly adsorbed on the β-, and γ-carboxyl groups, H^+. Figure 2 shows how the binding energy of this ion increases or decreases sharply with changing c-value. If both the fundamental theory of molecular connectedness of protoplasm and the postulation that many isolated pure proteins contain PCS that react with real life cardinal adsorbents, then one would expect that the exposure for a suitable duration of time of say 10.0 ml of a 0.5% solution of protein X would lead to a change of the association constant, K_H, of the β-, and γ-carboxyl groups of the protein. What that could tell is that that PCS acts as a EWC or EDC. The basic method used in determining the acid binding constants is by the titration method used, for example, by Foster and Sterman (1956) in their study of the effect of urea upon the pK_a values of bovine serum albumin. The employment of a truly good pH electrode is vital.

Since the total amount of the drug or cardinal adsorbent added to the solution is known, comparison with the number of the β-, and γ-carboxyl groups that have altered their K_H could yield information of the extent of the one-on-many factor demonstrated. Additional insight can be obtained by including in the protein solution either KCl or NaCl as follows.

As pointed out above, with c-value rise or fall, the preference of the β-, and γ-carboxyl groups for either K^+ or Na^+ could reverse itself as shown in Figure 2. One can experimentally investigate the impact of a drug or cardinal adsorbent on a protein X by monitoring the acid binding constant K_H as described in the preceding section, only the solution beside the protein will also contain say 25 mM of either KCl or NaCl. Since K^+

and Na^+ compete against H^+ for the same β-, and γ-carboxyl groups, the apparent K_H determined would be affected. From the observed changes, one can calculate the relative adsorption constants of both K^+ and Na^+. And from their relative magnitude, one can easily determine whether that drug (or cardinal adsorbent) behaves as an *electron donating cardinal adsorbent* (EDC) or an EWC and how effective they are in either capacity.

2.2 Bulk-phase water molecules

According to the polarized-oriented multilayer (POM or PM) subsidiary theory of the AI Hypothesis, the exposed NHCO groups of fully extended protein chains could polarize and orient the bulk phase water molecules to varying degree. Thus, if a drug or other cardinal adsorbent brings about a change in the c-value of the β-, and γ-carboxyl groups of a protein X, it is expected that the surrounding bulk-phase water molecules would also undergo extensive changes. The following outline shows one experimental approach to investigate these predicted changes, including the validity of the postulation of pseudocardinal sites

The basic method planned is the equilibrium dialysis method such as that employed in many similar studies made in our laboratory in the past (Ling and Ochsenfeld 1989, Ling *et al* 1993.) In general a much higher concentration of protein X is needed for dialysis studies than for the β-, and γ-carboxyl group studies described in the preceding section. And, for the same reason, the choice of the protein would have to be limited to very inexpensive varieties available. For probe molecules, two most useful ones would be Na^+ (Cl^-), sucrose (or trehalose, which is more stable than sucrose.) In order to determine the true equilibrium distribution coefficient or q-value (rather than the apparent equilibrium distribution coefficient or ρ-value), a plot of the final equilibrium concentration of the probe inside the dialysis sac against the final equilibrium concentration in the external solution is required. If a straight line if obtained, the slope of the line equals the q-value of that probe in the protein solution inside the sac (for example, see Ling *et al* 1993.) The lower the q-value obtained, the clearer it shows a cogent connectedness between the PCS and the farthest water molecule in the sac. Insight gained in recent times from our extensive studies on solute distribution in living cells as well as model systems would provide valuable guideline in interpreting the data obtained (Ling *et al* 1993, Ling and Hu 2004, Ling and Fu 2005.)

I thank Dr. Raymond Damdian and the Fonar Corporation, Inc. and its many capable and helpful members, in particular, our Librarian, Anthony Collela and Director of Media and Internet Services, Michael Guarino. I also thank Margaret Ochsenfeld and Dr. Zhen-dong Chen for their dedicated and skillful cooperation.

References

Edelmann, L. (1977) Potassium adsorption sites in frog muscle visualized by cesium and thallium under the transmission electron microscope. *Physiol. Chem. Phys. 9:* 313.

Edelmann, L. (1980) Potassium binding sites in muscle: electron microscopic visualization of K, Rb, and Cs in freeze-dried preparations and autoradiography at liquid nitrogen temperature using ^{86}Rb and ^{134}Cs. *Histochemistry 67:* 233.

Edelmann, L (1983) Electron probe X-ray microanalysis of K, Rb, Cs and Tl in cryosections of striated muscle. *Physiol. Chem. Phys. 15:* 337.

Edelmann, L. (1998) Basic biological research with the striated muscle by using cryotechniques and electron microscopy. *Scanning Microscopy 12:* 1.

Foster, J.F. and Sterman, M.D. (1956) Conformation changes in bovine plasma albumin associated with hydrogen ion and urea binding. II. Hydrogen ion titration curves. *J,. Amer. Chem. Soc. 78:* 3656.

Kern, W. (1948) Die Aktivität der Natriumionen in wässrigen L`sungen der Salze mit polyvalenten Säuren. *Makromol. Chemie 2:* 279.

Ling, G.N. (1952) The role of phosphate in the maintenance of the resting potential and selective ionic accumulation in frog muscle cells. In *Phosphorus Metabolism* (W.D. McElroy and B. Glass, eds.), Vol. II , p. 748, Johns Hopkins University Press, Baltimore, Maryland.

Ling, G.N. (1957) Fixed-charge hypothesis for a key mechanism in change of Na-K-permeability during excitation *Fed. Proc. 16:* 81.

Ling, G.N. (1958) Fixed charge induction hypothesis for biological transmitter, amplifier and "mixer" at the molecular level. *Fed. Proc. 17:* 98.

Ling, G.N. (1961) The interpretation of selective ionic permeability and cellular potentials in terms of the fixed charge-induction hypothesis. *J. Gen. Physiol. 43:* 149.

Ling, G.N. (1962) *A Physical Theory of the Living State: the Association-Induction Hypothesis,* Blaisdell Publishing Co., Waltham, MA.

Ling, G.N. (1964) Association-induction hypothesis. *Texas Report Biol. & Med. 22:* 244.

Ling, G.N. (1965) The membrane theory and other views for solute permeability, distribution and transport in living cells. *Persp. Biol. Med. 9:* 87.

Ling, G.N. (1965a) Physiology and anatomy of the cell membrane: the physical state of water in the living cell. *Fed. Proc. (Symposium) 24:* S103.

Ling, G.N. (1969) A new model of the living cell: a summary of the theory and recent experimental evidence in its support. *Intern Rev. Cytol. 26:* 1.

Ling, G.N. (1986) The role of inductive effect in the determination of protein structure. *Physiol. Chem. Phys & Med, NMR 18:* 3. also available via http://www.physiologicalchemistryandphysics.com/pdf/PCP18-3_ling.pdf
A faster alternative is to go to "gilbertling.com" and select the volume (and article) from the drop-down list.

Ling, G.N. (1992) *A Revolution in the Physiology of the Living Cell*, Krieger Publ. Co., Malabar, FL.

Ling, G.N. (1997) Debunking the alleged resurrection of the sodium pump hypothesis. *Physiol. Chem. Phys & Med, NMR 29:* 123. Also available via http://www.physiologicalchemistryandphysics.com/pdf/PCP29-2_ling.pdf
A faster alternative is to go to "gilbertling.com" and select the volume (and article) from the drop-down list.

Ling, G.N. (2001) *Life at the Cell and Below-Cell Level: The Hidden History of a Fundamental Revolution in Biology,* Pacific Press, New York.

Ling, G.N. (2004) What Determines the Normal Water Content of Living Cell. *Physiol. Chem. Phys & Med, NMR 36:* 1. Also available via http://www.physiologicalchemistryand physics.com/pdf/PCP36-1_ling.pdf
A faster alternative is to go to "gilbertling.com" and select the volume (and article) from the drop-down list.

Ling, G.N. (2005) An updated and further developed theory and evidence for the close-contact one-on-one association of nearly all cell K^+ with β-, and γ-carboxyl groups of intracellular proteins. *Physiol. Chem. Phys & Med, NMR 37:* 1. Also available via <http://www.physiologicalchemistryandphysics.com/pdf/PCP37-1_ling.pdf>
A faster alternative is to go to "gilbertling.com" and select the volume (and article) from the drop-down list.

Ling, G.N. (2006) Chapter 1, A convergence of experimental and theoretical breakthroughs affirms the PM theory of dynamically structured cell water at the theory's 40th birthday.in: *Water*

and the Cell (Pollack, G.H., Cameron, I. L. and Wheatley, D.N., eds.) Springer Verlag, Berlin, New York.

Ling, G.N. (2007) Reinstating the (redefined) protoplasm as the physical basis of life. *Physiol. Chem. Phys. & Med. NMR 39:* xxx.
A faster alternative is to go to "gilbertling.com" and select the volume (and article) from the drop-down list.

Ling, G.N. and Fu, Y. (2005) What befalls the proteins and water in a living cell when the cell dies? *Physiol. Chem. Phys. & Med. NMR 37:* 141. Also available via: www.physiologicalchemistryandphysics.com/pdf/PCP37-141_ling_fu.pdf
A faster alternative is to go to "gilbertling.com" and select the volume (and article) from the drop-down list.

Ling, G.N. and Hu, W. (2004) How much water is made "non-free" by 36% native hemoglobin? *Physiol. Chem. Phys. & Med. NMR 36:* 143. Also available via: www.physiologicalchemistryandphysics.com/pdf/PCP36-143_ling_hu.pdf
A faster alternative is to go to "gilbertling.com" and select the volume (and article) from the drop-down list.

Ling, G.N. and Murphy, R.C. (1983) Studies on the physical state of water in living cells and model systems. II. NMR relaxation times of water protons in aqueous solutions of gelatin and oxygen-containing polymers which reduce the solvency of water for Na^+, sugars and free amino acids. *Physiol. Chem. Phys. & Med. NMR 15:* 137. Also available via: www.physiologicalchemistryandphysics.com/pdf/PCP15-137_ling_murphy.pdf
A faster alternative is to go to "gilbertling.com" and select the volume (and article) from the drop-down list.

Ling, G.N., Niu, Z. and Ochsenfeld, M. (1993) Prediction of the PM theory of solute distribution confirmed. *Physiol. Chem. Phys. & Med. NMR 25:* 177. Also available via: www.physiologicalchemistryandphysics.com/pdf/PCP25-177_ling_niu_ochsenfeld.pdf
A faster alternative is to go to "gilbertling.com" and select the volume (and article) from the drop-down list.

Received June 10, 2007;
accepted August 4, 2007.

APPENDIX I

The Model of the Biological Fixed-Charge System

(Reproduced from Chapter 4 of Ling, 1962)

4.1. Introduction—The 1951–52 Model

In 1951 and 1952, the author presented a version of the present hypothesis. According to this early version, selectivity of one alkali-metal ion over another is achieved by a difference in association energy and by an enhanced degree of ionic association through fixation of one species of ion; the fixed ions were called "fixed charges."

In the early model, the author followed Bjerrum's theory of ion-pair formation (1926). The treatment differed from that of Bjerrum in that it included the effect of dielectric

saturation, a phenomenon of particular importance to the present case. If *dn* is the average number of counterions within a spherical shell of thickness *dr* and at a distance *r* from the center of a fixed ionic group, then

$$dn = \frac{N_{\pm}}{V} 4\pi r^2 \exp\left(\frac{-Z_1 Z_2 \epsilon^2}{D(r) k T r}\right) dr. \tag{4-1}$$

Here $N_{\pm}$ is the number of counterions in the volume V; Z_1 and Z_2 are the valences of the charges; ϵ is the electronic charge; k is the Boltzmann constant; T is the absolute temperature; and $D(r)$ is the effective dielectric value, which varies with r as a result of the freezing in (dielectric saturation) of the water molecules in the intense field immediately surrounding an ion (Sack, 1926, 1927; Debye, 1929; Webb, 1926; Hasted *et al.*, 1948; Grahame, 1950). We considered *pdr*,

$$pdr = \frac{dn}{N_{\pm}/V} \tag{4-2}$$

as the probability of finding a counterion within the shell. Using the values of 2.0Å for the radius of the hydrated K^+ ion and 2.8Å for the hydrated Na^+ ion and a microcell radius of 20Å, we estimated a selectivity ratio K^+/Na^+ of 7. The details of this calculation are given in Appendix C; Figure 4.1 presents the results. We have reproduced Bjerrum's curve showing the probability of finding a cation in a shell *r*Å (abscissa) away from the anion as part B of this figure. The shaded area corresponds to the volume within the microcell of 12Å radius illustrated in part A.

This earlier model served many useful purposes, but the theory, as such, had serious limitations. First, despite its general acceptance (Fowler and Guggenheim, 1939; Harned and Owen, 1958; Kortüm and Bockris, 1951), the concept of hydrated ionic radii lacks clear physical significance. The hydrated ionic radius is usually only a few tenths of an angstrom unit larger than the crystal radius although a single water molecule is 2.7Å in diameter (see Appendix C; interpretation according to the present model is given in Section 4.4D). The use of the hydrated ion concept thus prevented quantitative improvement of the model. Second, the rigidity imposed upon the theory by the acceptance of a set of hydrated diameters of constant magnitude, and hence a fixed order of preference for different ions, is at variance with an increasing amount of evidence demonstrating the variability of ionic preference.

It was not until some years after 1952 that I became aware of any system, living or nonliving, that shows an unequivocal selective ionic accumulation of alkali-metal ions in any order other than $K^+ > Na^+$. Thus my early model seemed adequate. In the years that followed, however, it gradually became clear that, in a number of other systems in which ionic selectivity is a matter of greater simplicity, different and opposite orders of preference exist. Investigators. in these fields had, in fact, already offered qualitative explanations to account for the diverse orders of preference observed for the monovalent cations.

Following the work of Wiegner and Jenny (1927), Jenny (1932) concluded from studies of clays and permutites that "the observed irregularities in the lyotropic series of natural aluminum silicates may be interpreted as various stages in the reversal of the normal hydration order of the exchanging cations. From the viewpoint of hydration of ions, it is

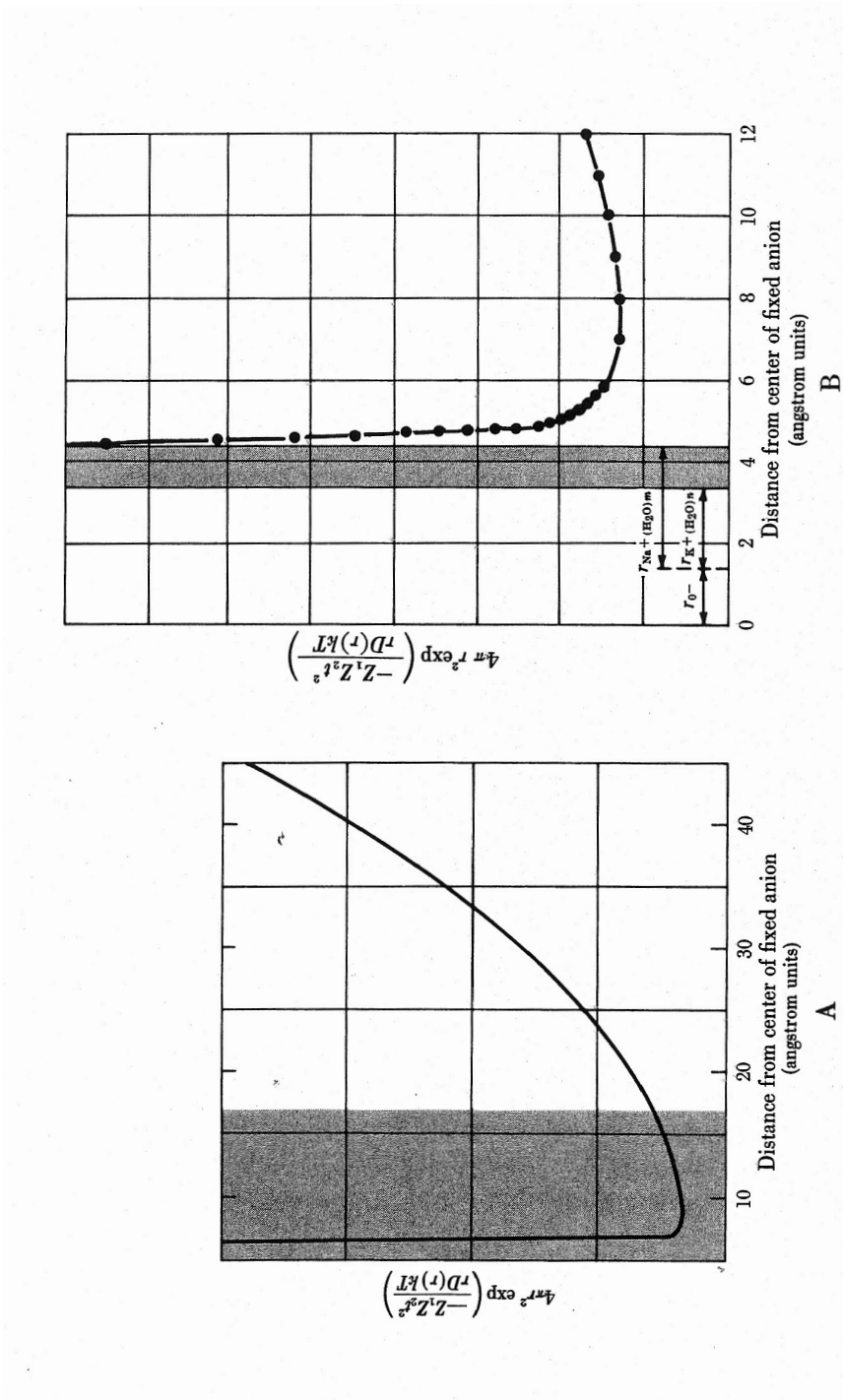

FIGURE 4.1. The probability of finding a countercation at various distances from the center of a microcell. The shaded area in A represents the volume available to the smaller hydrated K^+ ion (radius = $r_{K^+(H_2O)_N}$) but not to the larger hydrated Na+ ion (radius = $r_{Na^+(H_2O)_M}$); r_0 stands for the radius of the singly charged oxygen. In B, taken from Bjerrum (1926), the shaded area corresponds to the volume of a microcell of the size shown in A.

logical to connect the reversal of the lyotropic series with a dehydration of ions." Bungenberg de Jong (1949) ascribed the difference in the order of selectivity for different ions among systems possessing unlike functional groups to the different polarizabilities of these groups (see also Bregman and Murata, 1952; Bregman, 1953). After Eisenman *et al.* (1957),* as quoted by Isard (1959), postulated that the variation in the lyotropic series was due to a change in the electrostatic field strength of the fixed anionic sites, a convincing system could be erected to explain the selectivity orders observed in nature. These investigators hypothesized that with the increase of the field strength the interacting cations would lose their hydration shells in an orderly fashion, the least hydrated cations losing their hydration shells first.†

Eisenman and co-workers postulated eleven orders out of the 120 possible permutations for the five alkali-metal ions. They then showed that these eleven orders could account for a large number of the "irregular" lyotropic orders encountered in various ionic studies.** This hypothesis led to refinements in the calculation of the association energies of the various ions mentioned in the introduction (for an abstract, see Ling, 1957).

4.2. The Present Model

A. THE DEFINITION OF *c*- AND *c′*-VALUES AND THEIR ANALOGUES

Acids bearing the same carboxylic groups may have widely varying acid-dissociation constants: the *p*K value of acetic acid is 4.76, but the *p*K value of trichloroacetic acid is less than 1.0; the *p*K value of the carboxyl groups of uncharged glycine $NH_2CH_2COO^-$ is 4.30 (Edsall and Blanchard, 1933), that for the charged glycine $NH_3^+CH_2COO^-$ is 2.31 (Zief and Edsall, 1937). Thus, although the three substituent chlorine atoms of trichloroacetic acid and the amino group of glycine are spatially separated from the dissociating carboxyl group, they markedly weaken the attractive force between the carboxyl group and its proton. This phenomenon is called the inductive effect.

G. N. Lewis in 1916 and 1923 proposed that the inductive effect is a result of an electrical dissymmetry caused by the unequal sharing of electrons between unlike atoms. Pairs of shared electrons are thus displaced without being dissociated from their original atomic octets; this produces a similar displacement in the next link and the effect is propagated along a multiatomic molecule. The electronegativity of an atom or group in a molecule is the measurement of the tendency of this atom or group to draw electrons toward itself (Pauling, 1948). Substitution of hydrogen atoms by the more electronegative chlorine atoms, as in trichloroacetic acid, leads to withdrawal of electrons from an attached residue and hence a reduction of electron density in it. This is a negative inductive effect, $-I$-effect. The NH_3^+ group which is electronegative also exerts a $-I$-effect. Substitution

* The theories of Jenny and Bungenberg de Jong, as well as that of Eisenman, and coworkers, up to 1957 all dealt with the effects of hydration and dehydration in a qualitative manner. In deriving a quantitative theory one must take into account the effects of dielectric saturation as well as the hydrated diameters; only in this way can a significant selectivity between K^+ ion and Na^+ ion be theoretically derived.

† This order of dehydration is the reverse of that envisioned by Jenny (1932); he stated that the most hydrated ion will be the first affected by the dehydration process.

** Eisenman (1962) has summarized the views of these authors.

of hydrogen by less electronegative groups releases electrons and increases the electron density of a connected atom creating a + *I*-effect (Ingold, 1953).

The inductive effect is an electrostatic effect mediated through intervening atoms and intimately dependent upon their number, polarizability, and other characteristics. Another electrostatic effect emanates from substituent groups and is transmitted through space along the axis of shortest separation of the interacting atoms. This is called a direct effect, *D*-effect. The difference between the acid dissociation constants of acetic acid and of glycine may be accounted for by the combined *D*-effect and *I*-effect, together termed the *F*-effect. This nomenclature, used mostly by European authors (see Hermans, 1954), has been adopted in this monograph for its simplicity.

Let us begin with a singly charged and isolated oxygen ion O^- and assume that it is associated with a monovalent cation G^+ (Figure 4.2A). Let us also assume that the equilibrium distance between the "center of gravity" of the extra electron of this singly charged oxygen and the geometrical center of the cation is r_f. We now build up a complex molecule such as that shown in Figure 4.2B, bearing one or more chains of varying dipolar groups as well as single charges. These groups interact with the cation G^+; their interaction energy may be analyzed and resolved into three terms.

(1) Direct electrostatic effects produced by charge-bearing monopolar or dipolar groups and transmitted through the shortest spatial distance. Resolving the dipoles into single charges one may represent this class of effects by

$$\sum_{i=1}^{n} \frac{Z_G Z_i \epsilon^2}{D_i r_i}.$$

Here Z_G and Z_i are the valences; ϵ is the electronic charge; r_i is the shortest distance in space between the charge-bearing group and the center of the cation G^+; and D_i is the effective dielectric constant for that particular interaction.

(2) The *I*-effect, which produces induced dipoles along the whole molecule. The induced dipoles may again be resolved into single charges and absorbed in the first term.

(3) The *I*-effect and the *M*-effect (mesomeric or resonance effect), which create a change of electron density and a displacement of the center of gravity of the electron cloud of the oxygen atom on the functional group. This displacement of the center of gravity of the functional group is analogous to other induced dipoles mentioned under (2); it too will be absorbed in the first term. The varying electron density may be represented by a varying charge $\eta\epsilon$, where η is a positive number and ϵ is the electronic charge located at a distance r_f from the center of the cation G^+. D_f is the effective dielectric constant within this distance. The net effect corresponds to the sum of (1) the *D*-effect, and (2) and (3), the *I*-effects:

$$\frac{Z_G \eta \epsilon^2}{D_f r_f} + \sum_{i=1}^{n} \frac{Z_G Z_i \epsilon^2}{D_i r_i}.$$

Although the detailed meaning of this expression may be quite complex, its net effect is an increase, a decrease, or no change in the energy of interaction between the anion and the cation G^+. Exactly the same increase or decrease may be simulated by assuming a

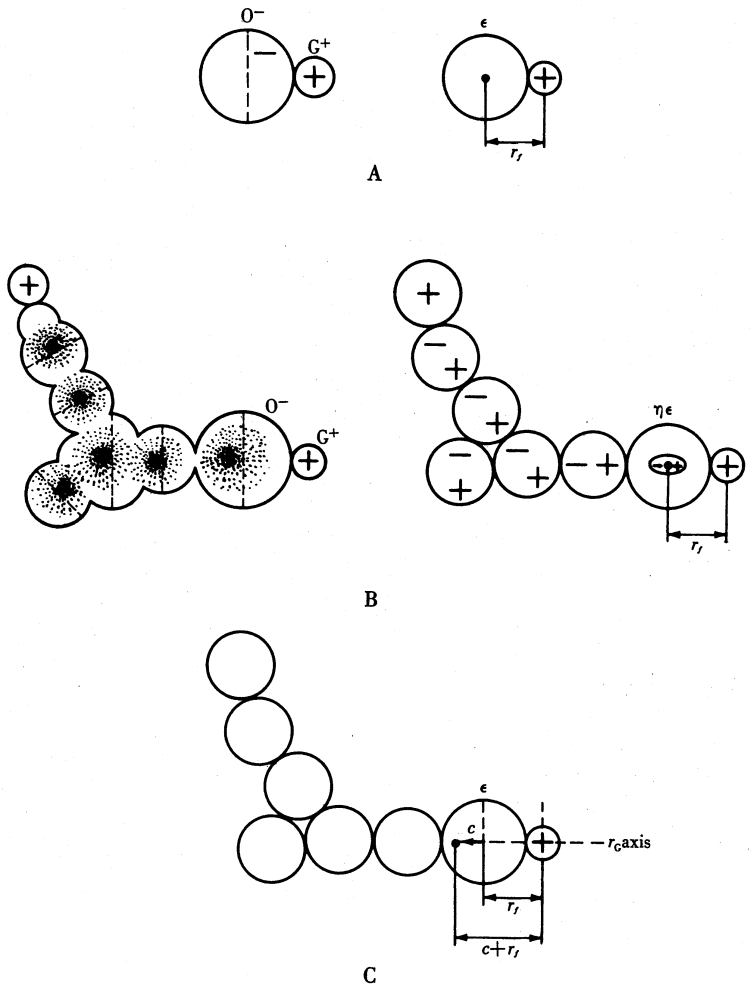

FIGURE 4.2. The definition of the *c*-value.

constant unit excess charge (valence electron) on the anion and by moving this excess charge along the r_G axis toward or away from G^+. This change in the separation of the unit excess electron from G^+ may be represented in angstrom units; it will be called *c*. The distance *c* is positive if the excess electron is displaced toward G^+, negative if it is displaced away from G^+. Thus, the total separation, as shown in Figure 4.2, will be $r_f - c$. We may then set $Z_G\epsilon^2/(r_f - c)$ equal to the combined actions of the three terms above. Cancelling $Z_G\epsilon^2$ and rearranging, we have the definition of. the *c*-value:

$$c = r_f - \frac{1}{\dfrac{\eta}{D_f r_f} + \displaystyle\sum_{i=1}^{n} \frac{Z_i}{D_i r_i}}. \tag{4-3}$$

In this treatment, the *c*-value is defined to be independent of the nature of the cation G^+ and its exact location. That part of the interaction which does depend on the nature and location of G^+ is absorbed in another variable, the group polarizability α (see Section 4.3A).

A fall of the *c*-value (a change from 0 to −1Å) parallels a decrease in the electron density of the functional group; for example, acetic acid (a weak acid) → trichloroacetic acid (a strong acid). A rise of *c*-value parallels an increase of electron density; for example, trichloroacetic acid → acetic acid. A c'-value may be formulated for a change in the density of the excess positive charge on an amino group; we use a hypothetical NH_3^+ group. Here, a rise of c'-value parallels a decrease of electron density and a fall of c'-value parallels an increase of electron density.

We can broaden the concepts of the *c*- and c'-values so that their application will include proton-accepting and proton-donating groups such as alcoholic, amide, ester, and ether groups as well as charged or dipolar groups other than O– and NH_3^+. In these cases, the particular group is matched by a hypothetical. singly charged O– or NH_3^+ group with the equivalent *c*- and c'-values. These values are then called the *c*- and c'-analogues of these different groups.

B. THE LINEAR MODEL AND THE FOUR CONFIGURATIONS

Having defined the *c*-value, the c'-value, and their analogues, let us insert a hypothetical cylindrical cavity in a microcell of a fixed-charge system. One end of the cavity encloses a negatively charged oxyacid group, represented as a negatively charged oxygen atom (Figure 4.3). Adjacent to the oxygen atom and near the middle of the cavity, we place a cation; farther away, we place two water molecules in a linear array. This configuration is called configuration 0. We then insert, between the fixed anion and its countercation, one, two, and three water molecules successively and call these configurations, respectively, configurations I, II, and 111.* We assume that all the water molecules within this cavity are completely frozen in (dielectrically saturated) and that variation of polarization outside the cavity from one configuration to another may be neglected.

C. THE VALUE OF THE DIELECTRIC COEFFICIENT D

Dielectric saturation in the immediate vicinity of an ion has long been recognized (Sack, 1926, 1927). According to the Debye theory of dielectric saturation (1929), the radial dielectric coefficient has a constant value of 3 in the space extending from the center of a monovalent ion radially to a distance of about 3Å, where it begins to rise gradually to the macroscopic value of 81, at about 16Å. The more recent calculations of Hasted *et al.* (1948) and of Grahame (1950) show a more abrupt rise of dielectric coefficient immediately beyond the first layer of water. Nevertheless, the consensus of opinion is that the first layer of water is almost completely saturated dielectrically.

Hasted assumed that the first layer of water around an anion is much less saturated than the first layer around a cation. This opinion is quite widely held (Hasted *et al.*, 1948;

* There is not enough room to accommodate the two water molecules distal to the anion within the microcell of 20Å radius. However, the linear arrangement is a model of the three-dimensional system in which water molecules are joined, not end-to-end, but in a zigzag. In that case, the problem disappears. Calculations were also made with the two distal water molecules removed from the model; the results showed no significant change except that the crossover points, to be discussed later, occurred at lower *c*-values.

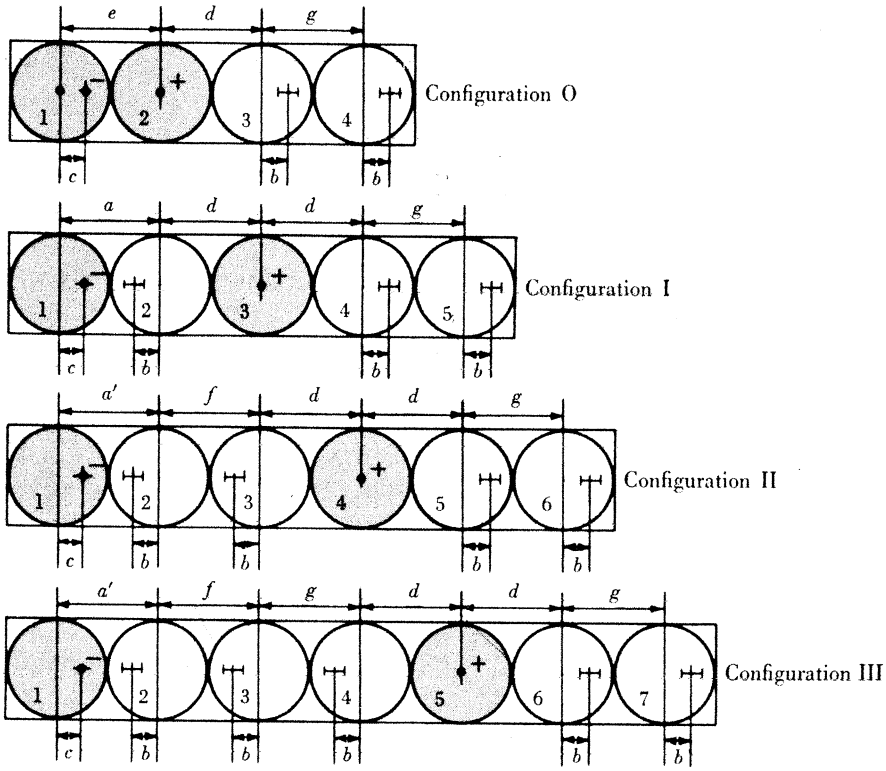

FIGURE 4.3. The linear model. The interaction energies were calculated for each of the monovalent cations in each of the four configurations of fixed anions and water.

Grahame, 1950). I adopted this assumption in my treatment of the 1951–52 model; however, little experimental evidence exists to support this view. Lorenz and Posen (1916) presented measurements of the mobilities of a large number of polyatomic organic anions. Applying Stokes' law, they calculated the effective volume of the ions and then compared these effective volumes with the molecular volume and concluded that no room could be left for an additional layer of water. Judging from the uncertain applicability of Stokes' law and the large ionic size, one sees no conclusive evidence for a general lack of hydration around anions, although the particular contention of these authors may prove correct. On the contrary, anions are known to possess both greater heats of hydration and greater entropies of hydration than cations of equal size; for example, K^+ (crystal radius = 1.33Å) has a ΔH of −75 kcal/mole and a ΔS of −11 cal/deg/mole; the corresponding values for F^- (crystal radius = 1.36Å) are −121.5 kcal/mole and −26 cal/deg/mole, respectively (Ketelaar, 1953, Table 13; Verwey, 1942). Water molecules oriented in the first hydration shell of an anion should thus be more rigidly frozen and have less freedom than water molecules around a cation of equal size. We may conclude that the first layer of water in immediate contact with either anions or cations is dielectrically saturated. Therefore, the water molecules between the anionic oxyacid group and a cation in configurations I and II should be completely saturated.

The third water molecule in configuration III, found between the two water molecules immediately adjacent to the carboxyl group and the cation, should also be completely saturated dielectrically. The following facts suggest that this middle water molecule is more polarized than any second-nearest neighboring water molecule around a single isolated cation or anion: (1) The interaction between the permanent dipole moment of a water molecule and the cation and that between the permanent dipole moment of the water molecule and the anion are additive. (2) The interaction between induced dipole and permanent dipole and that between induced dipole and induced dipole are enhanced through reinforcement of cationic and anionic induction. (3) These effects combine to shorten the equilibrium distances between the interacting molecules and ions, and thereby secondarily further intensify the cohesive forces of all these as well as those of the London dispersion energies.

4.3. Calculation of the Association Energies and Distribution Ratios

The difference in thermodynamic internal energy between the appropriately defined associated and dissociated states ($\Delta E = E_{\text{assoc}} - E_{\text{dissoc}}$) is represented by ΔE, which is usually a negative quantity. The terms "association energy" and "dissociation energy" are both used in this monograph. These energies are equal in absolute magnitude but differ in sign. We have chosen to represent the association energy by ΔE; the dissociation energy, then, is given by $-\Delta E$. We use the terms "adsorption energy" and "association energy" as synonyms. Having presented the basic assumptions of the linear model, we can calculate the association energy ΔE for each cation at varying c-values. Two steps are involved in this process; first, given a cation, a particular c-value of the fixed anion, and an unlimited number of water molecules, we want to find the statistical probability of having no water molecule, one water molecule, two, or three water molecules between the cation and the fixed anion pair; that is, we want to determine the probability of finding each of the configurations 0, I, II, III. To evaluate this, we must find the total of all energies between cation and anion, between ions and water, between water and water on an absolute basis for each configuration. By comparing the total energies of the various configurations, we can calculate their relative abundance at a given temperature. Having found this, we can calculate the association energy ΔE for each particular cation in its particular statistical distribution (for example, 95 per cent in configuration III, 4 per cent in configuration II, and 1 per cent in configuration I). The association energy ΔE is the difference between the energy of the cation in the fixed-charge system as a counterion of a fixed anion of a given c-value and the energy of the same cation in an infinitely dilute solution at an infinite distance. In a truly accurate three-dimensional model, ΔE could be obtained by comparing the energy calculated from the first step, properly weighted statistically, with the experimentally measured energy of the hydrated cation extrapolated to infinite dilution. Since we have only a linear model, this comparison cannot be made; instead we use the charging method of Born (1920). Since the major energy difference between the associated ion pair and the dissociated ion pair is the electrostatic interaction energy between the cation and the fixed anion, we can determine the approximate ΔE by evaluating the work done in bringing the cation from infinity to the particular equilibrium location estimated in the first part of our calculation. Once the association energies have been evaluated we can find the macroscopic equilibrium distribution ratios between various ion pairs.

A. CALCULATION—PART I. THE EVALUATION OF THE STATISTICAL WEIGHTS OF THE VARIOUS CONFIGURATIONS AT EQUILIBRIUM

We shall follow the treatment of ionic hydration of Moelwyn-Hughes (1949). We represent a water molecule as one that has a permanent dipole located bÅ away from the geometrical center of an otherwise spherically symmetrical molecule. The repulsion constant between the oxygen end of the water molecule and a cation is then assumed to be similar to that between the same cation and a fluoride ion (which resembles oxygen, Moelwyn-Hughes); the repulsive field is represented as inversely proportional to the ninth power of the distance between the centers of the two interacting atoms. The whole array is first assumed to be at 0°K. The total potential energy $\mathcal{U}$ of a particular configuration can be calculated from the equation:

$$\mathcal{U} = \underset{(1)}{\sum_i \sum_{j>i} \frac{Z_i Z_j \epsilon^2}{|r_{ij}|}} - \underset{(2)}{\sum_i \sum_{j\neq i} \frac{Z_i \epsilon \mu_j (r_{ij} + b_j)}{|r_{ij} + b_j|^3}}$$

$$- \underset{(3)}{\sum_i \sum_{j\neq i} \sum_{k\neq i} \frac{\alpha_i Z_j Z_k \epsilon^2 r_{ji} r_{ki}}{2|r_{ji}|^3 |r_{ki}|^3}} - \underset{(4)}{\sum_i \sum_{j>i} \frac{2\mu_i \mu_j}{|r_{ij} - (b_i - b_j)|^3}}$$

$$- \underset{(5)}{\sum_i \sum_{j\neq i} \sum_{k\neq i} \frac{2\alpha_i Z_j \epsilon r_{ji} \mu_k}{|r_{ji}|^3 |r_{ki} - b_k|^3}} \tag{4-4}$$

$$- \underset{(6)}{\sum_i \sum_{j>i} \frac{2}{|r_{ij}|^3} \left(\sum_{k\neq i} \frac{\alpha_i Z_k \epsilon r_{ki}}{|r_{ki}|^3} \right) \left(\sum_{l\neq j} \frac{\alpha_j Z_l \epsilon r_{lj}}{|r_{lj}|^3} \right)}$$

$$- \underset{(7)}{\sum_i \sum_{j>i} \frac{9}{4} \frac{\alpha_i \alpha_j}{|r_{ij}|^6} \frac{U_i U_j}{U_i + U_j}} + \underset{(8)}{\sum_i \sum_{j>i} \frac{A_{ij}}{|r_{ij}|^9}}.$$

In succession, the terms on the right-hand side of the equation represent (1) the classical energy of interaction between charge and charge, (2) the energy of interaction between charge and permanent dipole, (3) the energy of interaction between charge and induced dipole, (4) the energy of interaction between permanent dipole and permanent dipole, (5) the energy of interaction between permanent dipole and induced dipole, (6) the energy of interaction between induced dipole and induced dipole, (7) the London dispersion energy, and (8) the Born repulsion energy.

We number the ions and molecules consecutively from the fixed site to the end of the linear array, and define the positive direction as that of increasing numbers. The valency (0, +1, or −1) of the ith entity is represented by Z_i; ϵ is the electronic charge; r_{ij} is a scalar quantity representing the distance from the ith to the jth entity and is positive if $i < j$; μ_j is the scalar permanent dipole moment of the jth entity and is positive or negative as the dipole lies parallel or antiparallel to the positive direction; b_j is equal to $\pm b$, the sign being determined by the direction of displacement of the permanent dipole from the geometrical center of the species in a particular configuration. Thus the quantity

$$\frac{b_j}{\pm b} = \frac{\mu_j}{|\mu_j|} \tag{4-5}$$

depends only upon the orientation of the dipole within the species. We determine the equilibrium orientation of the dipoles with respect to the linear system by minimizing the total energy as a function of the possible orientations. The polarizability of the jth entity is represented by α; A_{ij} is the specific energy constant of the repulsive field between the ith and jth entities in immediate contact; U_j is the zero-point energy of the jth entity. The zero-point energy of a cation is taken as the second ionization potential; that of an anion is taken as the electron affinity (see J. E. Mayer, 1933). The zero-point energy for water molecules is calculated from the value of refractive indices of Tilton and Taylor (1938) to be 20.92×10^{-12} ergs per molecule.* This agrees closely with the ionization potential of water, 21.1×10^{-12} ergs per molecule (International Critical Tables).

In calculating the dispersion energy, we introduce the additional factor of 3/2 into the London expression,

$$-\frac{3}{2}\frac{\alpha_i\alpha_j}{|r_{ij}|^6}\frac{U_iU_j}{U_i + U_j}$$

following Born and Mayer (1932) and Bernal and Fowler (1933). other constants adopted and their sources are listed in Table 4.1.

Constant	H	Li	Na	K	NH_4	Rb	Cs	H_2O	Carboxyl oxygen
$d \times 10^8$ cm	1.61	2.21	2.50	2.90	3.06	3.09	3.38		
$g \times 10^8$ cm	2.42	2.50	2.53	2.55	2.55	2.56	2.58		
$\alpha \times 10^{24}$ cm	0[c]	0.075[g]	0.21[g]	0.87[a]	1.65[b]	1.81[g]	2.79[g]	1.444[a]	0.876[c]
$U \times 10^{12}$ erg/mole	0[c]	120.6[d]	75.4[d]	50.7[d]	50.7[c]	43.8[d]	37.5[d]	20.9[e]	3.4[f]
$\mu \times 10^{18}$ e.s.u.								1.834[a]	
$A \times 10^{32}$ erg/cm^9 (against oxygen end of water molecule)	0.208[i]	3.38[i]	8.5[h]	26.5[h]	35.01[i]	42.5[h]	82.5[h]	14.14[j]	14.14[j]
(against fluoride ion)			(6.29)[k]	(28.4)[k]		(49.4)[k]	(90.3)[k]		

Table 4.1. PHYSICAL CONSTANTS USED IN THE COMPUTATION OF INTERACTION ENERGIES.

[a] B. E. Conway, 1952 (Table II 3).
[b] Ketelaar, 1953.
[c] See text.
[d] Handbook of Chemistry and Physics, 1956–57 (p. 2347, II).
[e] Calculated from refractive indices of Tilton and Taylor, 1938.
[f] Latimer, 1952 (p. 18).
[g] Moelwyn-Hughes, 1949.
[h] Calculated from experimental heat of hydration, Moelwyn-Hughes, 1949.
[i] Calculated.
[j] Calculated from Searcy, 1949.
[k] Calculated from Lennard-Jones, 1936 (Table 32, p. 327).

* Sellmeier's equation of the form

$$n_i = 1 + \frac{a}{\nu_0^2 - \nu_i^2}$$

was used. Here n_i is the refractive index at wave length λ_i; ν_i is the corresponding frequency; ν_0 is assumed to be the only natural frequency; and a is a constant. The wave lengths λ_i chosen correspond to the following: 7065.2Å (He), 5892.6Å (Na), 4861.3Å (H), 4046.6Å (Hg), and $\nu_i = c_{\text{light}}/\lambda_i$ (c_{light} is the velocity of light). The ν_0 values calculated for each pair of frequencies were averaged, giving 20.92×10^{-12} ergs per molecule.

(1) The polarizability, zero-point energy, and other constants

The value α, assigned to the oxyacid group, represents the polarizability of the negatively charged oxygen and includes contributions from nearby atoms and other secondary effects (see the top of page 60). Consequently, we choose two values representing a reasonable range, rather than a single value. The lower value is arbitrarily taken as 0.876×10^{-24} cm^3. This is not an unreasonable lower limit since the carboxyl oxygen has a polarizability of 0.84×10^{-24} cm^3; the fluoride ion has a polarizability of 0.81×10^{-24} cm^3; the hydroxyl oxygen, 0.59×10^{-24} cm^3; and the ether oxygen, 0.64×10^{-24} cm^3 (Ketelaar, 1953, Table 9). For the upper limit, we choose the value 2.0×10^{-24} cm^3 (the OH^- group has a polarizability of 1.89×10^{-24} cm^3, Ketelaar, 1953).

The H^+ ion is given zero values for both its polarizability and its zero-point energy. The zero-point energy for the ammonium ion NH_4^+ is not available. Mulliken (1933) pointed out the chemical similarity between the ammonium ion and the potassium ion, and showed that the ionization potential of the NH_4^+ ion is very close to that of the potassium ion. We have assumed that the NH_4^+ ion has the same value for its second ionization potential as the potassium ion has. The best approximation for oxyacid oxygen is that of the electron affinity of a singly charged oxygen atom (Latimer, 1952).

The Born repulsion constants for the Na^+ ion, the K^+ ion, the Rb^+ ion, and the Cs^+ ion against either the oxyacid oxygen or the oxygen end of a water molecule were calculated from experimentally determined heats of hydration using Moelwyn-Hughes' equation 3 (1949, p. 479). For comparison, the repulsion constants between alkali-metal ions and the fluoride ion (which resembles oxygen) are also listed (Lennard-Jones, 1936, p. 327). We calculate the repulsion constant between water molecules from the data of Searcy (1949), who equated the repulsion term to C/r^{12}, while we use the approximation A/r^9. The value of C a constant, is obtained from Searcy. The equilibrium distance r between water molecules in ice is 2.76Å (Pauling, 1948). Equating C/r^{12} to A/r^9, we obtain $A = 14.14 \times 10^{-82}$ erg cm^9. We assume the same value for the repulsion between the hydrogen end of a water molecule and an oxyacid oxygen atom.

(2) Calculation of equilibrium distances

Figure 4.3 represents a scheme for the linear arrangement in the cylindrical cavity mentioned earlier and the designation of the distances: a, a', b, d, e, f, g. The next step is to select or calculate the equilibrium values of these distances. The value of b, the distance between the center of a water molecule and the center of its permanent dipole moment, is 0.274Å; d-values (roughly the sum of the radii of the cation and a water molecule) for the Na^+ ion, the K^+ ion, the Rb^+ ion, and the Cs^+ ion are, respectively, 1.55Å, 1.57Å, 1.61Å, and 1.69Å greater than their respective Pauling crystal radii. Adding the average value of 1.61Å to the crystal radius of zero for proton and of 1.45Å for the ammonium ion (Ketelaar, 1953, Table 3E), we obtain an equilibrium d-value equal to 1.61Å for the H^+ ion and to 3.06Å for the ammonium ion. Substituting these into a_0 of equation 3 of Moelwyn-Hughes, we obtain the repulsion constant A with a value of 0.208×10^{-82} erg cm^9 for the H^+ ion and 35.0×10^{-82} erg cm^9 for the NH_4^+ ion. It now remains only to find the values of a, a', e, f, and g.

(*a*) *The distance g*. The g-value represents the center-to-center distance between the two water molecules distal to the anion (Figure 4.3). Since this distance is far removed

from the anionic charge we assume that it varies only with the nature of the cation and that it does not depend on the anion. Neglecting the less important terms, we solve for the equilibrium distance g by assuming d constant for each cation and equating the repulsion force to the combined cohesive forces* due to the dispersion energy and to the energy of interaction between ion and dipole. We obtain

$$\frac{9A}{g^{10}} = \frac{2\epsilon\mu_w}{(d+g+b)^3} + \frac{6\alpha_w\mu_w\epsilon}{(g+b)^4 d^2} + \frac{6\mu_w^2}{g^4} + \frac{54}{8}\frac{\alpha_w^2 U_w}{g^7} \tag{4-6}$$

where A represents the repulsion constant, equal to 14.14×10^{-82} erg cm^9 between a pair of water molecules; and the subscript w refers to the water molecule. The equation is then solved for the different cations with the results given in Table 4.1. These and following equations are solved by the method of successive approximation.

(*b*) *The distance e*. After similar simplification by neglecting less important terms, one obtains at equilibrium

$$\frac{9A'}{e^{10}} = \frac{\epsilon^2}{(e-c)^2} + \frac{2\alpha_-\epsilon^2}{e^5} + \frac{2\alpha_+\epsilon^2}{(e-c)^5} \tag{4-7}$$

where A' is the repulsion constant between a cation and the oxygen end of a water molecule; and the subscripts + and − refer to the cationic and anionic groups, respectively. Defining a variable k by the equation $e - c = ke$, we substitute ke for $(e - c)$. Rearranging the above equation, we obtain

$$e^8 + \left(2\alpha_- k^2 + \frac{2\alpha_+}{k^3}\right)e^5 - \frac{9A'k^2}{\epsilon^2} = 0 \tag{4-8}$$

which we then solve for different cations and different k-values. From the relation $e - c = ke$, we find the value of c that corresponds to each k-value; a plot of e versus c for each alkali-metal ion is shown in Figure 4.4.

(*c*) *The distances a and a′*. Letting $a - c = k'a$, we find that

$$\frac{9A}{a^{10}} = \frac{2\alpha_w\epsilon^2}{(k')^5 a^5} + \frac{2\mu_w\epsilon}{(k')^3\left(a - \frac{b}{k}\right)^3} + \frac{27}{2}\frac{\alpha_-\alpha_w U_- U_w}{U_- + U_w}\frac{1}{(k')^7 a^7} + \frac{\epsilon^2}{(k')^2\left(a + \frac{d}{k'}\right)^2}. \tag{4-9}$$

Calculations of a-values using the above equation, first with the smallest d-value for the H^+ ion and then with the largest d-value for the Cs^+ ion, show that these differences of d-value affect the a-value very little. We decided to use the average d-value of 2.68Å for all cation calculations and 2.68 + 2.7Å (2.7Å is the diameter of a water molecule) = 5.38Å for the calculation of all a'-values. The result is also given in Figure 4.4.

* Both the repulsion force and the combined cohesive forces are derived from equation (4-4) for the various energies and from the relation that the force between two interacting particles is equal to the derivative of the energy between them with respect to r, the distance of separation.

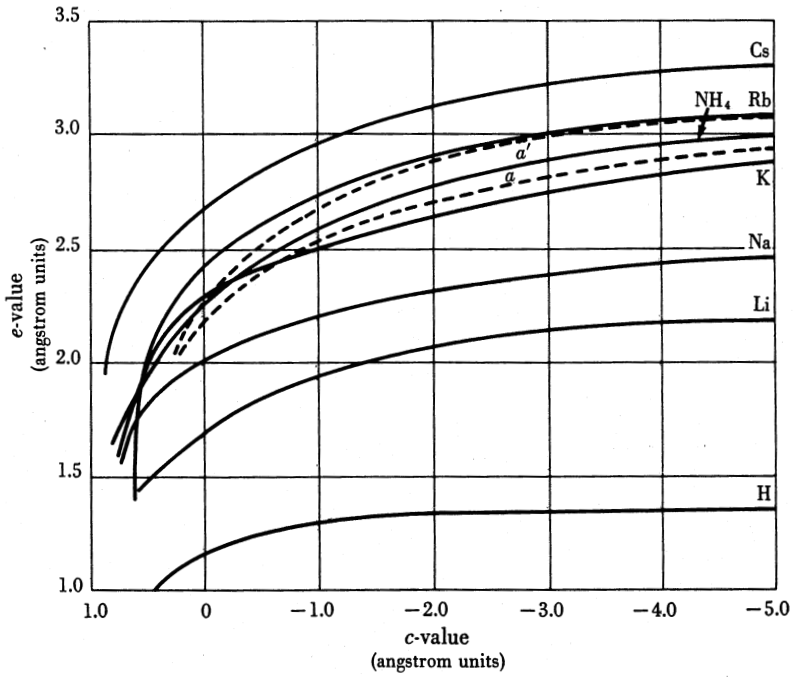

FIGURE 4.4. The relation between the c-value and the computed value of e, a, and a'. The equilibrium distance e between the centers of the fixed anion and the countercation in the 0-configuration is represented by the solid line. The dotted lines show the distances a and a' as functions of the c-value. Here a is the distance between the center of the fixed anion and the first water molecule in configuration I and a' is the analogous distance in configurations II and III.

(*d*) *The distance f.* Following the same reasoning as above, and again neglecting the lesser terms, we derive

$$\frac{9A}{f^{10}} = \frac{2\mu_w\epsilon}{(d+f)^3} + \frac{\epsilon^2}{(d+f+a-c)^2} + \frac{6\mu_w^2}{f^4} \qquad \textbf{(4-10)}$$

for configuration II. The same i-values were used for configuration III. The results are plotted in Figure 4.5.

(3) The calculation of the total potential energies of the various configurations

Having determined all the equilibrium distances, we calculate the total potential energies of the various configurations. In summing the individual terms, we neglect a particular term in equation (4-4) only after computing that term for each cation and finding that the term for the ion with the highest value is less than 0.15 kcal/mole. The total energy for each ion at each c-value is then plotted against the c-value after subtracting the value $n \times$ 4.98 kcal/mole; here n represents the number of water molecules inserted between the cation and the anion for that configuration and 4.98 kcal/mole corresponds to the energy

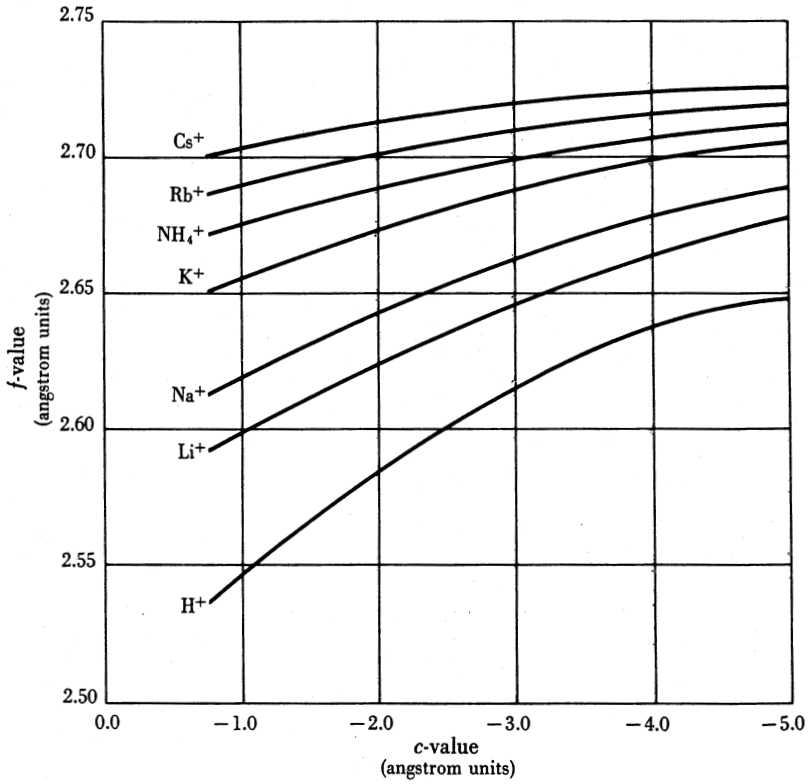

FIGURE 4.5. The relation between the *c*-value and the computed value of *f*. The distance between the first and second water molecules in configurations II and III is represented by *f*.

needed to bring a water molecule from pure liquid water at an infinite distance into the linear array.*

Figures 4.6, 4.7, and 4.8 plot the computed energies of the various configurations of the different ions against the *c*-value. In Figure 4.6, the polarizability of the oxyacid group is assumed to be 0.876×10^{-24} cm^3; in Figure 4.7, 1.25×10^{-24} cm^3; and in Figure 4.8, 2.0×10^{-24} cm^3.

(4) The calculation of the contributions of different configurations

For each ion at a particular *c*-value, one configuration represents a state of lowest energy. In general, the relationship for each ion is such that at lower *c*-values the higher configuration with a greater number of water molecules intervening between the fixed anion and the countercation is preferred. As the *c*-value increases, the preference is shifted to lower

* Each oriented water molecule possesses a total energy equal to the latent heat of vaporization (9.955 kcal/mole) minus *RT* (0.582 kcal/mole at 20°C). Each water molecule has four "half bonds" (coordination number = 4. each bond counted twice) of 2.489 kcal/mole each. We assume that two of these half bonds are altered in transplanting one water molecule to the linear array.

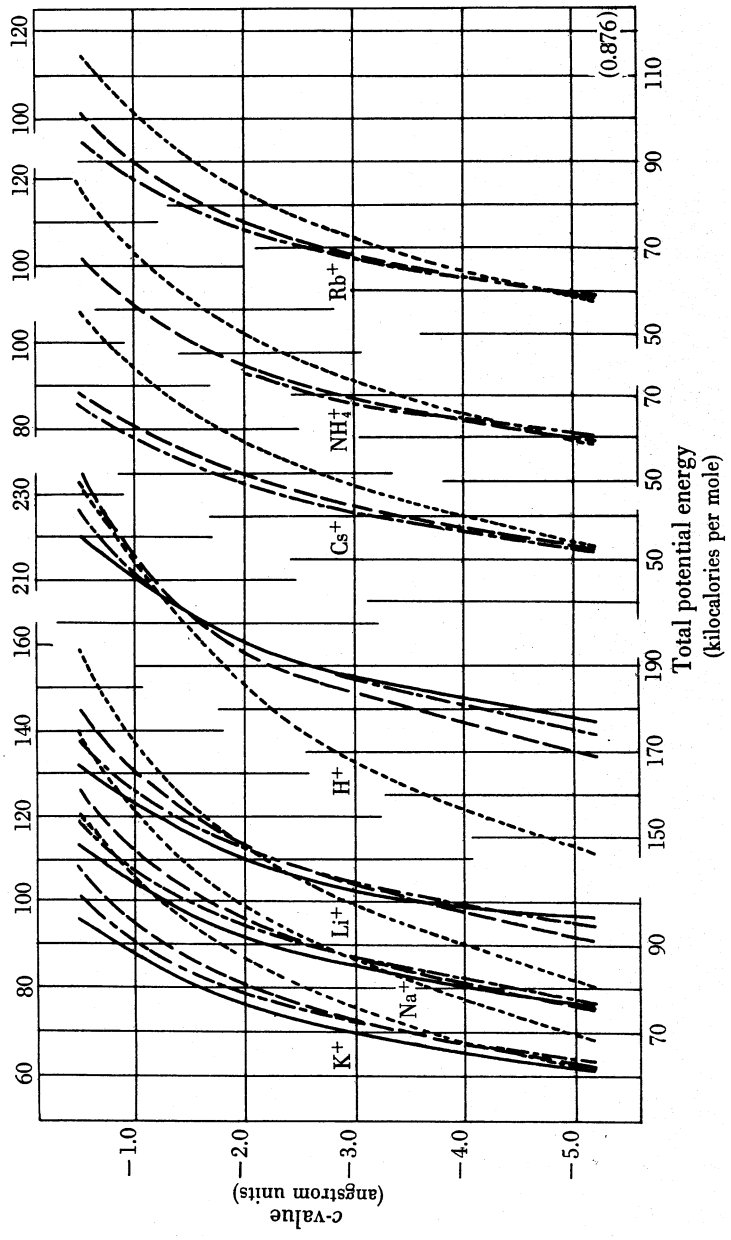

FIGURE 4.6. The variation of the total potential energy $\mathcal{U}$ of the fixed anion-countercation-water systems as a function of the c-value at 0°K. In this figure, the fixed anion has a polarizability of 0.876×10^{-24} cm^3. Values are plotted for each cation in each of the configuration 0 – – – –, I — — —, II – — – —, III ——.

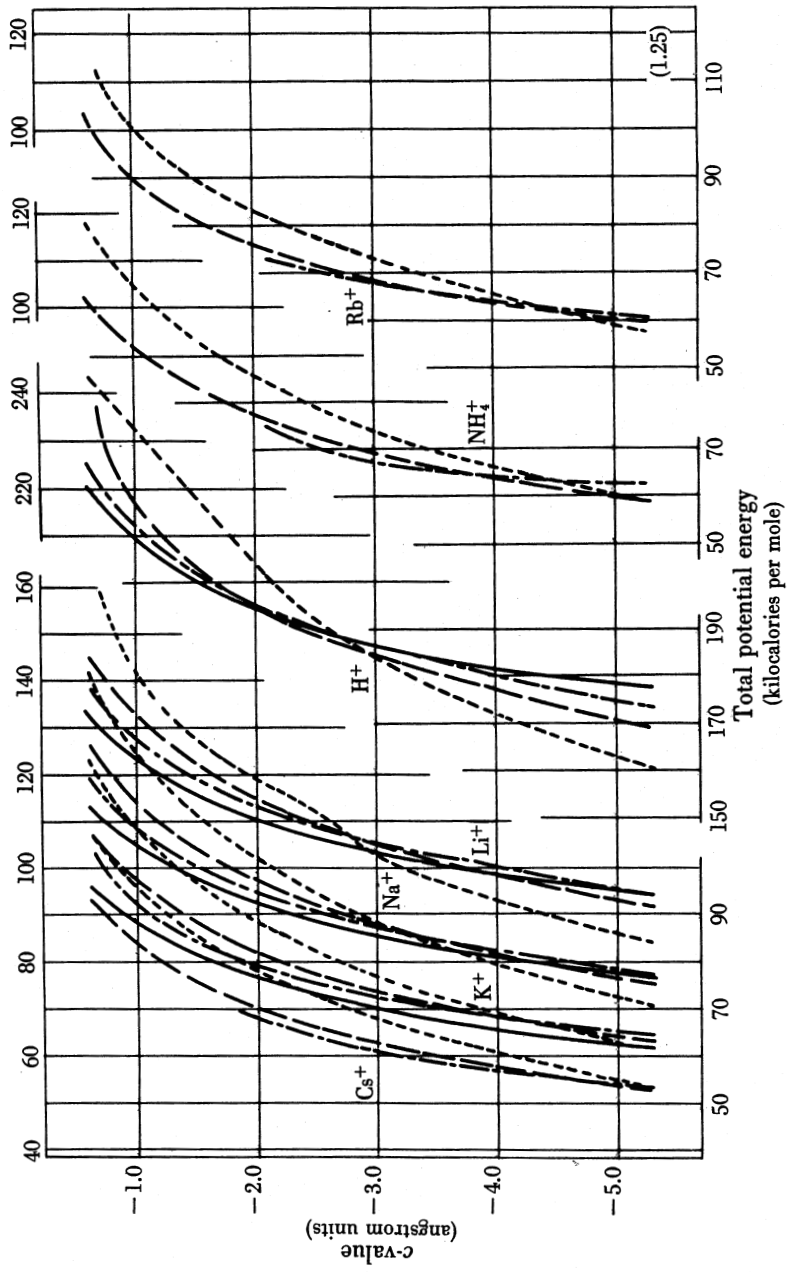

FIGURE 4.7. The variation of the total potential energy ^0U of the fixed anion-countercation-water systems as a function of the c-value at 0°K. In this figure, the fixed anion has a polarizability of 1.25×10^{-24} cm^3. Values are plotted for each cation in each of the configuration 0 – – – –, I — — —, II – — – —, III ——.

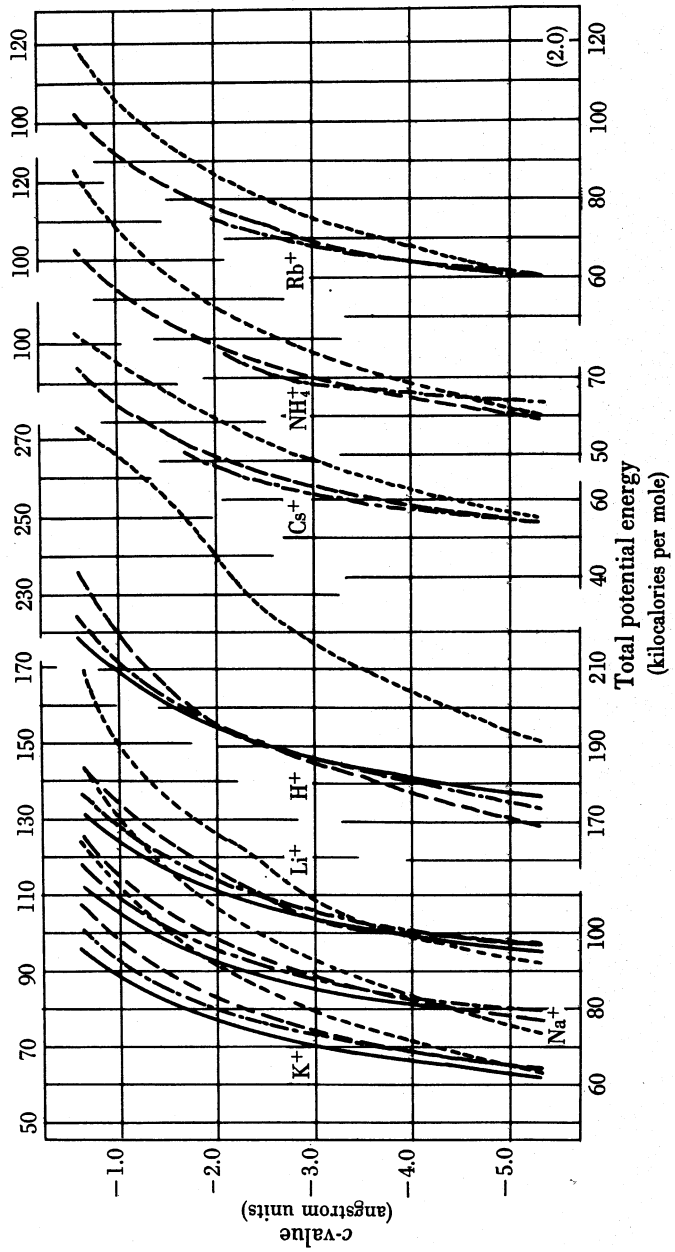

FIGURE 4.8. The variation of the total potential energy $\mathcal{U}$ of the fixed anion-countercation-water systems as a function of the c-value at 0°K. In this figure, the fixed anion has a polarizability of 2.0×10^{-24} cm^3. Values are plotted for each cation in each of the configuration 0 – – – –, I — —, II – — – —, III ——.

and lower configurations until eventually, at the highest c-value, the 0-configuration is invariably the preferred one. This trend is followed by each ion, although the c-value at which the preference changes from one configuration to another varies from ion to ion.

From Appendix B, we derive for the species p_i

$$\frac{n_i^s}{\sum_{s=0,I,II,III} n_i^s} = \frac{(\mathbf{p.f.})_i^s \exp(-\mathcal{U}_i^s/RT)}{\sum_{s=0,I,II,III} (\mathbf{p.f.})_i^s \exp(-\mathcal{U}_i^s/RT)} \tag{4-11}$$

where n_i^s is the number of p_i ions in a particular configuration s; $(\mathbf{p.f.})_i^s$ is the partition function for that ion in that configuration; and $\mathcal{U}_i^s$ is the total energy of the ith ion assembly in configuration s.

If we assume that only the configurational partition function varies significantly among the associated ions (see Section 2.4), the relative distribution of the same ion p_i in the different configurations would be

$$\frac{n_i^s}{\sum_{s=0,I,II,III} n_i^s} = \frac{\rho_i^s \exp(-\mathcal{U}_i^s/RT)}{\sum_{s=0,I,II,III} \rho_i^s \exp(-\mathcal{U}_i^s/RT)}. \tag{4-12}$$

where ρ_i^s is the number of sites (see Section 2.4A) available to p_i in configuration s, a function of the species of the ion, its configuration, and the c-value as shown in Figures 4.6 to 4.8. If r_i^s is the equilibrium distance from the center of p_i in configuration s to the center of gravity of the negative charges $(r_f - c)$, on first approximation the ion may be assumed to be constrained to move within a spherical shell of radius r_i^s and thickness h. We make the further assumption that the empirical equation

$$h = \left(\frac{RT}{\mathcal{U}}\right)^{1/2} \text{Å}$$

which holds for almost all diatomic molecules, also applies to the fixed anion-counterion pair (see Mayer and Mayer, 1940). In this equation, $\mathcal{U}$ stands for the absolute magnitude of the energy of the bond and one may write for ion p_i in configuration s

$$\rho_i^s = 4\pi \left(\frac{RT}{\mathcal{U}_i^s}\right)^{1/2} (r_i^s)^2.$$

Substitution into equation (4-12) yields

$$\frac{n_i^s}{\sum_{s=0,I,II,III} n_i^s} = \frac{[(r_i^s)^2/(\mathcal{U}_i^s)^{1/2}] \exp(-\mathcal{U}_i^s/RT)}{\sum_{s=0,I,II,III} [(r_i^s)^2/(\mathcal{U}_i^s)^{1/2}] \exp(-\mathcal{U}_i^s/RT)}. \tag{4-13}$$

In the present case, since only those configurations with the greatest (negative) total energies count, the ratio of $(\mathcal{U}_i^s)^{1/2}$ for two such configurations is always close to unity; hence

$$\frac{n_i^s}{\sum_{s=0,I,II,III} n_i^s} = \frac{(r_i^s)^2 \exp(-\mathfrak{U}_i^s/RT)}{\sum_{s=0,I,II,III} (r_i^s)^2 \exp(-\mathfrak{U}_i^s/RT)}. \quad (4\text{-}14)$$

This equation gives us the percentages of different configurations of the ion-fixed-charge pair at a particular value of c.

B. CALCULATION—PART II. THE CALCULATION OF THE ASSOCIATION ENERGIES OF VARIOUS IONS AT DIFFERENT c-VALUES

The problem of ionic association is always ambiguous because it depends intimately upon the definition of a state of association and the definition of a state of dissociation. The problem becomes even less clear when we deal with a fixed-charge system in equilibrium with a free solution. In this case, the dissociation of a counterion-fixed-charge pair could mean the assumption of a new position by the dissociated counterion either inside or outside the fixed-charge system. If it migrates out of the fixed-charge system, the process is complicated by the development of surface potentials (see Section 10.2 on cellular potential). Further, the association energy depends, in general, on both the spatial position of the counterion in the fixed-charge system and the history of the fixed-charge system itself. To eliminate these complications, we regard as associated any counterion that assumes one of configurations 0, I, II, or III. The fixed-charge system with its complete assortment of counterions is then broughi from 0°K to the ambient temperature. We now define the association energy, ΔE, to be the difference between the energy of the associated counterion and the energy of the first counterion that diffuses out of the fixed-charge system to an infinite distance in an infinitely dilute aqueous phase. This energy is not significantly different from that obtained if we compare the associated counterion in configuration 0, I, II, or III with a similar counterion in a hypothetical "beyond III" configuration within the fixed-charge system. The limit of association (equivalent to r_2 of Section 2.4A) in this case refers to the radius at which there is a sharp increase in the dielectric coefficient of the medium such that a volume of water which is not dielectrically saturated intervenes between the two charged particles (see Ling, 1952, inset of Figure 6).

Taking into account the freezing-in of the water molecules between the fixed ion and its counterion (Section 4.2B), we calculate the association energy by evaluating the work performed when the counterion is brought from infinity through a medium having the dielectric properties of water into a microcell at the equilibrium distance which that particular ion assumes. Instead of using a macroscopic dielectric coefficient, we take Debye's value for the dielectric coefficient $D(r)$ at a distance r from the center of a univalent ion.* In the present case, however, the sharp increase of dielectric coefficient with increase of r does not begin until r corresponds to a distance three water molecules away from the anion. Thus, within a region of 8.1Å (3 × 2.7Å) between the cation and anion in configuration III, we assume a uniform dielectric constant of three.

The energy of association of each ion at each c-value is then

* No significant variation would be created if the curve of Grahame (1950) or of Hasted *et al.* (1948) were used for the rising part of the effective dielectric coefficient.

$$\Delta E = \sum_{s=0,I,II,III} \frac{n_i^s}{\sum_{s=0,I,II,III} n_i^s} \int_{r_i}^{\infty} -\frac{\epsilon^2}{D(r)r^2}\, dr \qquad (4\text{-}15)$$

where $n_i^s \Big/ \sum_{s=0}^{III} n_i^s$ is given by equation (4-14). In Figures 4.9 to 4.11, the computed association energies of the various cations against anions of differing *c*-values are presented. For Figure 4.9, the polarizability of the oxyacid functional group is taken to be 0.876×10^{-24} cm^3; for Figure 4.10, as 1.25×10^{-24} cm^3; and for Figure 4.11, as 2.0×10^{-24} cm^3. We believe that Figure 4.9 gives the closest approximation to ion interaction with biological fixed-charge systems; most of this discussion will be based on this figure.

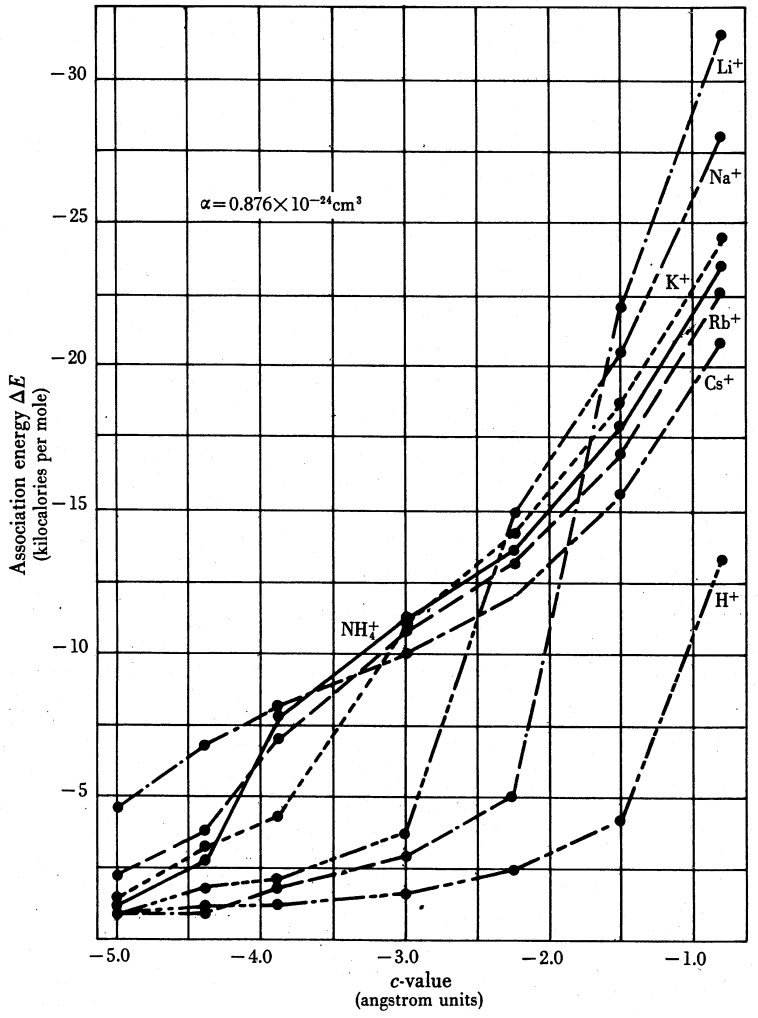

FIGURE 4.9. The relation between the calculated association energy ΔE of various cations and the *c*-value of the anionic group. The polarizability α is 0.876×10^{-24} cm^3.

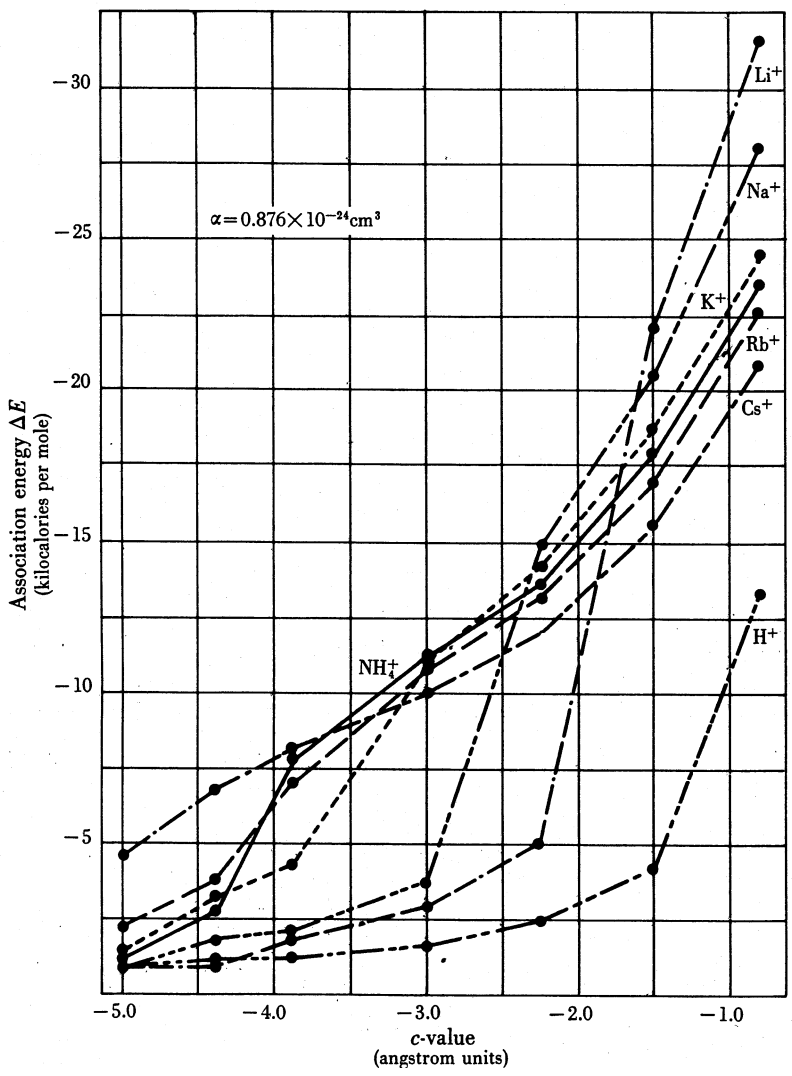

FIGURE 4.10. The relation between the calculated association energy ΔE of various cations and the c-value of the anionic group. The polarizability α is 1.25×10^{-24} cm^3.

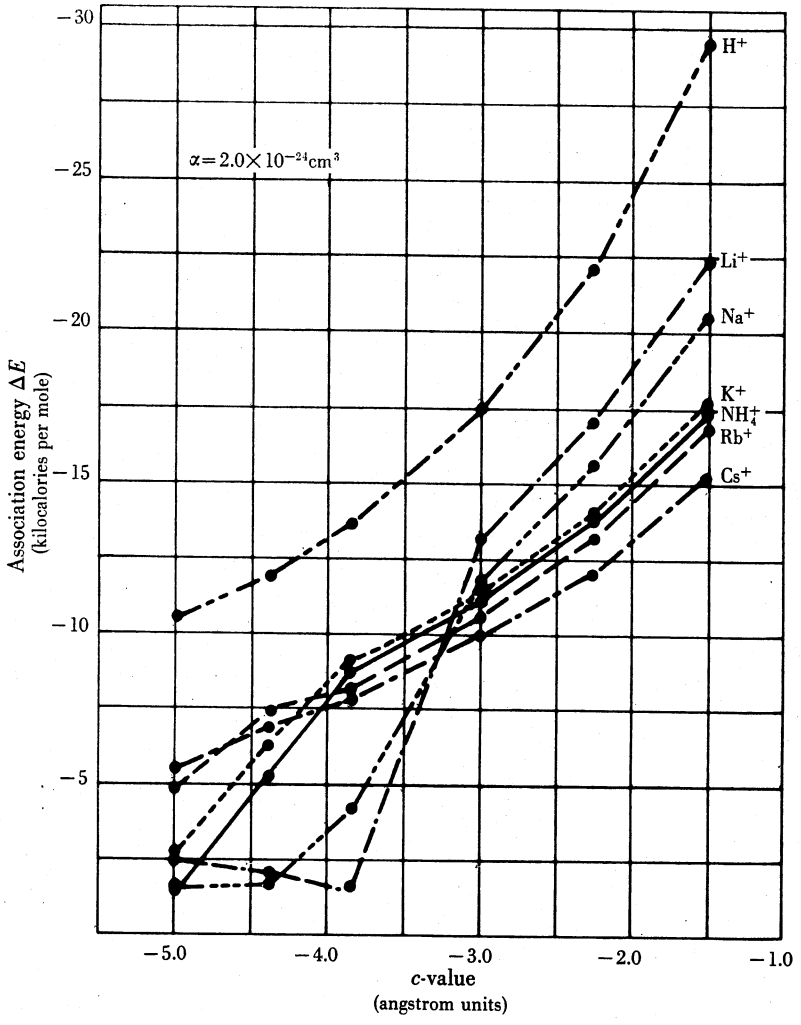

FIGURE 4.11. The relation between the calculated association energy ΔE of various cations and the c-value of the anionic group. The polarizability α is 2.0×10^{-24} cm^3.

4.4. Discussion and Comment on the Present Model

A. THE TENTATIVE NATURE OF THE ABSOLUTE *c*-VALUE AND ASSOCIATION ENERGIES

The adoption of the present linear model is a concession to the forbidding complexity associated with a three-dimensional model. Since transforming the linear model to a three-dimensional model would involve symmetrical changes only, one would not expect the ΔE-versus-c-value plot to involve any disorderly disturbance of the relations calculated, but only changes of absolute magnitude.

The linear model does discriminate against the higher configurations. Thus the calculation of the total energies of the 0-configuration would be virtually the same in the linear as in a three-dimensional model. On the other hand, for configurations I, II, and III, the energies calculated are a great deal less in the linear model than they would be in a three-dimensional one; in these higher configurations, a large part of the energy arises from the interactions between the ions and water molecules and these water molecules are obviously coordinated in three dimensions. In the linear model, therefore, only a fraction of the coordinated water molecules is taken into account; the higher the configuration the greater the discrepancy.

Another aberration is created by the adoption of the Born charging method for the determination of association energies. The assumption that the total hydration energy of the ions remains the same in the dissociated and associated states is implicit in this procedure. This assumption is closer to the truth for ions in the higher configurations than for ions in the 0-configuration. If we neglect the partial loss of ion-water interaction in the 0-configuration the calculation overestimates the 0-configuration energy. Consequently, (1) the aberration from the first part of the calculation is accented and this causes the crossover points to fall on lower c-values than they should, and (2) the dissociation energy at high c-values is overestimated.

When the three-dimensional model is developed, we do not expect the shape of the ΔE-versus-c-value plot to he changed significantly; but the c-values should be much higher than the present tentative values which we have calculated. One must remember that the c-value, as defined, is not a spatial location of a particular electron; thus, comparison of its value with, say, the diameter of an oxygen atom is quite meaningless and leads to erroneous conclusions.

The heat of hydration in kcal/mole is 114.6 for Li^+, 89.7 for Na^+, 73.5 for K^+, 67.5 for Rb^+, and 60.8 for Cs^+ (Latimer *et al*, 1939). The coordination numbers of these ions range from 6 for Li^+ to 2 for Cs^+ (B. E. Conway, 1952, Table III, p. 53). The overestimation of the energy of the 0-configuration thus consists essentially of one-sixth to one-half of the heat of hydration, a value that ranges from −20 to −30 kcal/mole. Therefore, the corrected association energies for the alkali-metal and ammonium ions at high c-values should have values no greater than −20 kcal/mole. For a rough quantitative estimation involving these association energies, we halve the calculated association energies. Figure 4.12 shows the distribution ratios (with K^+ as the reference ion) for an anion polarizability equal to 0.876×10^{-24} cm^3. (Compare with Figure 4.13, where the uncorrected values were used.)

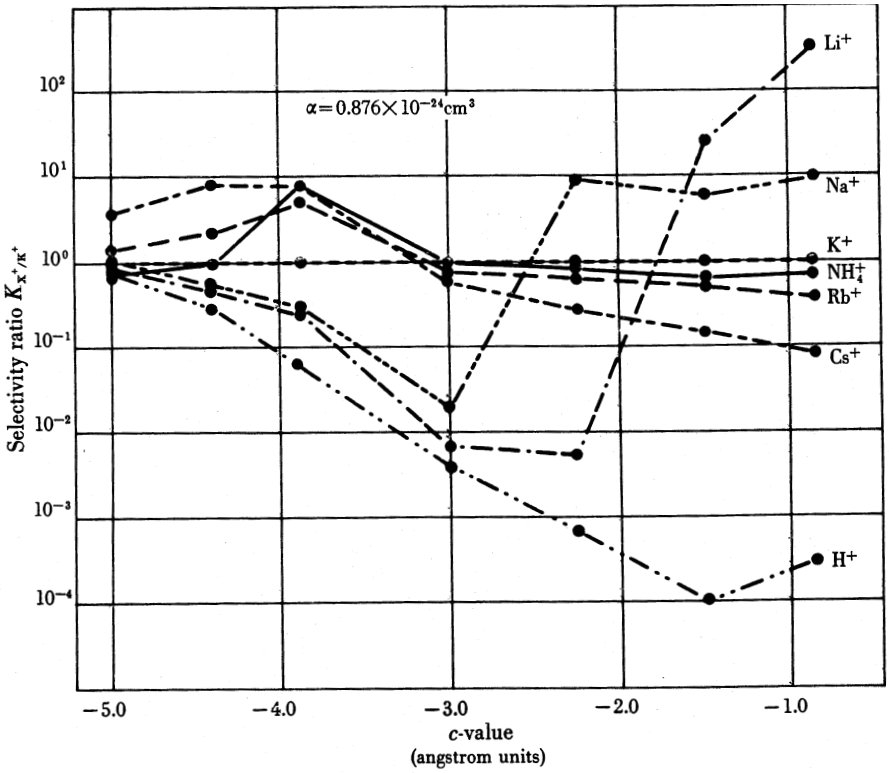

FIGURE 4.12. The relation between the selectivity ratios of various cations and the *c*-value. The K^+ ion is taken as unity and selectivity ratios are calculated from the association energies given in Figure 4.9, divided by 2 (see Section 4.4A).

B. INTERNAL ENERGY COMPARED WITH FREE ENERGY

Calculated as work, the association energy ΔE is equivalent to a standard free energy of association in a dilute salt solution. It does not correspond to the standard free energy of association in a fixed-charge system because a large positive entropy of dissociation that is not included in the free energy found by the Born charging method contributes greatly to the true free energy of adsorption. This large entropy change arises from the configurational- and rotational-entropy gain experienced by a counterion when it is taken from the associated state in a fixed-charge system to the dissociated state in free solution. The free energy that we obtained approximates the association energy ΔE more closely than the free energy of association ΔF. Since we are interested primarily in the relative values of the association energies with reference to other counterions, we do not need the absolute ΔF and have not attempted to calculate it.

C. THE HYDROGEN ION

Although the O—H bond in an alcoholic group is almost entirely nonionic, resonance greatly increases the ionic nature of the O—H bond in the carboxylate ion (Pauling, 1948; Branch and Calvin, 1941). In the present treatment, we do not take account of the covalent

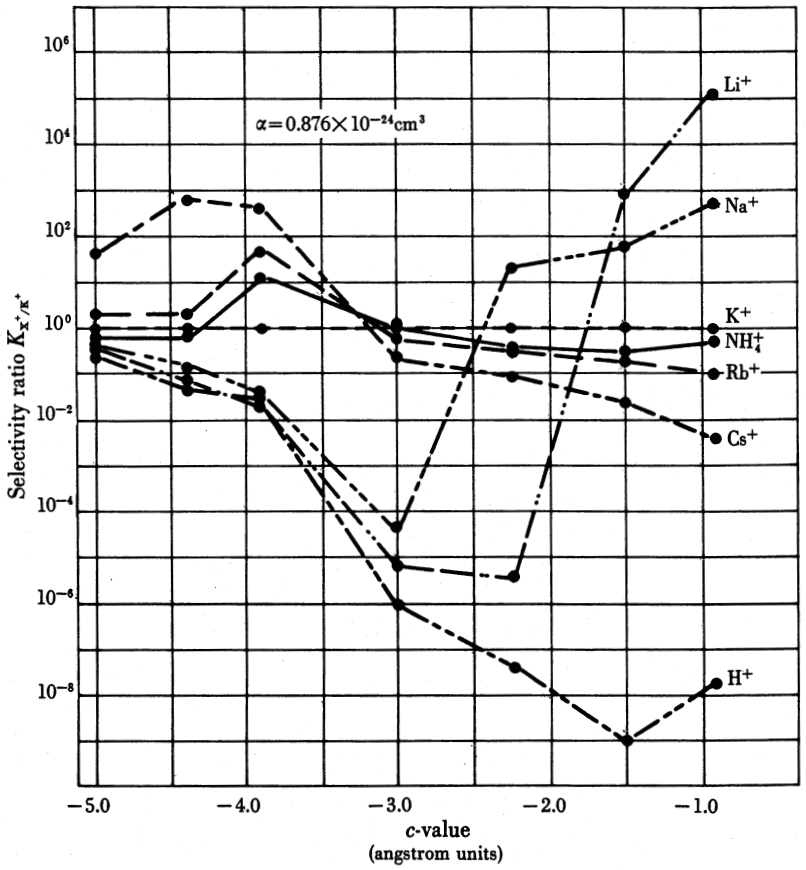

FIGURE 4.13. The relation between the selectivity ratios of various cations and the *c*-value. The K^+ ion is taken as unity and selectivity ratios are calculated from the association energies given in Figure 4.9. Here, the anionic polarizability is 0.876×10^{-24} cm^3. The assumption is made that all ions are completely associated and that there is no difference among the partition functions of the various adsorbed states (configurations) other than the configurational entropy.

contribution to the bond between the H^+ ion and the carboxyl oxygen; we assume that it is constant with respect to variation in *c*-value. This is justified. The *p*K's of a list of oxyacids vary from less than 1 (HIO_3) to 11 (HPO_4). Kossiakoff and Harker (1938) showed that variation in the nonexchange electrostatic part of the interaction energy alone can produce this wide *p*K variation. Thus the dissociation of an oxyacid with a *p*K-value between 1 and 11 may involve little additional contribution due to variation of the exchange energy. Bregman (1953) has shown that the sulfonic ion exchange resin (which has an average *p*K-value of about 1.6 for its sulfonate radicals) selects alkali-metal ions in the order $Cs^+ > Rb^+ > K^+ > Na^+ > Li^+$, whereas a carboxylic resin (with a *p*K-value of about 6.0) selects them in the reverse order, $Li^+ > Na^+ > K^+$ (see Chapter 9). This shows that the range of *c*-value variation corresponding to *p*K-value variation from 1.6 to 6.0 includes roughly the entire range of *c*-value variation for which we have made calculations. The wider range of variation that Kossiakoff and Harker demonstrated to be dependent only

on electrostatic variation assures us that it is safe to assume that variation of the covalent contribution has very little effect on variation of the acid dissociation within the *p*K range of interest to us.

The constancy of the covalent contribution does not reflect its magnitude. Although this constancy makes comparison between ΔE-values calculated at varying *c*-values valid, the absolute value for ΔE may not be so reliable. Neglecting the exchange energy has two untoward effects: (1) the 0-configuration is de-emphasized, and (2) the association energy is reduced. Thus, if we were to evaluate it properly for a particular ionic group, the exchange energy would be added to the 0-configuration both in the calculation of the total energies of the system (step I) and in the electrostatically calculated association energy (step II). The net result of adding the exchange-energy contributions may be simulated by increasing the polarizability value α of the anionic group, a change which primarily affects the 0-configuration. The result of this manipulation differs little from the change brought about by transposing the H^+-ion curve from Figure 4.10 (or even from Figure 4.11, with the higher polarizability) to Figure 4.9, without disturbing the values of the curves of the other ions.

D. THE STATISTICAL INTERPRETATION OF THE MEANING OF "HYDRATED IONIC RADII" IN THE CLASSICAL LYOTROPIC SERIES

At the lowest *c*-value, the free energy of association follows the same order as the classical lyotropic (Hofmeister) series, $Cs^+ > Rb^+ > K^+ > Na^+ > Li^+$; this order was found to depict the relative effectiveness of the action of these ions on colloidal systems as well as their mobilities in dilute aqueous solution (Hofmeister, 1888; Höber, 1945). From the point of view of the present theory, this is due entirely to the statistical nature of the number of water molecules found between the cation and the fixed anion. Thus if the same number of water molecules intervenes between the different cations and the same anion, the cation with the smallest crystal radius will always have the highest free energy of association. In fact, however, at the lowest *c*-value, the largest ion (Cs^+) has the highest energy of association because, statistically, it prefers to have fewer water molecules between it and the anion.

The water molecules between the cation and the anion clearly do not belong, as hydration water, to either the cation or the anion, exclusively. If we arbitrarily assign these water molecules to the cation only, the statistical nature of the water of hydration would explain the fact that a hydrated ion may have a radius only a fraction of an angstrom unit larger than its crystal radius although the water molecule has a diameter of 2.7Å. To calculate the hydrated diameter of a cation, one must include the crystal radius of the cation plus the statistical number of water diameters. For $c = -5.0$Å* and $\alpha = 0.876 \times 10^{-24}$ cm^3, given 2.7Å as the diameter of each water molecule, the theoretical, curve would give the hypothetical hydrated cation diameters: Li^+, 8.57Å; Na^+, 7.10Å; K^+, 6.67Å; Rb^+, 5.64Å; and Cs^+, 3.52Å.

The order of this series is the same as that in the classical lyotropic series. As the *c*-value changes, the relative preference for different counterions also changes. This variation includes both a reversal of preference for one or another of a pair of cations (for

*The hydrated radii of dissociated cations in free solution correspond to the case in which $c \to -\infty$. To approximate this condition the lowest value of *c* equal in our calculation to −5.0Å has been chosen for illustration.

example, a system may go from a class for which $Na^+/K^+ < 1$ to a class for which $Na^+/K^+ > 1$), and a wide variation in the selectivity coefficient within any class of preferences. Thus, in a mixture of Na^+ and K^+ at a given *c*-value (let it fall within the range that gives $Na^+/K^+ < 1$) the countercation population would be represented by both K^+ ions and Na^+ ions in all configurations. However, K^+ ions would be selectively accumulated because statistically more Na^+ ions would assume higher configurations than K^+ ions and consequently the K^+ ion would have a higher association energy. Conversely, there are high *c*-values at which there is no water between most of the Na^+ ions and the fixed anions (configuration 0), while K^+ ions remain mostly in configurations I and II. The selectivity coefficient for Na^+/K^+ would be very much higher ($Na^+/K^+ >> 1$) than at the *c*-values discussed above. At very high *c*-values, both K^+ and Na^+ assume the 0-configuration and the absolute energies of association are much higher; however, the Na^+/K^+ ratio again decreases because the interconfigurational advantages have vanished. But the ratio cannot fall to unity because the crystal radius of Na^+ is smaller than that of K^+.

E. THE IMPORTANCE OF THE PHYSICAL PROPERTIES OF WATER

It is perhaps obvious that the physical properties of the water molecules intervening in the various configurations are of critical importance because of their effect on short-range interactions. Thus the substitution of deuterium oxide (D_2O) for water (H_2O) affects acid dissociation constants, as mentioned in the introduction, and has a profound effect on the *c*-value versus total-potential-energy plots of the various ions in Figures 4.6 to 4.8. Such changes in interaction energies are the basis of the functional and morphological changes of cells kept in D_2O media, discussed on page xxviii.

F. THE CRITICAL IMPORTANCE OF AN OPTIMAL MICROCELL SIZE

Very high selectivity ratios have been calculated for the ratios of K^+, NH_4^+ Rb^+, or Cs^+ to Na^+ or Li^+ at various *c*-values. The reason is that at these *c*-values, Li^+ and Na^+ ions prefer high configurations, whereas K^+, NH_4^+, Rb^+, and Cs^+ ions prefer low configurations. A high configuration subsumes a sufficient microcell volume to permit a sizable number of water molecules around the ion pairs. If the fixed ionic sites are too close together, the preference for the higher configurations by, say, Na^+ or Li^+, is lost and the selectivity ratio falls. If the microcell is excessively large, the counterions will be dissociated and there will then be a loss of ionic selectivity. Thus, for optimal selectivity, a microcell is needed in which, for the particular association energies involved, there will he both a high degree of ionic association and sufficient water to allow the assumption of the higher configurations. It seems that nature has anticipated this need by providing living cells with an average microcell 20Å in diameter, and by providing effective charge fixation with a profusion of anchoring sites in the form of H-bonding and ionic groups.

G. THE OPTIMAL c-VALUE FOR MAXIMUM SELECTIVITY

Given an optimal microcell size, one can calculate the theoretical selectivity ratios for a particular pair of ions from the association energies given in Figures 4.9 to 4.11. Results of such calculations are illustrated in Figure 4.13, which demonstrates that for the maximal ratio of, say, Na^+/K^+, a particular range of optimal *c*-values exists. Variation in *c*-value beyond this range in either direction causes a decline in selectivity.

BIBLIOGRXPHY

BOOKS AND MONOGRAPHS

I. Molecular Forces

Debye, P., "Polar Molecules." Chemical Catalog Co., New York, 1929. Contains an important discussion of dielectric saturation of polar solvents.

Kortüm, G., and Bockris, J. O'M., "Textbook of Electrochemistry," Vol. I. Elsevier, Amsterdam and New York, 1951. Contains a lucid presentation of the forces in an ionic crystal.

London, F., The general theory of molecular forces. *Trans. Faraday Soc*. 33, 8–26 (1937).

II. Induction

Branch, G. E. K., and Calvin, M., "The Theory of Organic Chemistry, An Advanced Course." Prentice-Hall, Englewood Cliffs, New Jersey, 1941. In Chapter 4, modes of interaction of substituent groups of chemical compounds are briefly presented. In Chapter 6, resonance, polarizability, and inductive effects, are extensively discussed with respect to their effects on acid strength at equilibrium.

Cohn, E. J., and Edsall, J. T., eds., "Proteins, Amino Acids, and Peptides as Ions and Dipolar Ions." Reinhold, New York, 1943. Chapter 5 contains a discussion similar to that of Branch and Calvin on the effects of substituent groups on acid strength except that amino acids and peptides are primarily considered. Also included in this chapter are discussions of the theories of Bjerrum and Kirkwood and Westheimer on the effects of group substitution on acidity.

Ingold, C. K., "Structure and Mechanism in Organic Chemistry." Cornell Univ. Press, Ithaca, New York, 1953. The author, who has made very important contributions to the development of the induction theory, presents a complete theory of organic reactions. Chapter 2 on interaction between and within molecules is particularly useful to those not familiar with this subject.

Springall, H. D., Modern physico-chemical views on acids and bases and their application to organic substances, *in* "Chemistry of Carbon Compounds" (E. H. Rodd, ed.), Vol. 1, Part A, pp. 99–106. Elsevier, Amsterdam and New York, 1951. A review of the historical development of the induction theory through the important work of the British chemists, Ingold, Lapworth, Robinson, etc.

REVIEWS AND ORIGINAL ARTICLES

Bernal, J. D., and Fowler, R. H., A theory of water and ionic solution, with particular reference to hydrogen and hydroxyl ions. *J. Chem. Phys*., 1, 515–548 (1933).

Bjerrum, N., Untersuchungen über Ionenassoziation. I. Der Einfluss der Ionenassoziation auf die Aktivität der Ionen bei mittleren Assoziationsgraden. *Kgl. Danske Videnskab. Selskab, Mat.-fys. Medd*. 7, No. 9, 1–48 (1926).

Ling, G., The role of phosphate in the maintenance of resting potential and selective ionic accumulation in frog muscle cells, *in* "Phosphorus Metabolism" (W. D. McElroy and B. Glass, eds.), Vol. II, pp. 748–954. Johns Hopkins Press, Baltimore, 1952. The original version of the present association-induction hypothesis.

References for Appendix I

Bernal, J.D. and Fowler, R.H. (1933) *J. Chem. Phys. 1*: 515.

Bjerrum, N. (1926) *Kgl. Danske Videnskab. Selskab, Mat.-fys. Medd. 7*, No. 9, 1.

Born, M. (1920) *Z. Physik. 1*:45.

Born, M. and Mayer, J.E. (1932) *Z. Physic. 75*:1.
Branch, G.E.K. and Calvin, M. (1941) *The Theory of Organic Chemistry, An Advanced Course,* Prentice-Hall, Englewood Cliffs, NJ.
Bregman, J.I. (1953) *Ann. N.Y. Acad. Sci. 57*: 125.
Bregman, J.I. (1952) *J. Am. Chem. Soc. 74*: 1867.
Bungenberg de Jong, H.G. (1949) In: *Colloid Science*, (H.R. Kruyt, ed.), Vol. II, Elsevier, Amsterdam and New York, p.287.
Conway, B.E. (1952) *Electrochemical Data*, Elsevier, Amsterdam and New York.
Debye, P. (1929) *Polar Molecules*, Chemical Catalog Co., New York.
Edsall, J.T. and Blanchard, M.H. (1933) *J. Am.Chem. Soc. 55***:** 2337**.**
Eisenman, G. (1962) *Symposium on Membrane Transport and Metabolism*, (S. Kleinzeller and A. Kotyk, eds.), Academic Press, New York.
Eisenman, G., Rudin, D.O. and Casby, J.U. (1957) *Science 126*: 831.
Fowler, R.H. and Guggenheim, E.A. (1939) *Statistical Thermodynamics*, Cambridge Univ. Press, London and New York.
Grahame, D.C. (1950) *J. Chem.Phys. 18*: 903.
Harned, H.S. and Owen, B.B. (1958) *The Physical Chemistry of Electrolyte Solutions,* 3rd Ed., Reinhold, New York.
Hasted, J.B., Ritson, D.M. and Collie, C.H. (1948) *J. Chem. Phys. 16*: 1.
Hermans, P.H. (1954) *Introduction to Theoretical Organic Chemistry,* (edited and revised by R.E. Reeves), Elsevier, Amsterdam and NewYork.
Höber, R. (1945) *Physical Chemistry of Cells and Tissues*, McGraw-Hill (Blakiston), New York.
Hofmeister, F. (1888) *Naunyn-Schmiedebergs Arch. Exptl. Pathol. u. Pharmakol. 24*: 247.
Ingold, C.K. (1953) *Structure and Mechanism in Organic Chemistry*, Cornell Univ. Press, Ithaca, NY.
Isard, J.O. (1959) *Nature 184*: 1616.
Jenny, H. (1932) *J. Phys. Chem. 36*: 2217.
Ketelaar, J.A.A. (1953) *Chemical Constitution: An Introduction to the Theory of the Bond*, (transl. by L.C. Jackson), Elsevier, Amsterdam and New York.
Kortüm, G. and Bockris, J.O'M. (1951) *Textbook of Electrochemistry*, Elsevier, Amsterdam and New York.
Kossiakoff, A. and Harker, D. (1938) *J. Am. Chem. Soc. 60*: 2047.
Latimer, W.M. (1952) *The Oxidation States of the Elements and Their Potentials in Aqueous Solutions*, 2nd Ed., Prentice-Hall, Engelwood Cliffs, N.J.
Latimer, W.M., Pitzer, K.S. and Slansky, C.M. (1939) *J. Chem. Phys. 7*:108.
Lennard-Jones, J.E. (1936) In: *Statistical Mechanics*, 2nd Ed., (R.H. Fowler, ed.), Cambridge Univ. Press, London and New York.
Lewis, G.N. (1916) *J. Am. Chem.Soc. 38*: 762.
Lewis, G.N. (1923) *Valence and Structure of Atoms and Molecules*, Chemical Catalog Co., New York.
Ling, G.N. (1951) *Am. J. Physiol. 167*: 806.
Ling, G.N. (1952) In: *Phosphorus Metabolism*, Vol.II, (W.D. McElroy and B. Glass, eds.), Johns Hopkins Press, Baltimore, MD, p.748.
Ling, G.N. (1957) *Federation Proc. 16*: 81.
Lorenz, R. and Posen, I. (1916) *Z. anorg. U. allgem. Chem. 94*: 265.
Mayer, J.E. (1933) *J. Chem. Phys. 1*: 270.
Mayer, J.E. and Mayer, M.G. (1940) *Statistical Mechanics*, Wiley, New York,
Moelwyn-Hughes, E.A. (1949) *Proc. Cambridge Phil. Soc. 45*: 477.
Mulliken, R.S. (1933) *J. Chem. Phys. 1*: 492.
Pauling, L. (1948) *The Nature of the Chemical Bond*, Cornell Univ. Press, Ithaca, NY.
Sack, H. (1926) *Physik. Z. 27*: 206.
Sack, H. (1927) *Physik. Z. 28*: 199.
Searcy, A.W. (1949) *J. Chem. Phys. 17*: 210.

Tilton, L.W. and Taylor, J.K. (1938) *J. Research Natl. Bur. Standards 20*: 419.
Verwey, E.J.W. (1942) *Rec. trav. chim. 61*: 127.
Webb, T.J. (1926) *J. Am. Chem. Soc. 48*: 2589.
Wiegner, G. and Jenny, H. (1927) *Kolloid. Z. 42*: 268.
Zief, M. and Edsall, S.T. (1937) *J. Am. Chem. Soc. 59*: 2245.

Physiol. Chem. Phys. & Med. NMR (2006) *38*: 147–155

Analysis of Homologous Derivatives of Cephalothin by Multivariate Methods for Clinical Efficacy

Ronald Bartzatt

University of Nebraska
College of Arts and Sciences
Department of Chemistry
Omaha, Nebraska 68182
E-mail: rbartzatt@mail.unomaha.edu

Abstract: This work presents the analysis of pharmacological properties of a homologous set of cephalothin derivatives formed after inserting an aliphatic ester substituent having from one to ten carbon atoms (ie. -CH_3 or -$CH2CH_3$) in place of the former carboxyl group (-C(O)OH). These compounds were shown to have significant correlations and associations in their properties after analysis by pattern recognition methods including cluster analysis, detrended correspondence analysis, and K-means cluster analysis. Formula weight of all derivatives is directly correlated and increases with molar volume, parachor, and molar refractivity. Index of refraction decreases as formula weight of derivatives increases. Polar surface area of all derivatives remains constant at 102.02 A^2 as formula weight increases. Partitioning between 1-octanol/water values of Log P increases as the length of the aliphatic ester group increases. The number of nitrogens, oxygens, -NH and -OH groups, remains constant for all derivatives remains the same at 2, 6, and 1, respectively. Homologs 1 to 7 (based on number carbon atoms of ester group) show zero violations of the Rule of 5, which indicates effective drug bioavailabilty. Values of polar surface area indicate that more than 25% of any derivative present in the intestinal system would be absorbed. The ethyl and propyl derivative of cephalothin have Log P values indicating efficient permeation of the central nervous system. Detrended correspondence analysis and K-means cluster analysis showed associations and interrelationships among these derivatives that will be clinically useful for the treatment of bacterial infections.

KEY WORDS: cephalothin; antibacterial agents; antibiotics

CEPHALOSPORINS ARE generally considered bactericidal, have low toxicity, and inhibit mucopeptide synthesis in bacterial cell walls [1]. Cephalothin is a first generation cephalosporin that is a semisynthetic derivative of cephalosporin C and is active against

both gram-negative and gram-positive bacteria [1]. Cephalothin is not well absorbed from the gastrointestinal tract, however it is rapidly disseminated from intramuscalar sites of injection [1]. Cephalothin is widely distributed in body tissues but does not normally enter the cerebrospinal fluid (but will reach low levels due to meningeal inflammation) and has a larger relative volume than some penicillins [1]. Approximately 60% of administered cephalothin is bound to plasma protein and 60% to 80% is eliminated in unchanged form by renal tubular secretion [1]. Bacterial resistance to cephalosporins has been on the increase and documented on a world wide basis [2, 3, 4, 5]. Substantial resistance that is specific to cephalothin has been observed in various clinical isolates [6].

Many important pathogens have become resistant to multiple classes of antimicrobial agents, covering most clinically useable antimicrobials, making such infections costly to treat and increasingly subject to failure [7]. Modes of drug resistance include various mechanisms of drug inactivation, target site modifications, and the events of reduced drug uptake or enhanced efflux [7]. For gram-negative pathogens (E. coli) the mechanism of drug efflux is recognized as an important cause of multidrug resistance [7].

Statistical analysis methods are applied to determine the source of property differences, side effects, and variation in activities for drugs that have similar structural features [8]. An important approach to these studies is the alteration of the size and shape of a drug by instituting the following: (1) changing the number of methylene groups; (2) changing the degree of unsaturation; and (3) adding or removing a ring system [8]. The addition of methylene groups along a chain increases the lipophilicity of a drug, increases permeation of lipid cell membranes, and may increase the activity [8]. The addition of a methylene group (-CH2-) along a chain constitutes the formation of a homologous series [9]. Many studies have shown that the addition of 1 to 6 or 7 methylene groups results in the increase of drug activity [9]; however, the chain lengthening beyond this point results in a decrease of activity. A 2-way plot of the number of methylene groups versus the drug potency results in a unimodal figure [9]. Statistical analysis of properties can elucidate beneficial characteristics of a drug candidate before they are put through expensive and time-consuming biological testing. Studies using multivariate methods have successfully elucidated properties for improvement of various drug delivery and dosage forms [10, 11]. The aliphatic chain imparts useful effects on molecular properties that have been revealed here through application of pattern recognition analysis.

MATERIALS AND METHODS

Molecular Modeling and Properties Determination

Molecular modeling and molecular properties were determined by utilizing ChemSketch v. 5 (90 Adelaide Street West, Toronto, Ontario, M5H 3V9, Canada) and Molinspiration (Liscie udolie 2, SK-841 04 Bratislava, Slovak Republic).

Pattern Recognition Analysis

Multivariate data matrix is analyzed by the following algorithms to show pattern relationships within their numerical values. Detrended correspondence analysis and K-means cluster analysis determined by PAST Version 0.45 (copyright May 2001, Oyvind Hammer, D. A. T. Harper). Cluster analysis was determined by KyPlot Version 2.0 beta 15

(copyright 1997-2001, Koichi Yoshioka). Analysis of similarities (ANOSIM) on properties of the homologous series was accomplished by PAST Version 0.45.

RESULTS AND DISCUSSION

Previous studies have shown the propyl and butyl esters of cephalothin have antibacterial activity against Eshcerichia coli that is similar to that of the parent compound, and with substantial inhibitory effect on ampicillin resistant E. coli [12]. These findings suggest that a homologous series of cephalothin derivatives could have substantial clinical efficacy in the treatment of bacterial infections. By back altering the length of the aliphatic ester substituent it is possible to vary important pharmacological attributes that will enhance the effectiveness of antibacterial action and benefit the pharmacokinetic profile of these agents. The analysis presented in this work shows clearly inter-relationships of the homologs and to the parent compound cephalothin. In addition, the favorable conclusion of these analysis shows clearly the efficacy of exploring the potential uses of other homologous sets of antibacterial agents.

The molecular structures of cephalothin and its homologous derivatives is presented in Figure 1. The carboxyl group (-C(O)OH) of the antibiotic is replaced by an ester substituent having a single methyl group (homolog 1) to as many as 10 carbon atoms (9

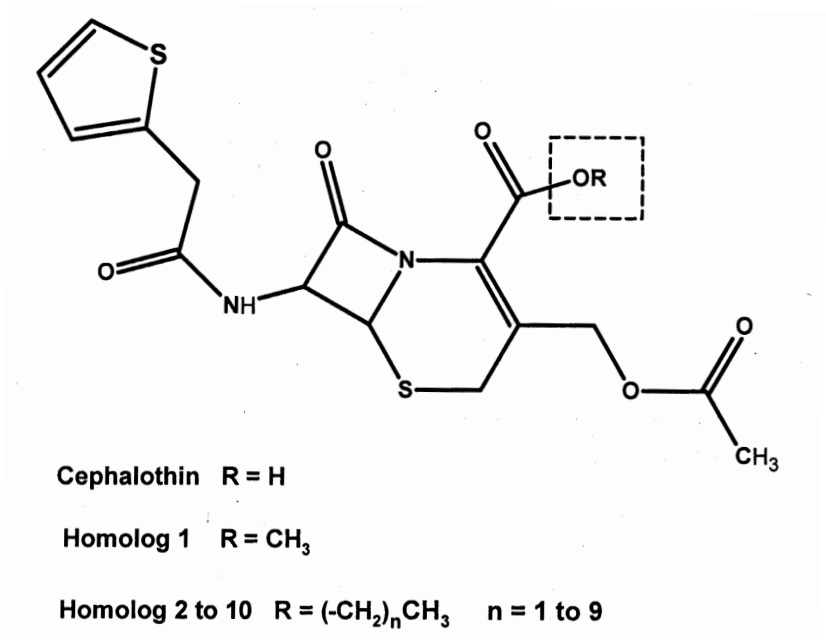

FIGURE 1. The molecular structures of members of the homologous series are presented here for comparison to the parent antibiotic cephalothin. Note that the beta-lactam ring is intact. The parent cephalothin has a carboxyl group whereas the homologs have an ester substituent. The homologs 1 to 10 have carbon atoms within an aliphatic chain and are designated as to their number of carbon atoms.

methylene groups and 1 end methyl group) along an aliphatic chain (ie., no branches). All other components of the parent structure remain the same, inclusive of the beta-lactam ring. Cephalothin itself is a first generation semisynthetic cephalosporin and a derivative of cephalosporin C, which is active against both gram-negative and gram-positive bacteria [1].

Numerical values of important pharmacological properties are shown in Table I for each homolog. Derivatives are identified by the number of carbon atoms in the aliphatic chain of the ester substituent. Properties presented in Table I appear to vary according to the length of the ester chain. Molar volume, molar refractivity, and parachor are polarizability parameters. Index of refraction is the speed of light in a vacuum divided by the speed of light within the agent, these values having a range of 0.1. Molar refractivity is a measure of steric factors, a constitutive-additive property, and a measure of the volume occupied by a group of atoms. Molar refractivity also increases as the formula weight and molar volume increases, indicating the concurrent increase in steric effects.

Homologs 1 to 7 show zero violations of the Rule of 5, which indicates that these homologs should have favorable bioavailability [13]. The Rule of 5 states that a drug may show poor permeation when two or more of the following occur: (1) formula weight is > 500; (2) Log P > 5; and (3) there are >10 H-bond acceptors [13]. Only homologs 8, 9, and 10 show violations of Rule of 5, with homolog 9 and 10 being the only homologs falling in the category of poor bioavailability (ie., FW > 500 and Log P > 5). The number of oxygens, nitrogens, -NH groups, and -OH groups remains constant for homologs 1 through 10. These groups contribute strongly to the hydrogen bonding activity of the drugs in aqueous environment and the polar surface area. With the polar components remaining constant as the formula weight increases the lipophilic tendency of the homologs will increase, an observation substantiated by the steady increase of the Log P values for homologs 1 to 10. The increase in lipophilic propensity and therefore inclination for repositing in cellular membranes accompanies a concurrent inclination for reduced aqueous solubility. Polar surface area (PSA) for homologs 1 to 10 is 102.02 A^2 and parent cephalothin at 113.01 A^2. Values of PSA have been shown to be efficient in prediction of absorption in the intestinal tract and central nervous system [14, 15]. These PSA numerical values indicate that homologs 1 to 10 are expected to have absorption of approximately 30% within the intestinal tract, while the parent cephalothin is approximately 20% absorbed. The presence of the ester group enhances absorption within the intestinal tract.

K-means cluster analysis designates subjects (homologs) in clusters of highest similarity but limits the number of clusters to a target value designated by the investigator (ie., there is no hierarchy) [16, 17, 18, 19]. In this study, K-means cluster analysis was performed on properties shown in Table I into a maximum of 4 clusters. Results of K-means cluster analysis are as follows (homologs identified by number of carbon atoms within the ester chain): Cluster 1) Homolog 3; Cluster 2) Homolog 7, 8, 9, 10; Cluster 3) Cephalothin and homolog 1; Cluster 4) Homolog 2, 4, 5, and 6. Interestingly homolog 3 is designated into a cluster all its own, however homolog 2 is clustered with 4, 5, and 6, which suggests the properties of these lower weight homologs demarcates 3 as distinct. The parent cephalothin and the lowest weight homolog 1 are grouped together and thereby considered most similar. The highest weight homologs 7, 8, 9, and 10 feature the most similarity to one another. Resolution of the homologous series can be increased through K-means analysis into 5 clusters. The results of analysis follows: Cluster 1)

TABLE I
Molecular Properties of Cephalothin and Homologs

	1	2	3	4	5	6	7	8	9	10	11
Number of Carbons in Ester Group	Formula Weight	Molar Volume (cm^3)	Parachor (cm^3)	Molar Refractivity (cm^3)	Index of Refraction	Polar Surface Area ($Angstroms^2$)	Log P	Number of Oxygens	Number of Nitrogens	Number of -NH and -OH	Violations of Rule of 5
0*	396.44	252.7	751.4	95.07	1.675	113.01	0.566	6	2	2	0
1	410.47	277.6	794.8	99.91	1.639	102.02	1.182	6	2	1	0
2	424.49	293.7	934.9	105.54	1.63	102.02	1.558	6	2	1	0
3	438.52	309.9	874.9	109.17	1.622	102.02	2.061	6	2	1	0
4	452.55	326	915	113.8	1.615	102.02	2.62	6	2	1	0
5	466.57	342.1	955.1	118.43	1.608	102.02	3.125	6	2	1	0
6	480.6	358.3	995.2	123.6	1.602	102.02	3.63	6	2	1	0
7	494.63	374.4	1035.2	127.69	1.597	102.02	4.136	6	2	1	0
8	509.65	390.5	1075.3	132.32	1.592	102.02	4.641	6	2	1	1
9	522.68	406.6	1115.4	136.96	1.588	102.02	5.146	6	2	1	2
10	536.71	422.6	1155.5	141.59	1.584	102.02	5.651	6	2	1	2

* = cephalothin

Homolog 8, 9, and 10; Cluster 2) Homolog 3 and 4; Cluster 3) Cephalothin and homolog 1; Cluster 4) Homolog 5, 6, and 7; Cluster 5) Homolog 2. Again the lowest weight homolog 1 is grouped with cephalothin. The highest weight homologs 8, 9, and 10 are clustered together and most similar. The intermediate homologs are separated into two clusters as 3 and 4, with 5, 6, and 7.

Standard cluster analysis utilizing single linkage with standard euclidean distance produces a vertical dendrogram which is presented in Figure 2. The low molecular weight homologs 1 and 2 along with the parent cephalothin (indicated by object 0) are considered distinct from the intermediate and high molecular weight homologs. However cephalothin and homolog 1 are determined to be the most similar. Interestingly this analysis determines homolog 2 to be distinct unto itself and a break point between the low weight and higher weight compounds, all other compounds separated into the supercluster initiated at node A. Homologs 3 to 10 are contained within a supercluster (node B) that is further differentiated into other subclusters. Homologs 4 and 8 are within a subcluster that is contained within the higher cluster bearing 6, 7, 9, and 10 (going from greater divergence to greater convergence). Intermediate weight homologs 3 and 5 are most similar to each other and considered distinct from homologs 4, 8, 6, 7, 9, and 10 (placed in order of increasing convergence) within the supercluster at node B.

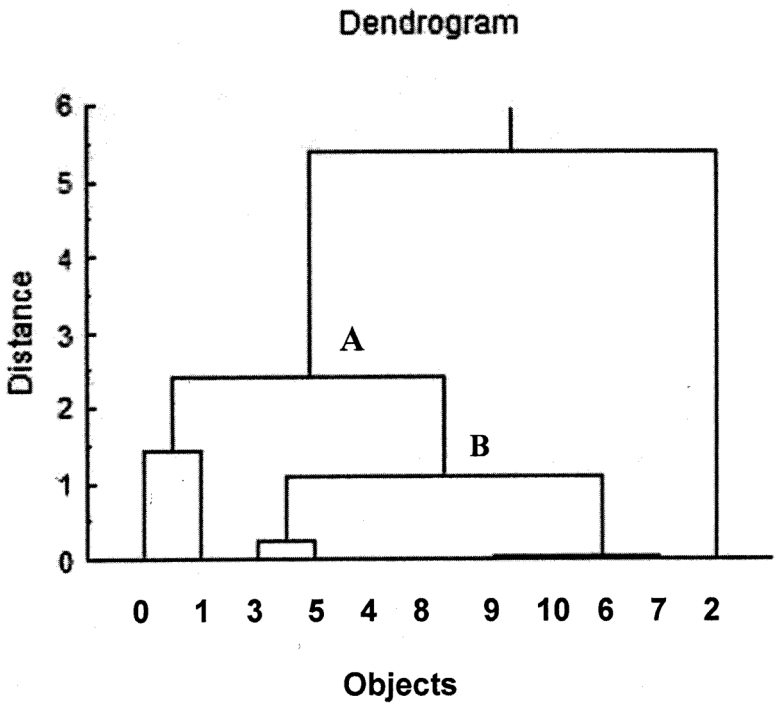

FIGURE 2. This vertical dendrogram reveals the results of cluster analysis of properties presented in Table I, accomplished by single linkage analysis utilizing standard euclidean distance. Objects are homologous derivatives of the parent compound cephalothin designated by the number of carbon atoms in the aliphatic chain of the ester group. Where the cephalothin parent structure is designated by "0" (ie., zero carbons) and homologs defined accordingly from 1 carbon to 10 carbons.

Correspondence analysis is a method of factoring categorical variables and displaying them so that associations can be studied in 2 or more dimensions (ie., a 2-way plot) [20]. Routine correspondence analysis can suffer from 2 problems: (1) arch effect owing to unimodal distribution; and (2) compression of data at initial and terminal ends [20]. Detrending removes the arch effect and compression of data [20]. Detrended correspondence analysis is performed on properties of Table I and results shown in the 2-way plot of Figure 3. Clearly by this analysis the parent cephalothin (enclosed rectangle) is considered distinct (least similar) to all homologs 1 to 10. The highest molecular weight homologs 9 and 10 are most similar and considerably distinct from 1 through 8. Homologs 1 to 7 (enclosed circle) are determined to be most similar and plotted along axis 1 and axis 2 in an approximate linear fashion. The roughly lineal configuration suggests identification of non-random attributes within the molecular properties. ANOSIM (analysis of similarity) provides a statistical analysis to determine whether a significant difference exists between 2 or more groups. A positive test statistic *R* value approaching 1 indicates

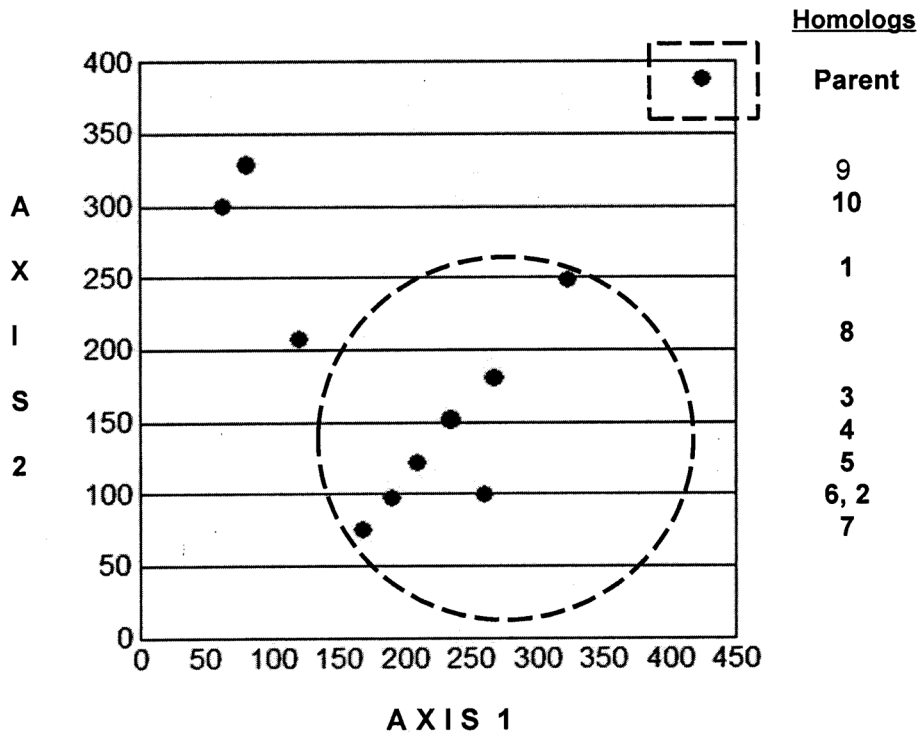

FIGURE 3. Detrended correspondence analysis of properties in Table I show associations among homologs based upon those pharmaceutical descriptors. Clearly the parent compound cephalothin is distinct from the homologous derivatives (inset rectangle). Homologs 1, 2, 3, 4, 5, 6, and 7 (based on number of carbons in aliphatic chain of ester substituent) are in closest proximity (see inset circle), a result that suggests these homologs have greater similarity among themselves than with the parent cephalothin and homologs 8, 9, and 10. Homologs 9 and 10 lie in closest proximity with homolog 8 centered between these two groupings, results suggesting distinct characteristics among these members of the homologous series.

dissimilarity between groups. The numerical result (R) shows the level of dissimilarity and can range as high as 1.000, which indicates maximum dissimilarity. ANOSIM computation between the parent cephalothin antibiotic and all homologs 1 to 10 determined an R = 0.8089, which indicates a high level of dissimilarity.

Neonatal meningitis requires antibiotic therapy which includes ampicillin and a third-generation cephalosporin. Strains of Escherichia coli (E. coli) are carried to the meninges after invading the blood stream from the gastrointestinal tract or nasopharynx. Neuroinflammatory conditions and bacterial infections increase the permeability of the blood-brain barrier to various substances [21]. Previous studies have shown that the major determinant of antibiotic penetration of the cerebral spinal fluid is passive diffusion along a concentration gradient and lipid solubility [22, 23]. Escherichia coli is the most common gram-negative bacteria that causes meningitis in neovates and invades the microvascular endothelial cells [24]. The propyl and butyl esters of cephalothin are homologs 3 and 4 of the series studied here and have been shown to inhibit ampicillin resistant E. coli [12]. The ester substituent increases the lipophilicity of the parent cephalothin (ie., higher Log P values). The relationship of Log P to penetration of the blood-brain barrier (BBB) has been studied and concludes that the optimum Log P value for entry through the BBB is 2 ± 0.5 [25]. Homolog 2 and 3 have Log P values of 1.558 and 2.061, respectively, suitable for BBB penetration and presumably treatment of meningitis. Therefore, the use of cephalothin homologs may benefit the clinical treatment of neonatal meningitis.

In summation, the properties of a homologous series of cephalothin have been analyzed by pattern recognition methods and shown to have clinically beneficial inter-relationships. Properties of molar volume, molar refractivity, and parachor increase as formula weight increases. Values of Log P increase as the length of the aliphatic ester substituent increases. Homologs 2 and 3 should penetrate the BBB and be useful in the treatment of neonatal meningitis. The values of PSA for homologs 1 to 10 remains constant at 102.02 A^2.

This work was funded by the Department of Chemistry, University of Nebraska, College of Arts & Sciences, Omaha, Nebraska 68182.

References

1. Goodman, L.S. and Gilman, A. (1970) *The Pharmacological Basis of Therapeutics*. The MacMillan Company: New York.
2. Erdem, H., Kilic, S., Pahsa, A. and Besirbelloglu, B.A. (2005) *J Chemother., 17(1)*: 61–65.
3. Moosdeen, F. (1997) *Clinical Infectious Diseases, 24(3)*: 487–493.
4. Miller, M.L., Obert, C.A., Gao, G., Daw, N.C., Flynn, P. and Tuomanen, E. (2005) *Emerg. Infect. Dis., 11(8)*: 1192–1196.
5. Brinas, L., Lantero, M., de Diego, I., Alvarez, M., Zarazaga, M. and Torres, C.J. (2005) *Antimicrob. Chemother*., *20*: 27.
6. Cornelissen, J.J., de Graeff, A., Verdonck, L.F., Branger, T., Rozenberg-Arska, M., Verhoef, J. and Dekker, A.W. (1992) *Antimicrob. Agents Chemother., 36(4)*: 801-807.
7. Deshpande, L.M., Fritsche, T.R. and Jones, R.N. (2004) *Diagn. Microbiol. Infect. Dis., 49*: 231–236.
8. Gareth, T. (2000) *Medicinal Chemistry.* New York, NY: John Wiley and Sons.
9. Silverman, R. (1992) *The Organic Chemistry of Drug Design and Drug Action.* San Diego, CA: Academic Press.

10. Hardy, I. and Cook, W. (2002) *J. Pharm. Pharmacol*., *55*: 3–18.
11. Mareno, M., Magalhaes, N., Cavalcanti, C. and Alves, A. (1996) *Quim Nova*., *19*: 594–599.
12. Bartzatt, R., Cirillo, S.L.G. and Cirillo, J.D. (2007) *Med. Chem., 3(1)*: 45–49.
13. Lipinski, A., Lombardo, F., Dominy, B. and Feeney, P. (1997) *Advanced Drug Delivery Review, 23*: 3–25.
14. Palm, K., Stenberg, P., Luthman, K. and Artursson, P. (1997) *Pharmaceutical Research*, *14*: 568–571.
15. Ertl, P., Bernhard, R. and Selzer, P. (2000) *J. Med. Chem., 43*: 3714–3717.
16. Johnson, R. and Wichern D. (1992) *Applied Multivariate Statistical Analysis.* Englewood Cliffs, NJ: Prentice Hall Inc.
17. Dundteman, G. (1984) *Introduction to Multivariate Analysis.* Beverly Hills, CA: Sage Publication.
18. Anderberg, M. (1973) *Cluster Analysis for Applications.* San Diego, CA: Academic Press.
19. Fossler, M., Chang, K. and Young, D. (1990) *Acta Pharm. Jugosl*., *40*: 225–236.
20. Greenacre, M.J. (1993) *Correspondence Analysis in Practice.* London, UK: Academic Press.
21. De Vries, H., Kuiper, J., de Boer, A., van Berkel, T.J. and Breimer, D.D. (1997) *Pharmacol. Rev., 49*: 143–155.
22. Abbot, N. and Romero, A. (1996) *Mol. Med. Today, 2*: 106–113.
23. Scheld, W. (1989) *Rev. Infect. Dis., 11*(Supp 7): S1669–1690.
24. Sukumaran, S., McNamara, G. and Prasadarao, N. (2003) *J. Biol. Chem., 278(46)*: 45753–45762.
25. Hansch, C. and Leo, A. (1995) *Exploring QSAR*. Washington D.C., U.S.A.: American Chemical Society.

Received June 5, 2007;
accepted November 28, 2007.

Physiological Chemistry and Physics and Medical NMR
INDEX
Volume 38, 2006